To my husband Joaquim
and to my son Francisco

Acknowledgements

I wish to express my appreciation to University of Minho and all those who direct or indirectly were involved in this research, in particular, the departments of Mechanical Engineering and Production and Systems for their collaboration.

I am thankful to the Portuguese Foundation for the Science and Technology (FCT) who supported my work through a scholarship.

I am deeply grateful to my supervisors, Professors Senhorinha de Fátima Capela Fortunas Teixeira and José Carlos Fernandes Teixeira, whose advice and encouragement have guided me throughout this research. I cannot forget their patience and constant friendship we developed during these years.

A special thank to Júlio Caldas for his help during the course of the experimental work and, above all, for his craftsmanship in setting up the test facility. Without his skills and dedication this experimental work would be nearly impossible.

Also Leonor and Miguel, from the Mechanical Engineering Department, I want to express my gratitude for the help on treatment and measuring the weight of the particles.

To André Espaze, an Eramus student from France, I want to thank his help in developing the system to introduce the solid particles as well as the help on the measurements of pressure drop.

To Professor Celina Leão, I want to thank her help on the statistic study of the droplet distribution, but above all her friendship and constant encouragement, mostly during the later stages in writing the thesis.

I also would like to thank my colleague at the university, Eng. Filipa Carneiro for the all the discussion and faithfull discussion of ideas regarding the Gambit and Fluent code. Her friendship and excellent working partnership is deeply appreciated.

Last, but not least, I would like to express my gratitude to my husband Joaquim for having unlimited patience and constant faith in me, for his love and understanding during the course of this work.

Abstract

Understanding the hydrodynamics of two-phase annular flow in venturi geometries is always a demanding task. Several works have been reported in the literature, regarding experimental and modelling of pressure drop, droplet size, liquid split and collection efficiency. However, research work in large-scale venturis close to the industrial application is very scarce.

The experimental venturi scrubber facility built at the University of Minho has a throat diameter of 125 *mm* and a total length of 1.27 *m*. The throat gas velocity was within the range between 34 and 70 *m/s* and the liquid flow rate was set between 0.013 and 0.075 *kg/s*. The experimental work extends the available data into lower liquid concentrations where the atomisation process is more complex. The droplet size was measured by means of a laser diffraction instrument with a dynamic range between 15 and 1500 μm. The pressure drop was measured by an inclined multi tube manometer with phase separators between the pressure tappings and the manometer.

The data show strong evidence that in the atomisation process, competing mechanisms are present. The droplet size is closely linked to the pressure drop which shows that the effect of liquid flow rate is not monotonic throughout the entire range. The minimum observed in this work has not been previously reported.

The influence of the type of liquid introduction, on the pressure drop, is only important at high liquid loading. The atomisation and the initial interactions with the gas stream control the flow dynamics throughout the venturi. Furthermore, the changes in the droplet size distribution along the venturi are a clear indication of the phases interaction along the geometry.

These data taken in well known and controlled conditions have been used to validate a phenomenological model further improved in the research group. This model takes into account the boundary layer growth in the diffuser and improves the

description of the droplet population by including a distribution created at each step along the venturi, coalescence effects, entrainment and deposition. The comparisons have shown fairly good results, particularly for the pressure recovery in the diffuser.

In order to achieve a better correlation between experimental and simulated results, a three-dimensional computational two-phase fluid model was developed using the Fluent code. An Euler-Langrangian approach has been used and the turbulence effects have been included. The droplet distribution at the venturi inlet was taken as a RR, but the dynamics of annular flow were not included.

Some discrepancies were observed for the convergence pressure drop but the total pressure drop up to the throat was very well predicted for the experimental data taken from the large-scale venturi.

The assumption of Cruz *et al.* (2007) model for the divergence section, that droplets flow essentially at the core region and not in the boundary layer, was predicted by the Fluent model.

Both models produced comparative results and they must be further developed.

Resumo

O estudo do escoamento bifásico do tipo anular num venturi é uma tarefa complicada. Vários trabalhos têm sido publicados na literatura abordando quer a experimentação quer a modelação das principais variáveis: queda de pressão, tamanho de gotas, distribuição do líquido e eficiência na colecção de contaminantes. No entanto este conhecimento quando aplicado a venturis de grandes dimensões é muito escasso.

Neste contexto foi construido um limpador de venturi experimental na Universidade do Minho. Este é caracterizado por um diâmetro de 125 *mm* no gargalo e um comprimento total de 1.27 *m*. Os ensaios foram realizados para velocidades do ar no gargalo entre 34 e 70 *m/s* enquanto o caudal de água foi regulado entre 0.013 e 0.075 *kg/s*. Este trabalho experimental estende os ensaios para baixos caudais de líquido onde o processo de atomização é mais complexo. O tamanho das gotas foi medido através de um instrumento baseado na técnica de difracção laser com uma gama de medição entre 15 e 1500 μm. A queda de pressão foi medida com auxílio de um manómetro multi-tubos inclinado.

Os dados mostram que no processo de atomização competem vários mecanismos. O tamanho de gotas está directamente relacionado com a queda de pressão que, em função do caudal de líquido, apresenta não ser monotónica ao longo da gama de ensaios testada. A ocorrência de um mínimo não tinha sido reportada na literatura.

O método de introdução do líquido no interior do venturi tem uma influência significativa na queda de pressão e no tamanho das gotas. O processo de atomização e as interacções entre as fases na região de entrada do venturi controlam o escoamento a jusante. Acresce que, a observaçãode alterações à distribuição probabilística das gotas ao longo do venturi, é uma indicação clara da interacção entre as duas fases.

Os dados, que reflectem condições experimentais controladas, foram usados para validar um modelo fenomenológico do escoamento, desenvolvido pelo grupo de

trabalho. Este modelo considera o crescimento da camada limite na expansão, uma distribuição probabilística das gotas, coalescência e a interacção entre o filme e as gotas dispersas. A comparação com os resultados experimentais é muito aceitável, em particular para a recuperação de pressão no difusor do venturi.

Por forma a encontrar uma melhor correlação com os dados experimentais, um modelo computacional bifásico, tridimensional, foi desenvolvido no código Fluent. O método Euleriano-Lagrangeano foi usado para a modelação da fase dispersa. No entanto, não inclui o escoamento bifásico do tipo anular. Algumas deficiências foram encontradas no cálculo da queda de pressão na contracção. O modelo permitiu ainda validar a hipótese de não inclusão da fase dispersa na camada limite do difusor (Cruz *et al.*, 2007). Ambos os modelos apresentam resultados similares.

Contents

List of Figures ..... **xii**

List of Tables ..... **xv**

Nomenclature ..... **xvi**

CHAPTER 1 ..... **1**

Introduction **1**
1.1 Gas Cleaning Devices 2
1.2 Venturi Scrubber 3
1.3 Objectives of the Research 8
1.4 Thesis Outline 8

CHAPTER 2 ..... **10**

Literature Review **10**
2.1 Numerical Models 10
2.2 Experimental Work 18
2.2.1 Pressure drop 19
2.2.2 Droplet size 20
2.2.3 Collection efficiency 22
2.3 Conclusions 24

CHAPTER 3 ..... **26**

Experimental Arrangement **26**
3.1 Experimental Setup 26
3.2 Experimental Techniques 31
3.2.1 Gas flow rate 31
3.2.2 Pressure drop in the venturi 33
3.2.3 Laser diffraction technique 37
3.3 Experimental Uncertainties 41
3.3.1 Manometers 42
3.3.2 Rotameters 46
3.3.3 Malvern 2600 48

CHAPTER 4 49

Experimental Results and Discussion 49
4.1 Test conditions 49
4.2 Pressure drop 51
4.2.1 Experimental Data 51
4.2.2 Model validation 58
4.2.3 Conclusions 62
4.3 Droplet Size 63
4.3.1 Droplet size distribution 63
4.3.2 Droplet size data 68
4.3.3 Droplet size correlations 73
4.3.4 Conclusions 77

CHAPTER 5 79

CFD Model 79
5.1 Fundamentals of CFD Modelling 79
5.2 Eulerian-Lagrangian Approach 81
5.3 Governing Equations 84
5.3.1 Continuous phase description 84
5.3.2 Discrete phase description 89
5.3.3 Coupling Procedure 95
5.4 Numerical Procedure 97
5.5 Output Results from Fluent 99

CHAPTER 6 100

Numerical Simulation and Experimental Validation 100
6.1 Grid Generation 100
6.2 Numerical Simulation 102
6.3 Single Phase Results 103
6.3.1 Numerical results 104
6.3.2 Comparison with experimental data 106
6.3.3 Discussion 109
6.4 Two-Phase Flow Steady State 110
6.4.1 Continuous phase 110
6.4.2 Dispersed second phase 114
6.4.3 Experimental validation 117
6.4.4 Discussion 120

CHAPTER 7 121

Conclusions and Future Work 121
7.1 Conclusions 121
7.2 Future Work 123

APPENDIX A 124

Collection System 124
A.1 Solid Particle Introduction System 124
A.2 Solid Particle Measurement 126
A.3 Collection Efficiency Preliminary Results 128
A.4 Conclusions 130

REFERENCES 131

List of Figures

Figure 1.1 - Venturi scrubber. 3
Figure 1.2 – Vertical two-phase flow map (Dahl, 2005). 4
Figure 1.3 – Horizontal two-phase flow map (Dahl, 2005). 5
Figure 3.1 – Geometric variables of the venturi geometry. 27
Figure 3.2 – Schematic representation of the experimental rig. 28
Figure 3.3 – Schematic representation of venturi scrubber injections and droplet measurement points. 30
Figure 3.4 – Overall view of the test facility. 30
Figure 3.5 – Scheme and view of the bell mouth entrance to the ventilator. 32
Figure 3.6 – Digital manometer. 33
Figure 3.7 – Pressure tappings along the venturi. 34
Figure 3.8 – The inclined differential manometer. 35
Figure 3.9 – Inclined multi manometer TEM. 36
Figure 3.10 – Settling chambers for separating the water from the gas. 36
Figure 3.11 – Layout of the Malvern 2600. 38
Figure 3.12 – Available lens and corresponding particle size range (μm). (*Malvern Instruments,user manual, 1991*). 38
Figure 3.13 – Geometry of manometer with water. 43
Figure 3.14 – Geometry of the multi tube. 45
Figure 3.15 – Rotameters used for liquid measurements. 46
Figure 3.16 – Calibration curve of liquid flow rate for rotameter A. 47
Figure 3.17 – Calibration curve of liquid flow rate for rotameter B. 48
Figure 4.1 – Gauge pressure along the installation as a function of the air flow rate. 51
Figure 4.2 – Effect of gas flow rate upon the pressure along venturi, for different liquid injection systems. $W_L = 0.013$ *kg/s*. 52
Figure 4.3 – Effect of gas flow rate upon the pressure drop along venturi for different liquid injection systems. $W_L = 0.038$ *kg/s*. 53
Figure 4.4 – Variation the total pressure drop in the venturi with gas velocity and liquid loading. Liquid injected as a film. 54
Figure 4.5 – Variation of the total pressure drop in the venturi with liquid to gas ratio and gas throat velocity. Liquid is injected as a film. 55
Figure 4.6 – Variation of the total pressure drop in the venturi with liquid to gas ratio and throat gas velocity. Liquid injected as a spray. 56
Figure 4.7 – Variation in the total pressure drop along the venturi with liquid flow rate. Liquid injected as a film. $U_{GT} = 70$ *m/s*. 57
Figure 4.8 – Variation in the total pressure drop along the venturi with liquid flow rate. Liquid injected as a spray. $U_{GT} = 70$ *m/s*. 57

Figure 4.9 – Variation in the total pressure drop along venturi calculated by the model of Cruz (1997). U_{GT} = 61 *m/s*..... 59
Figure 4.10 – Comparative total pressure drop predicted by Cruz (1997) model and experimental data. Liquid injected as a film..... 60
Figure 4.11 – Comparative total pressure drop predicted by Cruz (1997) model and experimental data. Liquid injected as a spray..... 60
Figure 4.12 – Comparative pressure drop in the throat predicted by Cruz (1997) model and experimental data. Liquid injected as a film..... 61
Figure 4.13 – Comparative example of pressure drop profiles predicted by Cruz (1997) model and experimental data. U_{GT} = 52 *m/s*..... 62
Figure 4.14 – Mass fraction droplet size distribution along the venturi axis (sections A, B and C). Liquid is injected as a film. W_G = 0.861 *kg/s* and W_L = 0.075 *kg/s*..... 65
Figure 4.15 – Mass fraction droplet size distribution along the venturi axis (section A, B and C). Liquid is injected as a spray. W_G = 0.861 *kg/s* and W_L= 0.058 *kg/s*..... 65
Figure 4.16 – Mass fraction droplet size distribution along the venturi axis (section A, B and C). Liquid is injected as film and spray. W_G = 0.987 *kg/s* and W_L = 0.075 *kg/s*. . 66
Figure 4.17 – Mass fraction droplet size distribution for different gas velocities in the diverging section. Liquid is injected as film. W_L = 0.075 *kg/s*..... 67
Figure 4.18 – Mass fraction droplet size distribution for different liquid loading in the diverging section. Liquid is injected as film. *Wg* = 0.987 *m/s*..... 68
Figure 4.19 – Mean droplet size along the venturi comparisons between two methods for liquid injections. W_L = 0.038 *kg/s*..... 69
Figure 4.20 – Influence of the liquid flow rate on the mean droplet size for the spray nozzles..... 70
Figure 4.21 – Effect of the gas velocity upon the mean droplet size at the end of the converging section (A). Liquid introduced as a film and as a spray..... 71
Figure 4.22 – Influence of the liquid flow rate upon the mean droplet size. Liquid injected as a spray and as a film for various gas flow rates..... 72
Figure 4.23 – Comparison between experimental and predicted droplet size in the converging section of the venturi (A). Droplet size is predicted using the throat velocity. Liquid is injected as a film..... 75
Figure 4.24 – Comparison between experimental and predicted droplet size in the throat section of the venturi (B). Droplet size is predicted using the throat velocity. Liquid is injected as a film..... 75
Figure 4.25 – Comparison between experimental and predicted droplet size in the divergent section of the venturi (C). Droplet size is predicted using the throat velocity. Liquid is injected as a film..... 76
Figure 4.26 – Comparison between experimental and predicted droplet size in the divergent section of the venturi (C). Droplet size is predicted using the local velocity. Liquid is injected as a film..... 77
Figure 5.1 - Overview of the two-way coupling (Adapted from Fluent 6.2 User's guide) 96
Figure 5.2 - Overview of the Segregated Solution Method (Adapted from Fluent 6.2 User's guide)..... 98
Figure 6.1 – Computational mesh of the circular venturi scrubber. 101
Figure 6.2 – Axial velocity along the venturi centreline. 104
Figure 6.3 – Axial velocity along the venturi as function of gas flow rate..... 105
Figure 6.4 – Velocity vectors profiles at medium *z* plan (throat velocity 70 *m/s*)..... 105

Figure 6.5 – Effect of the gas velocity on pressure drop. 106
Figure 6.6 – Comparisons between experimental and predicted pressure drop. U_{GT} = 70 *m/s*. 107
Figure 6.7 –Experimental and numerical pressure drop comparison for various air flow rates. 108
Figure 6.8 – Experimental and numerical total pressure drop as a function of the throat gas velocity. 108
Figure 6.9 – Comparative pressure drop predicted by CFD and experimental data, for each section 109
Figure 6.10 – Influence of the liquid upon the velocity along the venturi. U_{GT} = 70 *m/s*. 111
Figure 6.11 – Influence of the liquid loading upon the velocity at the venturi axis U_{GT} = 34 *m/s* 111
Figure 6.12 – Velocity vectors for the continuous phase. W_G = 0.987 *kg/s* and W_L = 0.075 *kg/s*. 112
Figure 6.13 – Influence of the discrete phase onthe continuous phase kinetic turbulence (*k*). 112
Figure 6.14 – Interphase momentum exchange ($kg.m/s^2$). 113
Figure 6.15 – Discrete phase concentration (kg/m^3). W_G=0.987 *kg/s* and W_L=0.075 *kg/s*. 114
Figure 6.16 – Particle Trajectories identified by particle residence time (*s*) 115
Figure 6.17 – Particle Trajectories for the smaller droplets (15.5 μm) identified by particle residence time (*s*) 115
Figure 6.18 – Particle Trajectories for the larger droplets (1504 μm) identified by particle residence time (*s*) 116
Figure 6.19 – Particle trajectories identified by particle *x* velocity (*m/s*) 116
Figure 6.20 – Particle trajectories identified by particle diameter (*m*) 117
Figure 6.21 – Comparison of pressure drop profiles predicted by the CFD model and experimental data. U_{GT} = 70 *m/s*. 118
Figure 6.22 – Comparative total pressure drop predicted by CFD model and experimental data. 119
Figure 6.23 – Comparative total pressure drop predicted by CFD model and experimental data for each section. 119
Figure 6.24 – Comparison of pressure drop profiles predicted by the CFD model, the Cruz (1997) model and experimental data. W_G = 0.987 *kg/s* and W_L = 0.038 *kg/s*. 120
Figure A.1 – Schematic representation of solid particle introduction system 125
Figure A.2 - Calibration curve for mass flow rate of dust particles. 126
Figure A.3 – Solid particle collection system 127
Figure A.4 – Wet filter in the suction probe. 128
Figure A.5 - Collection efficiency: numerical prediction. 129

List of Tables

Table 2.1 – Main geometric characteristics and experimental operation conditions 19
Table 2.2 - Published sources of droplet size in venturi scrubbers 20
Table 3.1 – Geometric details. 28
Table 3.2 – Maximum distance between lens and sample (*Malvern Instruments, user manual, 1991*). 39
Table 3.3 – Manometer with water. 44
Table 3.4 – Manometer multi tube. 44
Table 3.5 – Digital manometer 45
Table 3.6 – Calibration tests for rotameter A. 46
Table 3.7 – Calibration tests for rotameter B. 47
Table 4.1 – Volumetric flow rates and liquid to gas ratios tested. 50
Table A.1 - Preliminary results of collection efficiency 129

Nomenclature

A	*Area*	m^2
$\overline{X}$	*Rosin-Rammler parameter*	m
C_μ	*Constant derived from the Renormalization Group*	-
$C_{1\varepsilon}$, $C_{2\varepsilon}$	*Constants of the k-ε model*	-
C_d	*Discharge coefficient*	-
C_D	*Drag coefficient*	-
C_i	*Molar concentration*	$mole/m^3$
c_p	*Specific heat*	J/kgK
d	*Local diameter*	m
d_{32}	*Sauter mean droplet diameter*	m
d_D	*Droplet diameter*	m
D_i	*Diffusion coefficient*	m^2/s
d_p	*Dust particle diameter*	m
Ep	*Uncertainties of pressure measurements*	Pa
F_D	*Drag force*	N
F_x	*Additional forces*	N
g	*Gravitational acceleration*	m/s^2
G_k	*Generation of turbulence kinetic energy due to the mean velocity gradients*	$kg/m.s^3$
h	*Specific enthalpy*	J/kg
h_c	*Heat transfer coefficient*	W/Km^2

H_D	*Volume fraction of droplets*	-
h_{lg}	*Latent heat of vaporization*	*J/kg*
I	*Turbulence intensity*	*%*
k	*Turbulent kinetic energy*	m^2/s^2
K	*Thermal condutivity*	*W/mK*
k_c	*Mass transfer coefficient*	*m/s*
l	*Length*	*m*
m_D	*Droplet mass*	*kg*
n	*Rosin-Rammler parameter*	-
n_p	*Number concentration of dust particles*	m^{-3}
Nu	*Nusselt number*	-
p	*Pressure*	*Pa*
Pr	*Prandtl number*	-
Q	*Volume flow rate*	m^3/s
r	*Random number*	-
R_ε	*Additional term in ε equation for RNG model*	kg/m^3s
Re	*Reynolds Number*	-
Rp	*Resoluiton of pressure equipment*	*Pa*
RR	*Rosin-Rammler cumulative weight*	-
Sc	*Schmidt number*	-
S_D	*Momentum Source*	$kg\ m/s^2$
Sh	*Sherwood number*	-
S_m	*Mass source*	*kg/s*
St	*Stokes number*	-
T	*Temperature*	*K*
t	*Time*	*s*
T_D	*Particle relaxation time*	*s*

T_L	*Particle lagrangian time scale*	*s*
U	*Velocity*	*m/s*
u',v',w'	*Fluctuanting gas velocity*	*m/s*
u,v	*Droplet velocity components*	*m/s*
u,v,w	*Instantaneous gas velocity*	*m/s*
U_{GT}	*Throat gas velocity*	*m/s*
u_i,u_j	*Gas velocity components*	*m/s*
U_r	*Relative velocity between gas and liquid*	*m/s*
W	*Mass flow rate*	*kg/s*
We	*Weber number*	-
x,y,z	*Droplet coordinates*	*m*
x_i,x_j	*Gas field coordinates*	*m*
Z	*Vertical elevation*	*m*

Greek Symbols

Δp	*Pressure drop*	N/m^2
λ_f	*Friction factor*	-
α,θ	*Angle*	
ε	*Dissipation rate of turbulence*	m^2/s^3
η	*Collection efficiency*	-
η	*Effectiveness factor*	-
η_i	*Target efficiency*	-
λ	*Length scale*	*m*
μ	*Viscosity*	*kg/m s*
μ_t	*Turbulent viscosity*	*kg/m s*
ρ	*Density*	kg/m^3

ρ_f	*Density of fluid*	kg/m^3
ρ_p	*Density of dust particles*	kg/m^3
σ	*Surface tension*	*N/m*
τ_e	*Eddy lifetime*	*s*
ζ	*Random number*	-

Subscripts

∞	*Free flow*
atm	*Atmospheric*
D	*Droplet*
f	*Fluid*
G, g	*Gas*
L, l	*Liquid*
LE	*Entrainment liquid*
m	*Manometer*

Abbreviations

CFD	*Computational Fluid Dynamics*
FS	*Full scale*
MI	*Independent Model*
pdf	*Probability distribution function*
RNG	*Renormalization Group*
RR	*Rosin-Rammler Distribution*

Chapter 1

Introduction

In many industries, the presence of fine particles is a source of concern for both the industrial process itself and the human health, as well. Of particular relevance for the textile industry, the presence of fibre dust is a real health hazard for the workers.

In addition to fibre dusts, fogs of lubricating oils are widely present, contributing significantly to the clogging of dry filtering systems. The application of wet collectors for filtering is a valid alternative over systems such as dry filters or cyclones which are often the prime option for dust removal.

Because the humidity levels are kept at higher levels in order to facilitate the industrial process, the applications of wet systems in the textile industry, is desirable. In dry climates, such humidification is often combined with evaporative cooling for temperature control inside the plant.

It appears that one could efficiently consider the cleaning process with temperature and humidity control into a single unit. The study of compact and efficient solutions becomes imperative in optimizing the filtering and humidification processes. Therefore, wet collectors proved to be very advantageous in such environments. Amongst those, the venturi scrubber presents high collection effectiveness, particularly for small, low inertia particles.

1.1 Gas Cleaning Devices

In many industrial processes sedimentation is the primary mechanism for particle removal from a gas stream. For the finer particles that may still be carried with the gas flow, additional particle/gas separation equipment is required (Holdich, 2002).

Several types of equipment are available for gas cleaning. Holdich (2002) described some of these equipments mentioned as follows:

- Settlement chambers, which are more appropriate for coarse particles that may be collected in turbulent flow;
- In centrifugal collectors, such as gas cyclones, the inertial separation between the particles and the carrier gas causes particle with greater inertia, to be thrown out of the gas stream and collected on a surface;
- Scrubbers collect the particles by liquid droplets or liquid surfaces. The venturi scrubber achieves the capture especially in the throat section. The main particle collection mechanism is inertial interception;
- Fibrous and bag filters capture the dust on a fibre. The principal collection mechanisms are the inertia and diffusion;
- Gravel bed filters, capture particles on larger ones, which need to be subsequently cleaned. The principle collection mechanism are the same as with fibrous and bag filters;
- Electrostatic precipitators use electrostatic forces to induce the particle motion onto collection surface.

Holdich (2002) also analysed some of the operating condition for various equipments by comparing the collection efficiency for different particles sizes (1, 5 and 50 μm) and relative cost per 1000 m^3 of gas treated. The venturi scrubber proved to be very efficient to remove the 50 μm particles, presenting even 100% of efficiency at a relative low cost

Venturi scrubbers, are amongst the most effective of such devices, due to its various competitive advantages: they efficiently remove both tiny particles and toxic gaseous components; are compact and simple to build, with lower initial investment costs when compared with electrostatic precipitators; are reliable; and possible to handle hot, explosive or corrosive atmosphere and sticky particles. This last advantage is one key aspect that makes bag filters unsuitable for such duties (Sun and Azzopardi, 2003).

Whatever the application, the system optimization is paramount to its effectiveness. Such optimization can be focused in terms of compactness, in the balance between the efficiency of dust collection and temperature/humidity control and the operating energy costs (pressure drop). Detailed knowledge in the physical process of venturi scrubbers has great relevance, particularly in systems that are closer in size to the industrial applications. They are the main focus of the present work, and will be described in detail over the following sections.

1.2 Venturi Scrubber

A typical design of a venturi scrubber is shown in Figure 1.1. This equipment is composed by three main parts: convergence, throat and diffuser or divergence. The cross section could be rectangular or circular.

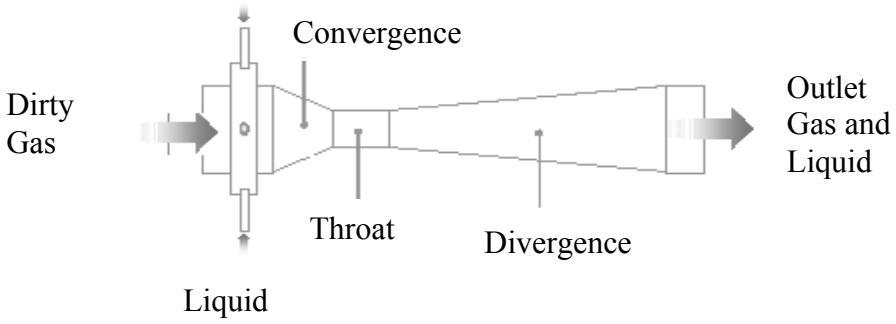

Figure 1.1 - Venturi scrubber.

The dirty gas contaminant is accelerated in the convergence section of the venturi. Liquid can be sprayed directly into the venturi throat or can be introduced at the inlet of the venturi as a film, which is subsequently atomised by the gas. In both cases, the high kinetic energy of the gas atomises the liquid into very small drops. Initially these droplets are flowing very slowly, and there is a large difference in velocity between the drops and the gas. The drops behave as very efficient inertial collectors, and the particles are transferred from the gas to the liquid droplets. In the divergent section, additional collection can occur because the dust decelerates more rapidly than the high inertia droplets and a part of the pressure lost is recovered (Gonçalves *et al.*,

2001). The venturi is followed by a separator that removes the droplets (with the dust particles) from the gas.

The different rates of acceleration between the gas and droplets are the basis of operation of the venturi scrubber. Because the acceleration is related to pressure drop, usually high collection efficiency yields high pressure drop and so high operation costs. This is the major limitation in the use of the venturi scrubber and has resulted in the development of several theoretical models to calculate the pressure drop across the venturi.

The study of the mechanisms involved in a gas-liquid flow becomes more difficult due to a number of additional variables that are not present in a single-phase system. In gas-liquid flow systems, the interaction between the two phases depends of several parameters, namely flow rate of each phase, pressure, heat flux at the wall, pipe geometry and flow direction, this interface takes a wide range of forms. Figures 1.2 and 1.3 show the flow patterns which have been generally accepted in vertical and horizontal flows, respectively. There are others physical parameters that affect the flow regimes that are not included in this graph like surface tension, viscosity, density of gas and liquid and also. Multiphase flow regimes also have no sharp boundaries but instead change smoothly from one regime to another (Dahl, 2005).

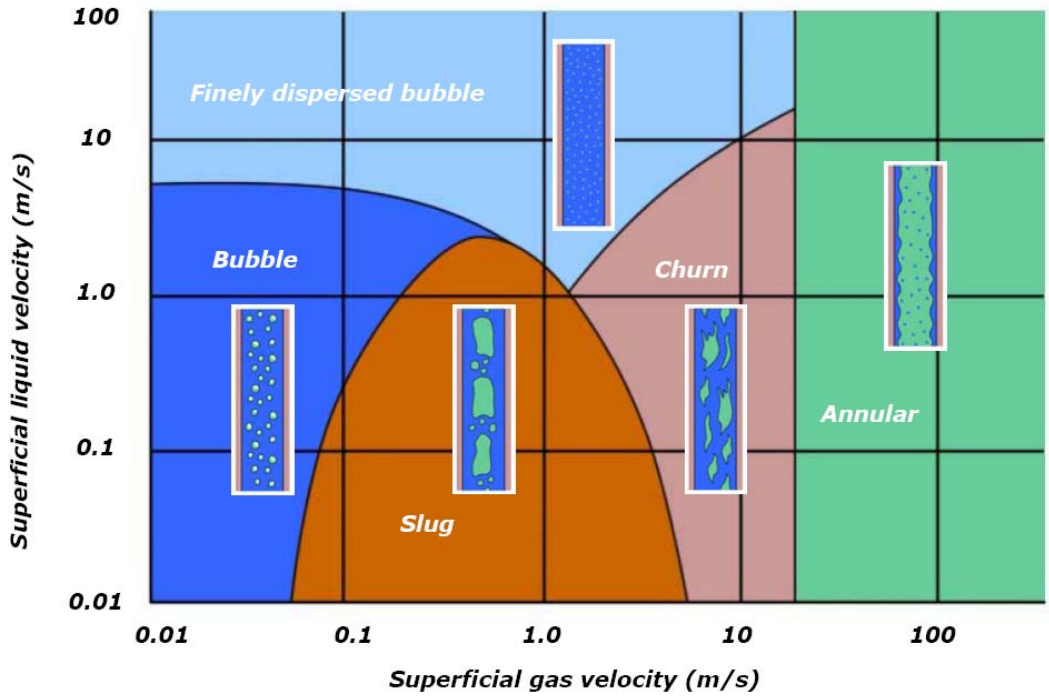

Figure 1.2 – Vertical two-phase flow map (Dahl, 2005).

The term superficial velocity is used on the axes of flow regime maps. The superficial velocity of a fluid is that obtained if the fluid would occupy all the cross section area of the tube. For the superficial liquid velocity analogous relation can be derived.

In vertical flows, as the superficial gas velocity increases the flow regime will change between all phases, bubble - slug - churn and annular. Note that for a particular superficial gas velocity, the flow regime is annular for all superficial liquid velocities.

In horizontal flows, the transitions are function of various factors namely pipe diameter and density of the phases. The Figure 1.3 is a qualitative map of the flow regime transitions in horizontal multiphase flow. This illustration will only be valid for a specific pipe, pressure and a specific pair of fluids.

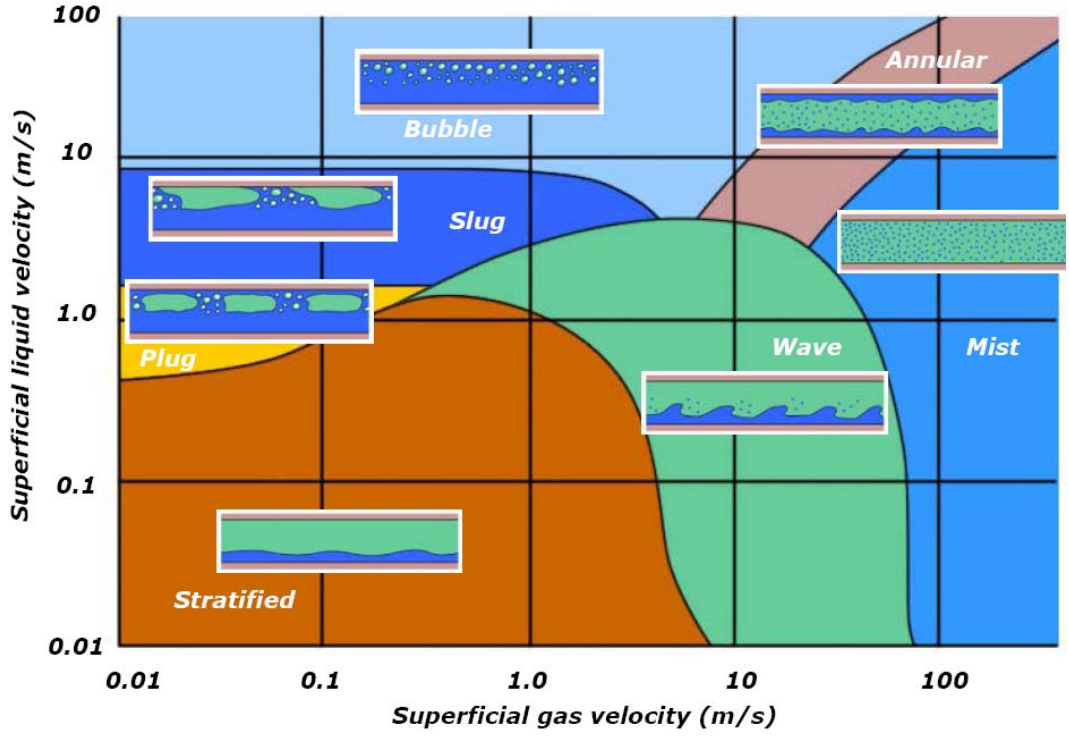

Figure 1.3 – Horizontal two-phase flow map (Dahl, 2005).

The hydrodynamics of an annular two phase flow is the core feature of a venturi scrubber: part of the liquid travels as a film on the wall and the rest is carried as droplets by the gas core. This is a very dynamic and complex flow because droplets can deposit, break-up or coalesce and new droplets are continuously entrained from the liquid film. The liquid splits between the film and the droplets, and the mass and momentum

interchange between the dispersed phase and the gas, is strongly dependent upon the droplet size (Azzopardi, 1997).

Venturi scrubbers have been extensively studied in order to foster their understanding and modelling. Great efforts have been dedicated to calculate the pressure drop as a major parameter in the venturi performance. The energy costs associated with gas pumping are the main drawback of these systems. It has been observed that an improvement in the efficiency of the equipment is always correlated to this parameter (Gamisans *et al*., 2002). Models of wide range of complexity have been presented in the literature, often validated with the experimental data.

The model of Azzopardi and Govan (1984) was tested and some improvements to this model were made by Teixeira (1989) and latter by Azzopardi *et al*. (1991). This model is based on the boundary layer theory and has been validated against different experimental data and proved to be very accurate.

Although some authors (Viswanathan *et al.*, 1985) have addressed the liquid flow split and the local entrained mass fluxes, a great deal of attention has been devoted to the study of droplets in venturi scrubbers. The efficiency of dust collection and gas absorption and humidification is strongly dependent upon the droplet motion inside the venturi. Furthermore, the momentum exchange of droplets accounts for 50-85 % of the total pressure drop inside the venturi. In both the size and distribution of droplets is of the greatest relevance (Gonçalves *et al.*, 2001).

The Cruz (1997) model is a variation of Azzopardi *et al*. (1991) model, discussed extensively in the literature. The modifications to this model concern the droplet distribution (classes and droplet coalescence) and they have been presented and discussed (Cruz *et al*., 1997).

Such analytical or phenomenological models can provide detail hydrodynamics of an annular two-phase flow, to predict the pressure drop, droplet sizes and collection efficiency in the venturi. They are also a versatile, flexible and cost effective technique. Researchers have been using this technique for all time.

The availability of affordable high performance computing hardware, together with new advances in numerical algorithms, visualization and programming techniques, have led to a recent increase of interest in Computational Fluid Dynamics (CFD) and to an improvement in the ability to solve and visualize complex problems in fluids engineering.

Ananthanarayanan and Viswanathan (1999) applied the CFD code Fluent to simulate the two-phase flow along a rectangular venturi scrubber. These results are encouraging and suggest that such codes can be used in optimizing equipment performance. However, it is impossible to assess the validity of the physical and chemical models embedded in a program as complex as a CFD code or the accuracy of its final results by any means other than comparisons with experimental test work. Anyone wishing to use CFD in serious way must realize that it is no substitute for experimentation, but very powerful problem-solving tool (Versteeg and Malalasekera, 1995).

Experimental data is important to validate these models and correlations. Over the years, several researchers published measurements in venturi scrubbers.

Most of the experimental work has been carried out in small laboratory-scale scrubbers rendering the extrapolation of results to industrial size designs open to question.

Detailed pressure drop analysis is rarely found in literature for large–scale venturi scrubbers. Gamisans *et al.* (2004a) presented experimental data in an ejector venturi with a small throat length and Allen and Van Santen (1996) present only film injection for the liquid introduction.

The work carried out on droplet size reports the droplet size distribution in venturi scrubbers as a mean diameter. Different droplet size distributions have also been used to characterize the distribution of droplet sizes.

Although most of the work has been reviewed, it may be summarised that very few published works have reported experiments in large scale test facilities. The experimental tests in venturi scrubbers, close to the industrial size, are needed. These data could be used to validate the existing numerical models in the literature.

Given that no modifications were required to scale-up, it seemed interesting to evaluate Cruz (1997) model with a new set of data from an industrial large scale venturi, with different liquid loadings and different methods of liquid injection.

The 3D numerical simulation of the two-phase flow on venturi scrubber using CFD code also appears to be an appropriate and effective technique to be used in order to get a detailed and complete description of the two-phase flow, inside a venturi scrubber.

1.3 Objectives of the Research

Taking into account the background previous outlined, two main goals are defined in the present work: to acquire experimental data of pressure drop and droplet size distribution along a large scale venturi scrubber constructed at the Mechanical Engineering Department at University of Minho, and to develop a three-dimensional computational model able to predict and characterize two-phase flow, air and droplets inside this geometry.

To achieve these goals four steps will be followed:

1. Reconstruction, adaptation and validation of the experimental setup initially designed by Lobarinhas (2003) for a large scale venturi close to the industrial size;

2. Obtain experimental data, on pressure drop and measuring the droplet sizes using the laser diffraction technique;

3. Validation of the experimental results against the phenomenological model developed by Cruz (1997) and numerical correlations of droplet size, available on the literature;

4. Development of a numerical model, using the CFD code, Fluent, to study the multiphase flow behaviour in a large-scale venturi scrubber.

1.4 Thesis Outline

In the following chapter, a more detailed review of the previous work on numerical models and experimental work on venturi scrubbers is point out.

Chapter 3 is a description of the experimental setup used to obtain the experimental data of pressure drop and droplet size. This setup was designed initially by Lobarinhas (2003), has been restructured and various modifications were introduced. The experimental techniques used are described as well as the experimental uncertainties.

The experimental results for pressure drop and droplet size are then presented in Chapter 4. The experimental results obtained are accessible being validated. The Cruz (1997) model, which was already been used by other authors and proved to be efficient, has been tested against these set of data for large scale venturi scrubber

A description of the CFD numerical code Fluent used is presented on Chapter 5. The model uses the finite volume method to discretize the conservation equations describing the two-phase flow in the venturi scrubber, in a turbulent regime.

For a better understanding of the results, a flow characterisation of the venturi scrubber is made in Chapter 6 through the velocity profiles and pressure drop along venturi; in this way, experimental and numerical results obtained using a CFD code are compared and discussed.

A brief set of conclusions along with future recommendations are finally presented.

Chapter 2

Literature Review

This chapter discusses previous work carried out by other authors in venturi scrubbers which is categorised into the following topics: modelling and experimental work. The numerical models reviewed are related to pressure drop and collection efficiency of the venturi. The experimental data available on the literature was reviewed to analyse the dimension of experimental apparatus, the range of the operating conditions and the geometric configurations used on pressure drop, droplets sizes and collection efficiency.

2.1 Numerical Models

The flow in a venturi scrubber is very complex: a dispersed multiphase mixture of gas, droplets, and dust particles. The interactions between gas and liquid droplets, atomization of the liquid jet, droplet breakup and collision, and interactions between liquid droplets and dust particles can also occur (Pak and Chang, 2006). Due to these complex phenomena, experimental correlations and numerical models have been used, so far, to predict the performance of the venturi scrubber.

Various models to study the hydrodynamics in the venturi scrubber have been proposed in the literature, from simple correlations to more complex CFD models.

As the main purpose of scrubbers is the collection of the dust particles, the different mechanisms of collection have been identified and modelled, in particular when the collector is a liquid droplet. The collection of dust particles can occur by a number of processes: inertial impaction, interception, diffusion, electrostatic attraction and thermal gradients.

In a typical venturi scrubber, dust particles are mostly collected by liquid droplets and the collection is mainly made by inertial impaction, interception and diffusion, being the first one by far the most important.

Understanding the physics of the flow inside the venturi, defining the main variables involved and formulating independent models for predicting pressure drop and collection efficiency, are the basis of the theoretical models.

One of the early models for pressure drop across a venturi was published by Calvert in the beginnings of the 70's (Calvert, 1970). It was based on the assumptions that all the liquid was atomized into droplets, and that they were subsequently accelerated up to the gas velocity at the end of the throat.

It was also assumed that pressure drop across the venturi scrubber is due only to the momentum change of droplets in the throat and that there was no pressure loss due to the gas acceleration and friction between the wall and the gas core. This results in a single explicit equation:

$$\Delta p = \rho_D \frac{Q_D}{Q_G} U_{GT}^2 \tag{2.1}$$

where U_{GT} represents the throat gas velocity, ρ_D is the droplet density and Q_D/Q_G is the liquid to gas ratio.

Although simple and easy to use, the model of Calvert (1970) does not consider the effect of the geometry of the venturi at all, and assumes that the liquid was introduced with a zero initial velocity.

All the well know models for the collection efficiency assume that inertial impaction is the main process of collection, and that collection is made only by liquid droplet assumed to be uniformly distributed along the cross section of the venturi.

The collection efficiency due to the inertia η_i is refered as the target efficiency and it has been derived for a single drop (Calvert, 1970) as a function of the Stokes number, as:

$$\eta_i = \left(\frac{\mathrm{St}}{0.7 + \mathrm{St}} \right)^2 \tag{2.2}$$

The Stokes number is a dimensionless number, known as inertial parameter, given by:

$$\mathrm{St} = \frac{1}{9} \frac{d_p^2 |U_G - U_D| \rho_p}{d_D \mu_G} \tag{2.3}$$

The dust particles of a given diameter and density (d_p and ρ_p) are assumed uniformly distributed at each section of the venturi and moving with the gas velocity.

A differential equation to describe the collection efficiency was initially derived by Calvert (1970) based on mass balance for dust over a differential volume:

$$-\frac{dn_p}{dx} = \frac{3|U_G - U_D| n_p H_D}{2 d_D U_G} \eta_i \tag{2.4}$$

where H_D represents the volume fraction of the droplets and η_i is the target efficiency of a single droplet defined above (Equation 2.2).

A further differential equation is needed to describe the motion of the liquid droplets. Assuming that the droplets move in one direction only (along the venturi), their velocity perpendicular to the direction of the flow is neglected. The drag force is taken to be the only important external force responsible for the droplet motion and the droplet velocity is calculated using Equation (2.5):

$$\frac{dU_D}{dx} = \frac{3}{4} \frac{\rho_G}{\rho_D} C_D \frac{|U_G - U_D| (U_G - U_D)}{d_D U_D} \tag{2.5}$$

Boll (1973) derived a differential equation for the pressure drop, which could be integrated over the entire length of venturi. It accounts for gas acceleration, wall friction and acceleration of the droplets, yielding a single explicit equation:

$$-\frac{dp}{dx} = \rho_G U_G \frac{dU_G}{dx} + \rho_D \frac{Q_D}{Q_G} U_G \frac{dU_D}{dx} + \frac{\left(\frac{Q_D \rho_D}{Q_G \rho_G} + 1\right) \lambda_f \rho_G U_G^2}{2d} \tag{2.6}$$

Boll (1973) modified the Equation (2.4) considering further parameters such as the acceleration due to friction of a monodisperse droplets population, the wall friction and the gas acceleration. The author assumes that once atomised, each droplet accelerates and decelerates as a function of the friction forces. The collection efficiency results become more feasible as the model is applicable to all the venturi.

Boll pressure model has been further developed by other authors (Hollands and Goel, 1975). Also Taheri and Sheih (1975) presented a model for collection efficiency which includes a new parameter to account for the droplet concentration at each axial position. The drawback of the final model is its complexity, requiring further equations for the eddy diffusivities of gas and droplets.

Placek and Peters (1982) allowed for a distribution of droplet size. They considered a more realistic model, pointed out that when the liquid is sprayed it breaks into a distribution of droplets with different sizes.

$$-\frac{dp}{dx} = \frac{W_G}{A}\frac{dU_G}{dx} + \sum_{i=1}^{n} \frac{W_{D_i}}{A}\frac{dU_{D_i}}{dx} + \frac{W_D + W_G}{W_G} \lambda_f \frac{1}{2}\frac{\rho_G}{d} U_G^2 \tag{2.7}$$

A more thorough analysis was presented by Azzopardi and Govan (1984). Their model is based on the description of annular two-phase flow which is characterized by the presence of a liquid film on the channel walls while, the gas and the entrained droplets flow in the centre of the tube. The basis of their model is a description of the change in liquid film flow rate due to the entrainment of liquid from the film and the deposition of droplets onto the film.

Azzopardi and Govan (1984) allowed for the existence of different groups of droplets, each one created at a different position along the venturi, although characterized by a single initial velocity and a mean diameter. The pressure drop is then

calculated from the sum of the five components: friction with the walls, gas acceleration, droplets acceleration, film acceleration and gravity. The model considers two types of liquid introduction: spray and film, allowing for a variation of the fraction of the liquid initially entrained. In spray injection, all liquid is entrained with a droplet diameter calculated from the nozzle diameter. The annular flow model describes the change in liquid film flow rate due to entrainment of liquid from the film when the liquid is introduced as a film.

Azzopardi and Govan (1984) also developed a 1D model to predict the collection efficiency, which includes the liquid film introduction and the atomization and deposition of the droplets. The mass balance equation for each group of droplets is described by the Equation (2.8):

$$-\left(\frac{dn_p}{dx}\right)_i = \frac{6\eta_i n_p |U_G - U_D| W_{LE_i}}{\pi d^2 U_G d_{D_i} U_{D_i} \rho_L} \tag{2.8}$$

The contribution of each group of droplets at each axial position is added up to calculate the total number of particles removed. It is considered that the particles move at the gas velocity and at a dilute concentration that they have no influence on the total pressure drop.

Following an analogous procedure, Viswanathan *et al.* (1985) presented a model to predict the pressure drop, based on annular two-phase flow. In their model the initial film fraction was provided from experimental information. They assumed a constant core quality all over the venturi, although the examination of experimental film flow data suggest a change in the liquid mass flowing on the wall along the scrubber length.

The model of Azzopardi and Govan (1984) tends to over predict the pressure recovery in the diffuser section. Teixeira (1989) attributed this phenomenon to the adverse pressure gradient observed in the diffuser section resulting in a rapid growth of the boundary layer. This growth reduces the gas and the droplets deceleration, decreasing the pressure drop recovery. Another effect that may be observed is the boundary layer separation with an additional loss of pressure recovery.

In order to describe the behaviour of the boundary layer, Teixeira (1989) developed a boundary layer integral model coupled to the annular two phase flow. Following the integral approach, the partial equations are integrated axially as a set of ordinary differential equations. The basic equations for the boundary layer region are

obtained from the momentum and mass balances for two-phase flow in cylindrical coordinates.

Teixeira *et al.* (1994) adapted the 2D model of pressure drop, which consider the boundary layer growth on the divergent section, for particle collection. The model used is similar to that presented by Azzopardi and Govan (1984). They investigated the various model parameters that affect the total pressure drop and dust collection efficiency and the results compared very favourably with available experimental data.

Fathikalajahi *et al.* (1996) developed a tridimensional model for the droplets dispersion, to describe the nonuniform concentration of the droplets in the divergent section of the venturi. Later, Ananthanarayanan and Viswanathan (1998) developed a simplified 2D model to predict liquid flux distribution and collection efficiency in a venturi scrubber. However, both models considered that all the droplets have the same diameter, which does not correspond to the reality.

Cruz (1997) following previous work (Teixeira, 1989), extended the 2D model by incorporating other features of the annular flow regime in venturi scrubbers and studied their effect upon their performance as gas cleaning devices (dust collection and gas absorption, Cruz *et al.*, 1997). They made a description of a stochastic model to predict droplet coalescence which is based on a probability of collision. For the description of the dispersed phase, a new droplet population is created at each position along the venturi and it is handled as a distribution of 16 size classes, which are updated throughout the venturi length. From the model analysis, the relevance of coalescence model is assessed. Particularly at high liquid loading, the coalescence model allows for a better prediction of the droplet distribution along the venturi. This combination of the inviscid model for the convergence section and a 2D boundary layer model in the throat and diffuser sections, with an improved treatment of the liquid phase, appears to be a good compromise in terms of efficiency and computational time. All variables are calculated using mathematical relations and the model does not require any calibration.

In this model, the liquid film on the walls and the continuous atomization of the droplets are considered. The collection equation for each group of droplets is expressed by the Equation (2.8). The collection efficiency is calculated for each of the sixteen classes of droplet sizes, which are updated at each step. Collection efficiency could in that way be predicted as a function of the diameter of each class droplet, taking into account the coalescence effect on the capture of the dust particles. The results obtained had been very satisfactory (Cruz, 1997).

Gonçalves (2000) presents a very detailed review of these models and Gonçalves *et al.* (2001) carried out an extensive evaluation of the available models for the prediction of pressure drop in venturi scrubbers. These models were compared with experimental data from venturis of different sizes (throat diameter from 1.9 to 16 *cm*), liquid injection systems and operating conditions. Although some future modifications have been suggested, the model of Azzopardi *et al.* (1991) was the only one to give good predictions for the entire range of variables studied.

Gamisans et al. (2002) adapted the model of Azzopardi et al. (1991) to handle an industrial scale ejector venturi. The model was formulated for a different type of liquid injection and so, it was necessary to change the correlation for the calculations of the Sauter mean diameter of droplets created and the calculation of the initial liquid fraction flowing as a film. Using this model, Gamisans et al. (2004) predicted the split of liquid between dropletss and film in the same ejector type venturi. The predictions, for the convergence and throat section, are fairly good but, for the divergent section, bigger discrepancies were found when compared with the experimental data. The authors suggested that further improvements may be achieved by using a two-dimensional model besides allowing the use of drop size distributions instead of mean diameters.

In order to widen the applicability and improve its accuracy the boundary layer formulation of the model of Azzopardi *et al.* (1991) was extended to the entire length of the venturi, known as the Full Boundary Layer Model (Sun and Azzopardi, 2003). The paper presented a test of this model and other published models when used to predict data from a high pressure system. The study has been confined to cylindrical, Pearce-Anthony type venturis and the model gave very good predictions for high-pressure conditions when compared with experimental results of Yung *et al.* (1984).

Also Van Werven *et al.* (2003) present an extension of the model Azzopardi *et al*. (1991) for modelling two-phase flow metering. Annular/dispersed flow on a film injection venturi type (wetted approach type) is considered. It is assumed that a liquid film at the wall is present in all the venturi sections (convergent, throat and divergent sections). The predictions are compared with experimental data obtained at high pressure with hydrocarbon fluids and showed a good agreement.

Rahimi *et al.* (2005) developed a realistic model to analyse the effects of heat and mass transfer on the venturi scrubber performance, considering that the venturi could operate under non-isothermal conditions. In their work, they included effects of droplet size distribution and liquid film on the walls. They concluded that for non

isothermal flow in a venturi scrubber, the overall collection efficiency decreases due to the cooling effects of evaporation in the throat section and in conditions when the gas relative humidity is high, the target efficiency of droplets decreases due to their growth by vapour condensation.

Because phenomenological methods have limits on the performance prediction when the venturi geometry or the operation condition changes, attempts have been made to implement other computational models in venturi scrubbers.

Different numerical methods are also used. Recently, Nasseh *et al*. (2007) have used artificial neural networks (ANNs), for estimating the pressure drop in venturi scrubbers. Three separate neural networks are designed. The experimental data are extracted from five different venturi scrubbers available in the literature: a rectangular venturi scrubber of the Pease-Anthony type, a circular and an adjustable prismatic venturi scrubber with wetted wall irrigation and two ejector venturi scrubbers with different throat diameter. The main parameters affecting the pressure drop namely the gas velocity in the throat of venturi scrubber, liquid to gas flow rate ratio, and axial distance of the venturi scrubber were analysed. Comparing the results of these ANNs and those calculated from available models shows that the results of ANNs are in a better agreement with experimental data.

With the recent achievements in the development of numerical solutions for the Navier-Stokes equations and the improvements of computing power and efficiency, the application of CFD has increased and proved a viable alternative in industry and science. In general, CFD is a powerful numerical tool that is becoming widely used to simulate many industrial processes (Norton and Sun, 2006).

The numerical simulations of multiphase flows, mostly gas-solid and gas-liquid flows, are the scope of various research works (Chen and Pereira, 2000; Huang *et al*., 2003; Kuan *et al*., 2007; Guilkey *et al*., 2007; Wasewar and Sarathi, 2008; Maliska *et al*., 2008). These include applications such as spray drying involving the motion of discrete droplets in a continuous gas stream similar to that in venturi scrubbers. However, applications describing CFD codes using droplet spray data, in venturi scrubbers, are limited.

Ananthanarayanan and Viswanathan (1999) studied the effect of nozzle arrangement on flux distribution inside a rectangular, pilot-scale, Pease-Anthony type venturi scrubber using the commercial CFD package Fluent. An Eulerian (continuous-phase)-Lagrangian (discrete-phase) approach is employed by this model. Liquid is injected through a series of nozzles perpendicular to the gas stream at the throat inlet.

The CFD model uses a simplified droplet atomization, considering that the droplets are inert particles. The simulation of annular, discrete, two-phase flow is validated with experimental data and the authors concluded that the proposed model could be used to study, design and improve large-scale industrial units. However, they suggest some improvements: the predictions of the model could be improved by providing more accurate information on the spatial mass and velocity of the drops as they atomize; the effect of drop size distribution could be studied for the same scrubber by incorporating distributions similar to Rosin-Rammler (RR) for the drop size spectrum; the effect of heat and mass transfer on the liquid distribution, like evaporation, could be studied by choosing appropriate models that are available in Fluent.

A mathematical model based on particle dispersion model, k-ε model of turbulence, and PSI-CELL model was developed to predict the particulate removal efficiency and pressure drop in an orifice scrubber (Mohebbi *et al*., 2003). Good agreement between experimental data and simulation show that the Eulerian/Lagrangian method can be a powerful model for predicting collection efficiency and pressure drop in orifice scrubber.

A dispersed three-phase flow of the Venturi scrubber was analysed numerically using the Eulerian-Lagrangian method (Pak and Chang, 2006). The gas was assumed to be a continuum while liquid droplets and dust particles were treated as discrete entities. Atomization of the liquid jet, interaction between gas and liquid droplets, dust capture of liquid droplets, droplet breakup and collision, and droplet deformation by aerodynamic force were all taken into account. The model was compared with data from a circular venturi with liquid sprayed into the throat. Some discrepancies were pointed out by the authors in the prediction of the total pressure drop up to the throat.

2.2 Experimental Work

The experimental validation of more complex models is always important but experimental data, in large-scale venturi scrubbers, are scarce in the literature. The review of experimental work is divided into three main parts: pressure drop, droplet size and collection efficiency.

2.2.1 Pressure drop

Table 2.1 summarizes the most relevant works reported in the literature on pressure drop in venturi scrubbers. The geometric characteristics of the venturis and the experimental operation conditions tested are high lighted.

Table 2.1 – Main geometric characteristics and experimental operation conditions

Source	Geometry	Injection System	Throat area (cm^2)	Throat length (cm)	U_{GT} (m/s)	L/G (l/m^3)
Yung *et al.* (1984)	Cylindrical	Spray	47.66	12.1,42.5	41.1-65.3	1.1-3
Allen and Van Santen (1996)	Cylindrical	Film	201.06	20.6	45-115	0.2-1.1
Viswanathan (1998)	Rectangular	Spray	203	26.7	45.7-76.2	0.4-1.9
Gonçalves *et al.* (1999a)	Cylindrical	Film/spray	2.84	1.5,6.4	50-90	0.5-2
Gonçalves *et al.* (1999b)	Rectangular	Spray	8.40	6.3,9,14	58.3,74.6	0.08-0.3
Gamisans *et al.* (2002)	Cylindrical	Ejector	50,150,300	5,10,20	8-24	2.9-23.5

Allen and Van Santen (1996) used a pilot plant to provide measurements of pressure drop for a wide range of operating conditions for both dry and wet flows. In their work, two venturi scrubber designs were tested: an industrial prismatic unit with an adjustable aspect ratio (5:1 down to 2:1), and a cylindrical long throat design with a length ratio of 1.3:1. The range of liquid to gas ratio tested was 0.2 – 1.2 (l/m^3) and gas velocity was varied between 79 *m/s* and 110 *m/s* for the cylindrical venturi and between 47 and 114 *m/s* for that of prismatic geometry.

Viswanathan (1998) have studied the liquid film characteristics in the venturi scrubber by measuring the liquid film flow on the wall, film thickness and the pressure drop in a rectangular pilot plant venturi. The scrubbing liquid was introduced through 17 orifices at the throat section. The experiments were carried out with liquid to gas ratios varying from 0.4 to 1.9 l/m^3, gas throat velocities between 45.7 and 76.2 *m/s* and injection orifices diameters of 2.108, 2.565, 3.175 and 3.860 *mm*.

Gonçalves *et al.* (1999a) reported experiments in a small scale venturi varying the length of the throat and the liquid injection arrangements. One venturi had a 15 *mm* long throat while in the second the throat was 64 *mm* long. In both cases liquid could be injected as a film or as jets. In the first option the liquid was introduced 30 *mm* upstream the convergence; in the jets injection, five holes of 1 *mm* diameter located 1 *mm* downstream throat inlet were used. The gas velocity was set at 50, 70 and 90 *m/s*. The liquid to gas ratio of 0.5, 1, 1.5 and 2 l/m^3 were employed. Data from a small scale rectangular geometry (Gonçalves *et al.*, 1999b) were also reported.

An industrial plant was built (Gamisans *et al.*, 2002) and the performance of an ejector type venturi scrubber has been studied experimentally. The effect of throat diameter and length was investigated as well as pressure atomizers with different cone angles. The apparatus consists basically of a venturi connected to a holding vessel, which also acts as a phase separator.

Later, Gamisans *et al.* (2004a, 2004b) have studied liquid distribution and the self-entrainment by a liquid jet, respectively, in the same ejector-venturi. In their experiments, the gas velocity was varied between 8 and 24 *m/s* and liquid flow rate was set at 2.5, 5 and 7.3 m^3/h.

2.2.2 Droplet size

Most of the work carried out on droplet size in venturi scrubbers report the data as a mean diameter. Different droplet size distributions have also been used to characterize the distribution of droplet sizes. Experimental data is important to validate these models and correlations and over the years, several researchers published droplet measurements in venturi scrubbers. Table 2.2 summarises the most relevant and their experimental conditions.

Table 2.2 - Published sources of droplet size in venturi scrubbers

Source	Convergence angle (^{o})	Diffuser angle (^{o})	Throat section/ diameter (*m*)	Liquid injection	Method of measurement
Yoshida *et al.* (1965)	25	3,5,9	0.016	Spray	-
Parker and Cheong (1973)	80	10	0.025	Film	MgO slide
Boll *et al.* (1974)	25	7	0.305x0.035	Spray	Light obscuration
Atkinson and Strauss (1978)	41	9.7	0.016x0.04	Spray	Photography
Bayvel (1982)	n/a	n/a	0.06	Spray	Laser diffraction
Roberts and Hill (1981)	25.5	7	0.076x0.15	Spray	Photography
Azzopardi and Govan (1984)	34	10	0.01	Film	Laser diffraction
Leith *et al.* (1985)	20	9.6	0.054	Spray	Photography
Teixeira *et al.* (1988)	68	19.4	0.019	Film	Laser diffraction
Alonso *et al.* (2001)	36	10	0.019	Spray/Film	Laser diffraction
Gamisans *et al.* (2002)	n/a	n/a	0.150;0.100	Ejector	Photography
Costa *et al.* (2004)	n/a	n/a	0.035x0.024	Spray	Laser diffraction
Viswanathan *et al.* (2005)	30	5,7,9	0.076x0.267	Spray	PDA

Although most of the work has been reviewed elsewhere (Alonso *et al.*, 2001), it may be summarised that very few published works have reported experiments in large scale test facilities. Most of the work has been carried out in venturis whose diameter is

on the order of 10^{-2} *m*. It is also worth referring that the experimental techniques for droplet sizing, used in some works, are either prone to statistical uncertainties, due to the limited size of the samples, or intrusive. Nonetheless the use of electro optical methods (Phase Doppler Analyser - PDA, laser diffraction) is currently of wide application. Another point that should be raised, concerns the method for liquid injection. Typically the liquid can be atomised directly into the venturi as a spray or can be introduced as a film upstream of the converging section. In this, droplets are atomised from the liquid film. Given that venturis are compact devices, the initial stages of droplet formation are of the utmost relevance and should have an important contribution to the collection efficiency and the total pressure drop.

Azzopardi (1993) reviewed the available published information and validated the predictions of a comprehensive model (Azzopardi *et al*., 1991) which incorporates most of the major physical effects. The model is then used to assess the influence of the most relevant parameters (geometry, flow rates, liquid injection method) on the split of liquid between film and droplets. This is a key aspect of the scrubber performance because the liquid in film is not available for dust collection. The calculations suggest that although in smaller units only a small part of the liquid travels as droplet if the liquid in injected as a film, most of the liquid travels as droplets from the start of the throat in large scale venturis. Thus, laboratory tests should be carried out in venturis with throat diameters as large as possible.

Alonso *et al.* (2001) reported new data taken in a cylindrical laboratory-scale venturi, using the Fraunhofer diffraction technique for size measurements. Two methods for the liquid injection were used. When liquid was injected as a film measurements were taken at the end of the diffuser. However, if the liquid was introduced as jets through orifices at the throat wall, measurements were carried out at three axial positions: two located in the throat and one at the end of the diffuser. Gas velocity and liquid to gas ratio varied from 50 to 90 *m/s* and 0.5 to 2.0 l/m^3, respectively.

As mentioned above, Gamisans *et al.* (2002) studied experimentally the performance of ejector venturi scrubbers presenting also data on droplet sizes. The high speed photography was used to describe the mean diameters. The tests were carried out with the gas delivery system disconnected due to the fact that the measurements of droplets are only function of the liquid pressure reaching the swirling chamber of the atomizer and its geometry. The method consists of freezing the droplets by adjusting the exposure time of the camera and the illumination supplied.

Costa *et al.* (2004) using the same technique as Alonso *et al*. (2001) measured the droplet size in a rectangular laboratory-scale venturi with a cross section 35 *mm* high and 24 *mm* wide. Water was injected through a single orifice with a 1 *mm* diameter located on the top wall of the throat, 15 *mm* downstream the throat inlet. Droplet size distribution was measured as a function of gas velocity (varying between 58.3 and 74.9 *m/s*), liquid to liquid to gas ratio (0.07 through 0.27 l/m^3) and the distance from the liquid injection point (64 to 173 *mm*). It was found that all these variables affect droplet size.

In the same venturi, Gonçalves *et al.* (2004) tested a different technique to examine the droplet dispersion. An isokinetically probe with a 2.7 *mm* internal diameter was used to remove liquid from several positions inside the venturi. The length of the throat effect was studied, so the concentration was measured at 29.5, 83.5 and 137.5 *mm* downstream from the liquid injection location.

Viswanathan *et al.* (2005) made a detailed characterization of droplet size, velocity and mass flux using PDA in the same venturi previously used (Viswanathan, 1998) varying the divergence angle (Table 2.2). The liquid was introduced at the throat section through 34 orifices, half of them on each side, perpendicularly to the gas stream. The measurements were carried out at three gas velocities (45, 60 and 75 *m/s*) and five liquid to gas ratio (0.4, 0.9, 1.2, 1.5 and 1.8 l/m^3).

2.2.3 Collection efficiency

A number of models to predict venturi scrubber efficiency can be found in the literature. Those models are useful to optimize and design new venturi scrubbers as well as predicting the effects of the different operating parameters.

The effective validation of such models has been limited because few data have been made available in the literature. Some of the experimental data available in the literature are presented in this section, describing the size and type of venturi used and the technique employed to measure the collection efficiency.

Rudnick *et al*. (1986) presented experimental data on the performance of three different venturis, over a wide range of operating conditions. All the venturis had a circular cross section with 127 *mm* inlet and outlet diameters, varying the length of the three sections as well as the diameter of the throat from 32 to 76 *mm*. The scrubbers were operated with four types of liquid injection. Velocity was varied between 21 and

160 *m/s*, and the liquid to gas ratio from 0.00019 to 0.0043. Isokinetic samples of aerosol were taken through probes of 7.5 *mm* aligned with the axis of the duct. Aerosol (Wesson oil) particles are counted and sized in 23 intervals covering a diameter range of 0.3 to 2.8 μm with a scattering optical aerosol spectrometer.

Allen (1996) carried out experiments in a large scale venturi scrubber to determine his grade efficiency curves using the contacting power law. The experiments were taken on the 2 m^3/s pilot plant described in Allen and van Santen (1996). Two geometries were tested: an industrial prismatic unit with adjustable aspect ratio and a classical long throat. In both units liquid was injected as a film (wetted wall irrigation). To measure the grade efficiency, the author used a dispersing pre-sized dust at a controlled rate into the inlet duct and measuring the fraction which penetrated the scrubber by extracting sampling in the outlet duct using an Andersen MkIII in stack cascade impactor. Two different particle sizes were used: 5 and 15 μm. The conditions investigated were: throat velocity (67 to 103 *m/s*), liquid to gas ratio (0.36 to 1.15 l/m^3) and the overall pressure drop (270 to 840 *mm* of water head). The curves are only dependent of the pressure drop across scrubber. No independent effect of the other parameters evaluated was observed.

Tsai *et al*. (2005) present a venturi scrubber system making use of heterogeneous nucleation and condensation growth of particles. This venturi was tested to remove submicron particles in the exhaust gas. The waste SiH_4 and dilution air are injected into a reaction chamber containing an electrical heater operating at 850ºC. Residual SiH_4 gas is abated because of high-temperature oxidation, in which a large number of SiO_2 particles are generated.

The experimental tests were made with 1 % of SiH_4 and a flow rate of 0.5 *l/min* and 1 *l/min*. The diameter of the throat is 1 *cm* and its length is 3 *cm*. The liquid to gas ratio was set between 1.17 and 1.8 l/m^3 and the liquid is injected tangentially at the entry of the venturi throat. A Scanning Mobility Particle Sizer system was used to measure the particle removal efficiency of the venturi scrubber. The sampling tube of the system was placed at the inlet and the outlet of the venturi for size distribution measurement of fine particles ranging from 50-480 *nm* in diameter. The removal efficiency of a certain particle size was calculated from the difference between the outlet and inlet number concentration divided by the inlet number concentration of the corresponding particle size. For SiO_2 particles larger than 0.1 μm, the removal efficiency is greater than 80-90%.

The performance of a laboratory scale rectangular venturi scrubber in the removal of fine mineral particles was tested experimentally by Costa *et al*. (2005). The experimental rig is horizontally mounted and the liquid is injected in the throat through a single orifice of 1 *mm*. The dust particles used are mineral rock, insoluble in water with a mean diameter of 5.8 μm and a density of 3030 kg/m^3. The variables analysed were the throat length (63, 90 and 117 *mm*), the gas velocity (58.3, 66.6 and 74.9 *m/s*) and the liquid flow rate (0.286, 0.586, 0.886 *l/min*). The aerosol isokinetic sampling system consisted of a probe, a Milipore filter, a vacuum pump and a flow meter. Two sampling points are located upstream the scrubber and downstream the cyclone. The sample was weighted and analysed for size distribution with the Malvern Mastersize particle sizer. The authors concluded that the collection efficiency increases with the throat gas velocity, present a minimum for particles of 0.3 μm, showing two collection mechanisms: inertial impaction, responsible for the collection of larger particles; and a diffusion mechanism acting primarily on the smaller particles.

Ribeiro *et al*. (2005) studied the effect of the operating parameters such as the liquid flow rate, throat length and number of liquid injection orifices in the collection efficiency of a small scale rectangular venturi scrubber very similar to the one presented above (Costa *et al.*, 2005). The dust particles used are phosphate rock with density of 2900 kg/m^3 and a mass flow rate of 3.16 *g/min*. The number of orifices on the throat walls varies from 1 to 5 orifices, each of 1 *mm* in diameter. Liquid flow rates tested varied from 300 to 900 cm^3/min and the throat length from 6.5 to 18.5 *cm* while the throat gas velocity was kept constant at 69.3 *m/s*. The authors concluded that the measured collection efficiency varied from 50 to 91% and show trend to increase with both liquid flow rate and throat length. Regarding the number of orifices the best results were obtained for a single orifice.

2.3 Conclusions

From the available literature, it may be concluded that although a systematic evaluation of the properties of venturi scrubbers has been addressed, experimental data in large scale venturi scrubbers is scarce. Droplet size data, when available, is limited, either because the measuring technique is open to question or because the influence of the liquid injection is not taken into account

In the present work, a large scale cylindrical venturi was built for measuring the most relevant operating parameters for industrial applications and to provide a reliable experimental data base that can be used for model validation. The experimental setup is a large facility which provides data close to the industrial scale, namely the use of higher air flow rates. It is worth remembering that the high air velocities obtained, especially at the throat section of the venturi, are accountable for the high pressure drop.

Two different methods of liquid injection are addressed and liquid flow rates have been extended into a range of low liquid loading where different mechanisms for droplet formation are expected to compete. The data may be of use to validate the applicability of models in the design of industrial applications.

A 3D numerical simulation of the two-phase flow on venturi scrubber using CFD code, Fluent, was used in this research work. The use of complete and robust commercial software is an important aspect; therefore it allows the test of different scenarios as well as the project optimization of a gas cleaning system.

Chapter 3

Experimental Arrangement

This chapter details the experimental setup and techniques. This accuracy is evaluated and an uncertainty analysis of the experimental results is carried out.

3.1 Experimental Setup

The experimental apparatus used in the present work was initially designed by Lobarinhas (2003) in his master degree project at the University of Minho. The limitations of physical space in the laboratory were the main argument in deciding for the horizontal flow configuration. Other works published in the literature also report the horizontal configuration for small scale venturis. In this setup, the main components of the rig are: a centrifugal ventilator, the venturi scrubber components and plenum chamber. For more details see Lobarinhas (2003).

In the initial design, the liquid was introduced as a smooth film through a porous section of the wall. In order to assess the influence of the liquid injection system, four standard atomizers were distributed along the perimeter of the experimental facility. In this way, the test facility enables the liquid introduction either as a film or as a spray and in this latter configuration the liquid is introduced upstream of the converging section. Such an arrangement is different from almost every work presented in the literature, where spray injection occurs at the throat section, even for small venturi

scrubbers. With this option, the droplets are under gas acceleration for longer periods with evident benefits in particle collection.

In addition, the test facility combines a long throat. This option can be used to evaluate the effect of a long throat upon the pressure drop, since it is in this section that most of the collection phenomena occur, as well as the break up and coalescence of the droplets. Most of the existing test facilities report shorter throat sections with a length to diameter ratio between 0.017 and 2.25 (ejector venturi). In the present design, that ratio is 2.45.

The apparatus was built with all the probes, tappings and windows necessary to measure the most relevant parameters in the scrubber operation.

The venturi dimensions are close to those used in typical industrial applications for such equipments. During the design and development of the present facility, several configurations were evaluated for the convergent and divergent sections together with various diameter ratios. In the end, the configuration built is such that it can be applicable to a typical industrial plant, making the industrial relevance of this project more appropriate.

The lengths of each section l_0, l_1 and l_2, the corresponding converging and diverging angles, α_0 and α_1, and the relevant diameters are schematically shown in Figure 3.1. The details are given in Table 3.1.

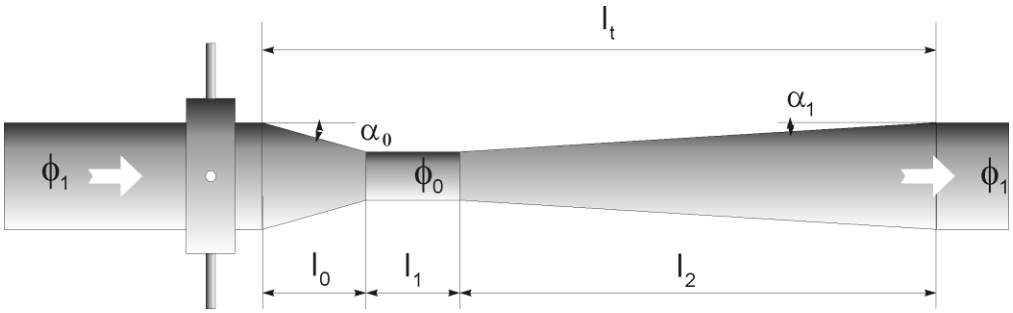

Figure 3.1 – Geometric variables of the venturi geometry.

Table 3.1 – Geometric details.

Dimensions of Venturi (*mm*)	
Inlet diameter	250
Throat diameter	122.5
Convergence length (l_0)	230
Throat length (l_1)	300
Divergence length (l_2)	740
Convergence angle (α_0)	17º
Divergence angle (α_1)	5º

The layout of the test facility is shown schematically in Figure 3.2.

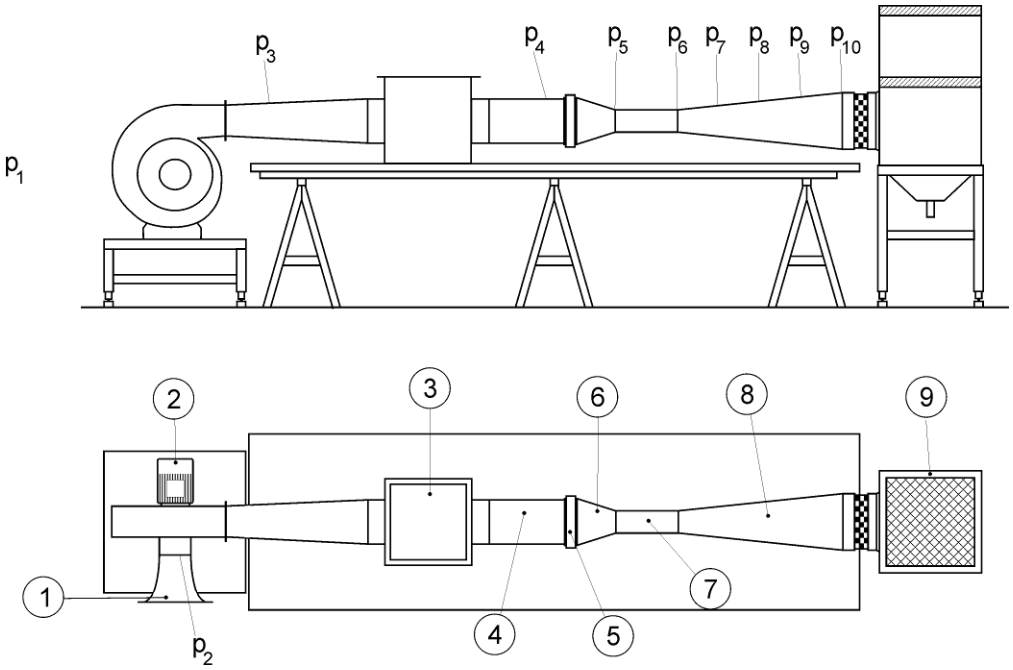

1. Bell mouth
2 Centrifugal ventilator
3. Solid particles introduction
4. Horizontal pipe
5. Liquid injection
6. Convergent section
7. Throat section
8. Divergent section
9. Plenum chamber

Figure 3.2 – Schematic representation of the experimental rig.

Air is blown by a centrifugal ventilator (2) into a horizontal pipe (4) made of galvanized steel, 250 *mm* in diameter. The flow is directed into the venturi scrubber (6-8) (throat diameter 122.5 *mm* with a length/diameter ratio of 2.45:1) where the water is injected just upstream (5). Downstream of the venturi a plenum chamber (9) filled with mesh screens is used to separate the water droplets flow the gas stream. The flow is subsequently discharged into the atmosphere.

Upstream of the venturi (3), if necessary, the dust particles may be introduced into the air stream at a controllable rate. The air flow rate is determined by measuring the static pressure at a bell mouth entrance (1) into the ventilator inlet (P_2). The flow is regulated by changing the current frequency powering the ventilator variable speed motor.

Water (metered by a bank of rotameters) is injected upstream of the convergence section either as a film through a porous wall or by a set of spray nozzles. Due to construction constrainments, the nozzles are located further upstream of the porous wall. Four equal nozzles with a 1.5 *mm* orifice diameter are equally distributed around the venturi perimeter, 220 *mm* upstream of the converging section. Pressure tappings are located along the venturi (P_4-P_{10}) and three sets of glass windows enable optical access into the flow.

For measuring the pressure drop in the venturi (tappings 3 through 10), a differential "U" manometer was used.

Droplets were measured along the throat and diffuser sections at x = 0.23, 0.53 and 1.27 *m* downstream of the venturi inlet. The positions are indentified by A, B and C respectively (Figure 3.3) and they are referred as such throughout the text.

The insert in Figure 3.3 depicts the experimental configuration of the optical windows. These consist of a set of two opposite apertures, sealed by optical windows of polished glass, 50 *mm* in diameter. In addition a small ring in the tube aperture prevents any remaining film going into the optical path of the laser beam. Compressed air is blown on the inner face to prevent droplets wetting the windows. The flow of compressed air is kept at a minimum necessary to avoid any droplet being diffused into the optical windows. Tests were carried out by varying the amount of air fed into the windows and the influence upon the droplet size was negligible. This is expected because: a) the droplet sizing technique does not depend upon the droplet velocity and; b) the additional flow of air does not change the breakup conditions in the vicinity of the apertures. Figure 3.4 shows the full view of the test facility.

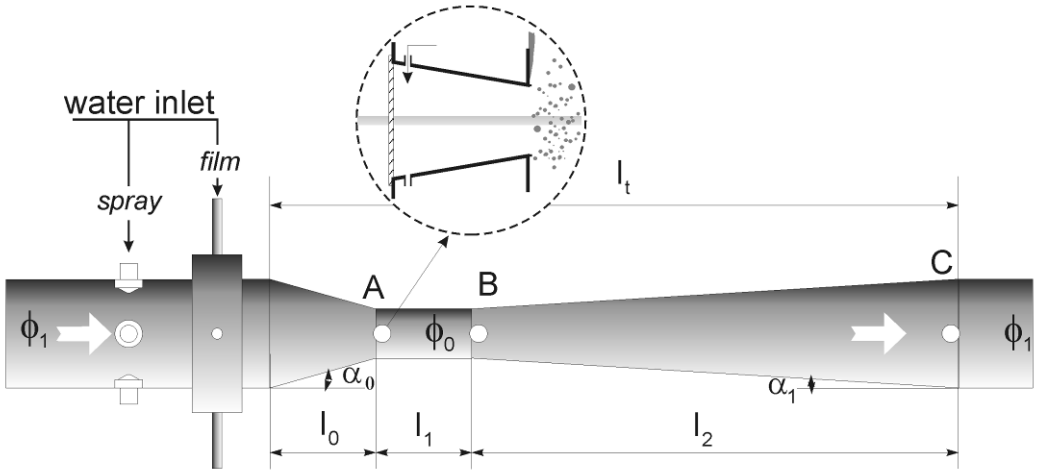

Figure 3.3 – Schematic representation of venturi scrubber injections and droplet measurement points.

Figure 3.4 – Overall view of the test facility.

3.2 Experimental Techniques

To measure the experimental data along venturi, various techniques were used. Taking into account the main objective concerning this project, special consideration is dedicated the measurements of pressure drop and droplet size. This section describes the experimental techniques to measure the pressure drop and droplet sizes, in addition to the gas flow rate.

Furthermore, some developments were made in order to obtain collection efficiency data in the venturi used in the present experimental work. Details are described on Appendix A.

3.2.1 Gas flow rate

The gas flow rate is determined by measuring the static pressure upstream of the ventilator. The Bernoulli equation could be used for steady state, inviscid, adiabatic and incompressible flow:

$$p_1 + \frac{1}{2}\rho_f U_1^2 + \rho_f g Z_1 = p_2 + \frac{1}{2}\rho_f U_2^2 + \rho_f g Z_2 = Cte \qquad (3.1)$$

where p is the static pressure, $\frac{1}{2}\rho_f U^2$ is the dynamic pressure and $\rho_f gZ$ is the pressure due to the gravity. In horizontal flows the gravity term could be neglected and assuming $U_1 = 0$ the Bernoulli equation could be simplified:

$$p_2 + \frac{1}{2}\rho_f U_2^2 = p_1 = p_{atm} \qquad (3.2)$$

Therefore the flow velocity U_2 can now be determined with only a single measurement.

Rearranging Equation (3.2), the flow velocity is easily expressed as:

$$U_2 = C_d \sqrt{\frac{2.(p_{atm} - p_2)}{\rho_f}} \tag{3.3}$$

$(p_{atm} - p_1)$ represents the static pressure drop obtained for each flow rate, ρ_f is the density of the fluid.

In order to validate the assumptions leading to Equation (3.3), a bell mouth was made of fibre glass, as schematically depicted in Figure 3.5. U_1 is assumed zero and the smooth entrance (an ellipse shape) guarantees that the boundary layer is limited to a very small thickness. Therefore the flow may be considered as inviscid and the velocity U_2 is uniform across the section.

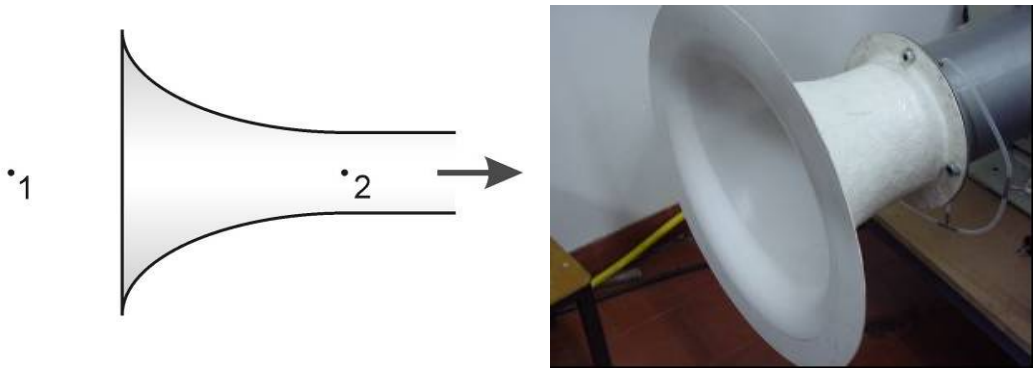

Figure 3.5 – Scheme and view of the bell mouth entrance to the ventilator.

This pressure is measured by a digital micro manometer (Figure 3.6), calibrated with a Betz type manometer.

Figure 3.6 – Digital manometer.

In Equation (3.3) the discharge coefficient C_d takes into account the deviations from the inviscid flow. It was calculated by integrating the velocity profiles measured by a two component LDA system. The calculated flow rate is then compared with that resulting from Equation (3.3) and the discharge coefficient is determined. A value of 0.98 was found within the range of flow rates tested and used throughout this work.

3.2.2 Pressure drop in the venturi

Pressure drop is a function of the losses due to the friction with the walls, gas, droplets and film acceleration, the gas-liquid interaction and droplet collisions.

Seven pressure tappings are located along the venturi in order to measure the static pressure data in different positions along venturi. Figure 3.7 presents a view of the various measuring points along the venturi. There were measuring points at the entrance of the venturi, at the beginning and end of throat section and at four points along the divergent section (see Figure 3.2).

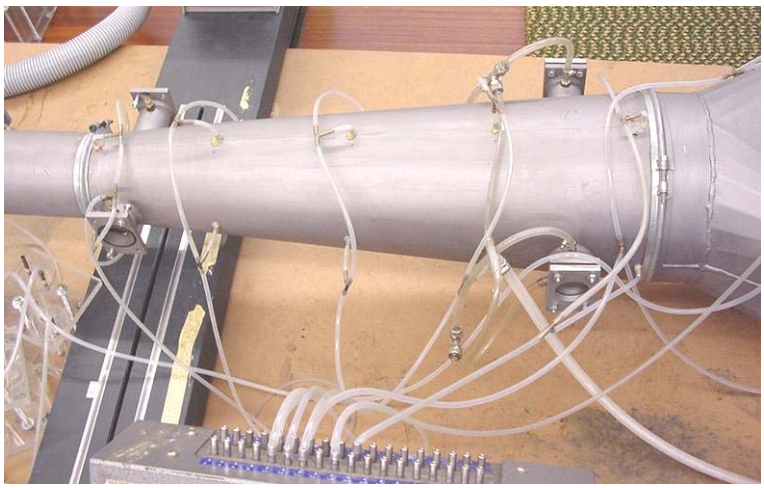

Figure 3.7 – Pressure tappings along the venturi.

At each location, 4 pressure tappings are distributed along the perimeter of the tube and the pressure averaged to provide the local gauge pressure. This was measured with a differential "U" manometer. This manometer is constituted by various manometric tubes that enable the simultaneous measurement of the static pressure in different points along the experimental rig (Figure 3.7). The gauge pressure is determined through the simple equation:

$$\Delta p = \rho_m g \Delta h \tag{3.4}$$

where ρ_m is the manometric fluid density. In order to improve the accuracy and sensitivity of the instrumentation, the manometer is tilted as depicted in Figure 3.8.

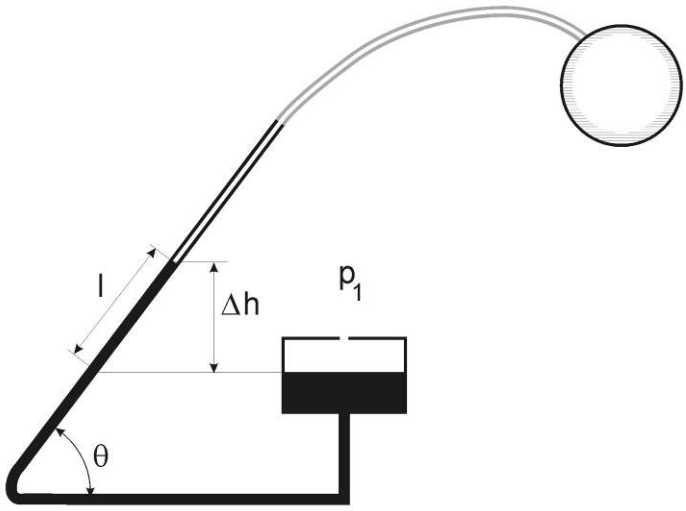

Figure 3.8 – The inclined differential manometer.

The scale reading relates with the pressure head through:

$$\Delta h = l\, sen\theta \tag{3.5}$$

By increasing θ, the sensitivity of the manometer is improved which is important for low pressure differences. However, instabilities may be observed preventing an accurate reading. A value of $\theta = 30^{\circ}$ was used in the present work.

The manometer used is a multi tube type designed by TEM (Figure 3.9). Each one of the pressure tappings was connected to one of the tubes of a multi tube manometer to record each pressure individually. The manometric fluid used is the alcohol. Before any experimental run, the reservoir (Figure 3.8) is adjusted along a vertical axis. In this way the level of the manometric fluid is made coincident with the zero in the scale.

A common reservoir, open to the atmosphere, is connected to all the manometers.

Ethyl alcohol is used in order to improve the accuracy of the readings. The alcohol is dyed for better reading. Its density was measured by weighting 100 *ml* in a precision scale and a value of 900 kg/m^3 was found. This value is higher than the standard reference (790 kg/m^3) due to the colouring.

Figure 3.9 – Inclined multi manometer TEM.

In order to avoid water from the test facility entering into the manometers, separators (with a purge at the bottom) were introduced between the pressure tappings and the manometers. They were built in plexiglass, as shown in Figure 3.10. All the lines are tightly secure.

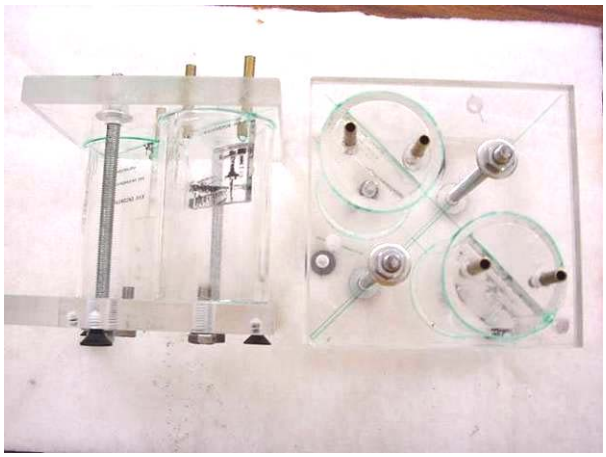

Figure 3.10 – Settling chambers for separating the water from the gas.

3.2.3 Laser diffraction technique

The technique employed for the droplet size measurements is based upon the Fraunhofer diffraction (Swithenbank, 1976). When a laser beam strikes droplets/particles, the angular variation of light scattered in the forward direction depends upon the particle size. Since the spray is dilute, some of the incident light is diffracted while the remaining is undiffracted. A lens forward of the sample collects all the light. That undiffracted is focused in a central spot and that diffracted is projected as a pattern of concentric rings in the lens focal plane. Large particles scatter at small angles and small particles scatter at a larger angle. The location of each ring is directly related to the volume fraction of a specific size in the spray. By using an array of photodetectors at the lens focal plane, the droplet size distribution can be measured.

There are many advantages using the laser light scattering principle: it is non intrusive; no calibration is required; it is simple, robust and highly versatile, providing highly repeatable measurements: it is fast, usually requiring approximately 3 minutes to complete a measurement; it is accurate, giving high resolution size discrimination; gives a large dynamic range (1:100); the sizing range can be easily adjustable; (Malvern Instruments, User Manual, 1991).

The Malvern 2600

The Malvern 2600 particle sizer, marketed by Malvern Instruments, has been applyed in this project (Figure 3.11). This instrument has been used for both in spray analysis (Swithenbank *et al*., 1976; Chigier, 1983) and annular flow (Azzopardi, 1984; Teixeira, 1988; Alonso *et al*, 2001) and it is based on the principle of laser light scattering.

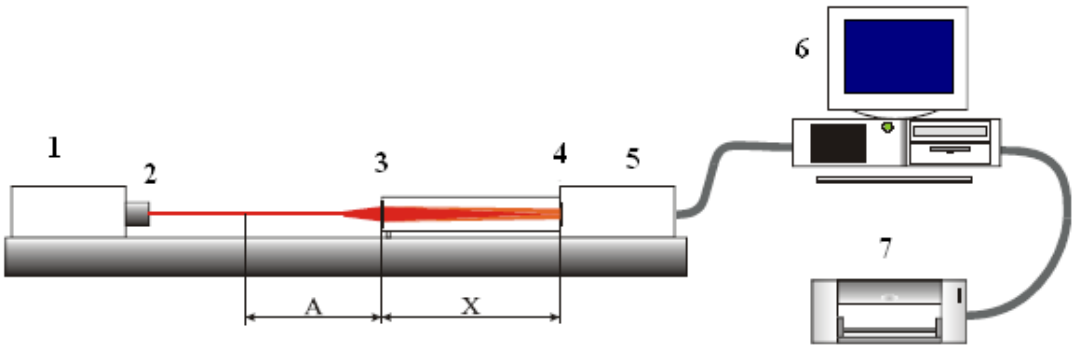

1. He-Ne laser
2 Beam expander lens
3. Receiver lens
4. Detector (rings)
5. A/D converter
6. Computer
7. Printer
A. Lens cut-off distance
X. distance to the detector

Figure 3.11 – Layout of the Malvern 2600.

The Malvern 2600 has six different receiver lenses, which, for a specific pattern of detectors and light wavelength (623 *nm)* from a HeNe Laser, give different particle size ranges (Malvern Instruments, User Manual, 1991), as presented in Figure 3.12.

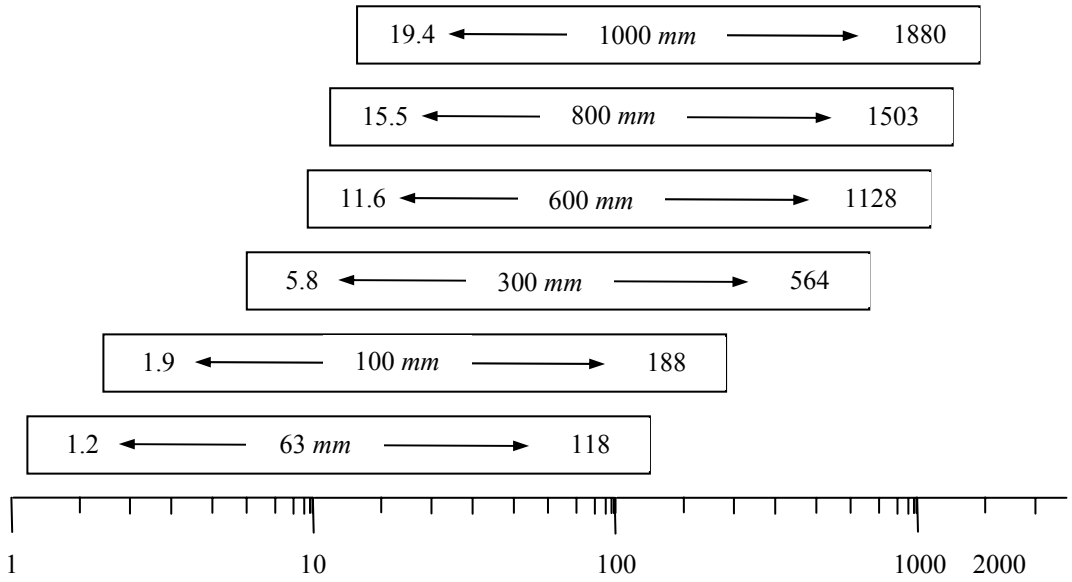

Figure 3.12 – Available lens and corresponding particle size range (μm). (*Malvern Instruments,user manual, 1991*).

The most adequate lens is selected by the resulting data fitting. The lens is such that the particle size distribution should be within the dynamic range expected for that lens.

Usually, a large number of particles are simultaneously present in the analyser beam, being the scattered light focused on the detector the sum of all individual patterns overlaid on the central axis. In this way, the system integrates the scattered light from all particles. It is very important to ensure that the particle concentration is in the range of acceptability for an accurate measurement (diffracted light below 50 % of the total incident light).

There is a time averaged observation of the scattered light as the dispersed material is continuously fed through the analyser beam.

When the particle field to be measured is located too far from the collection lens, the light scattered at large angles by the small particles is lost due to the limited lens aperture or window, causing the measured size distribution to be shifted towards large particles. This is called the *vignetting* or lens cut-off effect (Malvern Instruments, User Manual, 1991). Therefore, it is important that, for any measurement, all particles are illuminated by the beam within the lens cut-off distance (distance A in Figure 3.11), which depends on the lens used, being smaller for the smaller size ranges. The maximum value of this distance for each lens is summarized at the Table 3.2.

Table 3.2 – Maximum distance between lens and sample (*Malvern Instruments, user manual, 1991*).

Lens diameter *(mm)*	**Distance A *(mm)***
63	55
100	133
300	400
600	780
800	1050
1000	1300

In the present experiments, an 800 *mm* focal length lens provided a measurement of droplet size in the range of 15.5-1503 μm, which was found to be the most appropriate for the current work. This configuration proved adequate because for each experiment, the entire droplet distribution was confined within the lower and upper limits of the sizing range. In addition, the cut off distance is large enough to prevent the

vignetting effect. The results also proved to be reproducible by repeating each test at least three times over a period of time.

Despite the many advantages of the laser diffraction technique, it is limited to ensemble measurements of average size of spherical particles. Furthermore, no velocity information is provided. In addition, the theory is invalid for very small particles (bellow approximately 1 μm), where very large diffraction angles are expected and diffraction patterns also depend on the optical properties of the particles. More recent developments in the technique combine Fraunhofer and Mie scattering theory in order to expand the measuring range into the submicron size. On the other hand, if particles are too large, the reflection and the absorption of light can be significant (Bayvel and Jones, 1981). However, these effects are not relevant for droplets of the size range found in the present work.

In order to relate the droplet distribution with the measured light dissipation, the Malvern assumes a probability distribution function (*pdf*) for the droplet size. In this process, the function is iteratively adjusted in order to minimize the error between the measured light and that calculated for a given distribution. The instrument provides the user with 4 functions, 3 of them being defined by two parameters (Normal, Log-Normal and RR) and a fourth is a 15 parameter polynomial fitting (Model Independent, MI). Amongst the two parameters options only the RR was used. In fact, the RR distribution represents a good compromise in terms of efficiency and in easy of use (Mugele and Evans, 1951) and the overall performance is comparable to that shown by the upper limit log normal distribution (Teixeira, 1988). The distribution is usually presented by the cumulative weight of droplets:

$$RR = 1 - e^{-\left(d_D / \overline{X}\right)^n} \tag{3.6}$$

where *RR* represents the mass fraction in the particles with a diameter equal or smaller than d_D; $\overline{X}$ and n is the distribution parameters. $\overline{X}$ represents the diameter below which droplets carry 63,2% of the total mass and can be related to the Sauter mean diameter (d_{32}) by means of the gamma function. The parameter n provides a measure of the spread of the distribution.

Comparing to the RR function, the MI fitting can detect multiple peaks in the droplet distribution which may be of interest in complex atomization conditions.

During the course of the experimental work, great care was observed in the following aspects:

1. To obtain both a parallel beam and the detector perfectly aligned with the laser source;

2. Each time the glass windows were cleaned, their orientation relative to the beam was adjusted;

3. The ambient light was reduced to a minimum to avoid noise signals which may be particularly significant in the outer rings;

4. In order to ensure that all the diffracted light (for the present configuration of the detector, lens diameter and focal length) was collected by the lens, the maximum distance between the lens and the sample (A) was not greater than the cut off distance for the present length (focal length of 800 *mm*).

3.3 Experimental Uncertainties

No physical quantity could be measured exactly. All the measurements are subject to some uncertainty due to both limitations of the instrumentation and a wide range of errors and inaccuracies due to the operator. Measurements should be made with great care to reduce the possibility of error as much as possible.

The calculation of the uncertainty associated with a measurement provides a confidence level for the experimental data. So estimation of experimental uncertainties is an important part of an experimental project.

Experimental uncertainties can be classified as systematic or random. Systematic are those which apply to a particular experimental system and are caused by defects in the experiment or in the way which it is carried out. This type of error is difficult to detect and could only be “controlled” by repeating the experiment using a different apparatus or changing the experimental procedure by using different methods.

Random uncertainties are more frequent and can produce different results for successive measurements of a given quantity. To minimize this kind of uncertainties,

the measurements should be made with great attention to the experimental procedure and reading all the instruments as accurately as possible. The rigorous way to estimate random uncertainties in a quantity is to repeat the measurements a larger number of times and examine to the spread in the data obtained using rigorous statistical methods.

It could be said that there are three main sources of experimental uncertainties, such as: limited accuracy of the measuring equipment, limitations and simplifications of the experimental procedure and uncontrolled changes to the environmental (for examples small changes of the temperature).

Every instrument has an inherent uncertainty that is determined by the precision of the instrument. In this section the uncertainties related with the equipment used are studied.

3.3.1 Manometers

The air flow rate is determined by measuring the static pressure at a bell mouth entrance at the ventilator inlet. This variable is measured by a digital micro manometer, whose calibration was verified by a Betz type manometer.

To have confidence in the results, the accuracy of the manometers used needs to be checked. Three manometers were tested: one with water, the multi tube (alcohol) and the digital manometer.

Manometer with water

For the water manometer (Figure 3.13), the Bernoulli's equation yields for the gauge pressure:

$$p_2 = \rho_{water} g \Delta h + p_1 \tag{3.7}$$

being $\rho_{water} = 998\,kg/m^3$, $g = 9.81\,m/s^2$, $\Delta h = z_1 - z_2$ and $p_1 = p_0 = 0\,Pa$.

Δh is measured and the level of water on a scale is read with a resolution of 1 *mm*. Liquid curvature due to the surface tension, makes the exact location of the free surface

hard to distinguish. A resolution bellow 1 *mm* cannot be expected in the reading of Δh, which means that the resolution in the pressure, R_p is:

$$R_p = \rho_{water} g R_{\Delta h} = (998)(9.81)(0.001) \approx 10\,Pa \tag{3.8}$$

Then two values of height have to be taken, z_1 and z_2, which means an uncertainty E_p of:

$$E_p = 2\,R_p \approx 20\,Pa \tag{3.9}$$

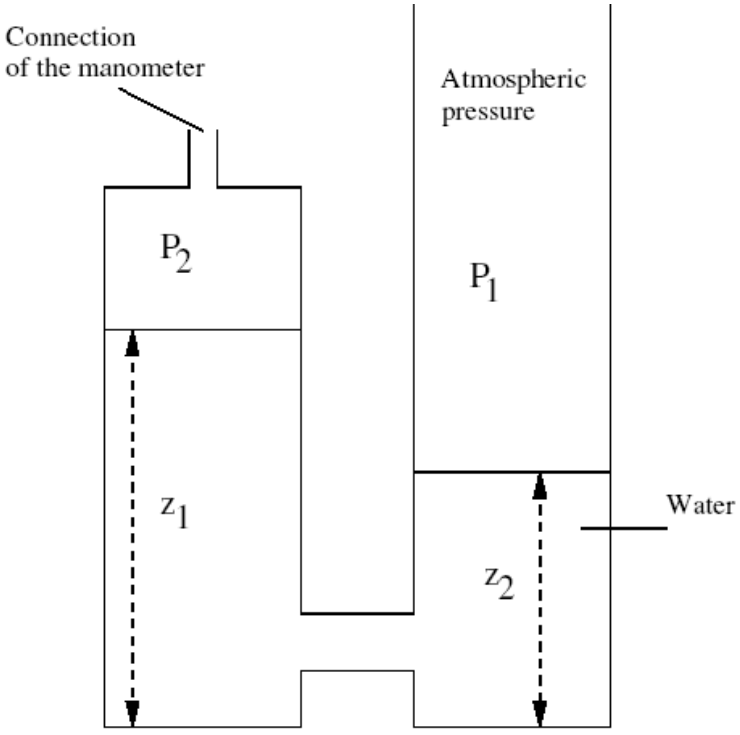

Figure 3.13 – Geometry of manometer with water.

The ventilator speed was controlled by an electronic circuit that varies the current frequency. The different tests were carried out by changing the frequency settings of the supply current. The four air flow rates correspond to frequencies of 20, 30, 35 and 40*Hz* respectively.

The results for the water manometer are presented in the Table 3.3. The height is given in *mm* and the pressure refers to the gauge pressure.

Table 3.3 – Manometer with water.

Air flow rate (*kg/s*)	z_1 (*mm*)	z_2 (*mm*)	**Pressure** *(Pa)*
0.483	8	10	176
0.736	18	20	372
0.861	26	27	518
0.987	33	33	646

Multi tube Manometer

For calculating the pressure with the multi tube (Figure 3.14), the density of the alcohol should be analysed. Usually this density is 790 kg/m^3 and by testing the alcohol from the bottle the same value was found. Nevertheless, when the alcohol from the manometer was measured, a density of about 900 kg/m^3 was found. It is important to note that the alcohol does not have the same density in the whole system, the alcohol from the measuring tubes tends to be heavier because it is contaminated sometimes by water. Evaporation also plays a role in its density.

Considering the alcohol density equal to 900 kg/m^3 and knowing that the scale for measuring the level has a resolution of 2 *mm*, the uncertainty of this manometer will be:

$$R_p = \rho_{alcohol} g(z_R - z_m) = (900)(9.81)(0.002) \approx 17\,Pa \tag{3.10}$$

The results are presented in the Table 3.4.

Table 3.4 – Manometer multi tube.

Air flow rate *(kg/s)*	z_m (*mm*)	**Pressure** *(Pa)*
0.483	18	159
0.736	41	362
0.861	56	494
0.987	72	636

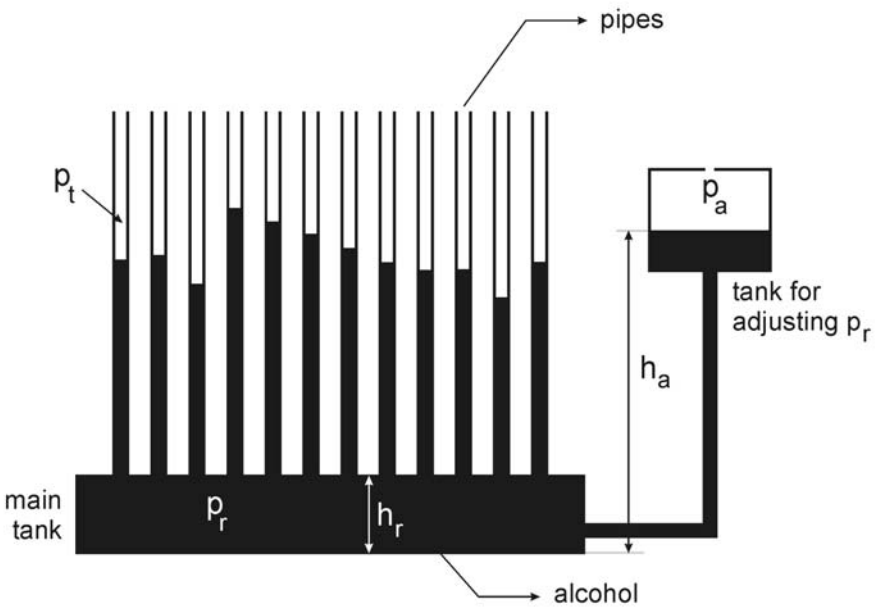

Figure 3.14 – Geometry of the multi tube.

Digital Manometer

The digital manometer can have a resolution of 1 *Pa* but was calibrated for a range of pressure of 7000 *Pa*. The data sheet from the manufacturer displays a full scale error of 0.05%, so there is accuracy in the result of:

$$E_P = \frac{(0.05)(7000)}{100} = 3.5\,Pa \tag{3.11}$$

The results are presented in Table 3.5 for the digital manometer. In conclusion the digital manometer appears to be correctly calibrated as well as the multi tube manometer.

Table 3.5 – Digital manometer.

Air flow rate ***(kg/s)***	**Pressure** ***(Pa)***
0.483	150
0.736	364
0.861	500
0.987	645

3.3.2 Rotameters

For the measurement of the liquid flow rates, a bank of two rotameters, A and B, was used as observed in Figure 3.15.

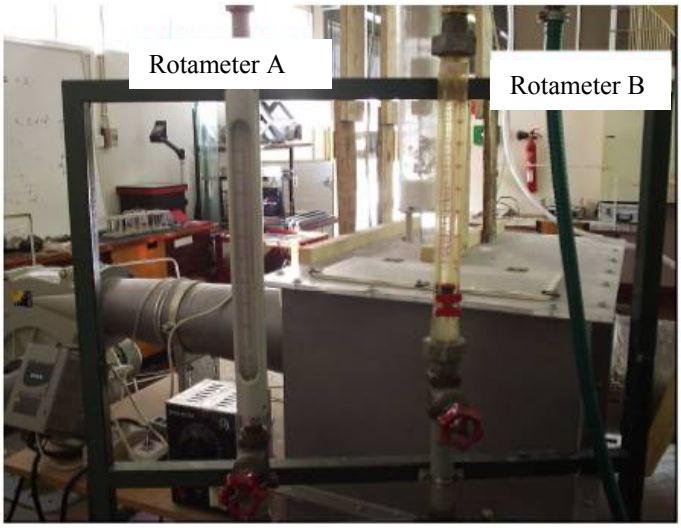

Figure 3.15 – Rotameters used for liquid measurements.

Although the rotameters are calibrated by the manufacturers their accuracy was tested. For this purpose, once the flow rate was stabilized at a certain level, the exact flow rate was directly measured by measuring the water volume in a vessel and stop watch.

For the rotameter A, the data obtained is presented in Table 3.6.

Table 3.6 – Calibration tests for rotameter A.

Reading ***(% FS)***	**Time** ***(s)***	**Volume** ***(l)***	**Flow Rate** ***(l/min)***
0	126	0.5	0.234
20	81	1.0	0.738
40	43	1.0	1.392
50	35	1.0	1.71
59	29	1.0	2.07
80	21	1.0	2.85
100	17	1.0	3.53

And the calibration curve can be determined and is shown in Figure 3.16.

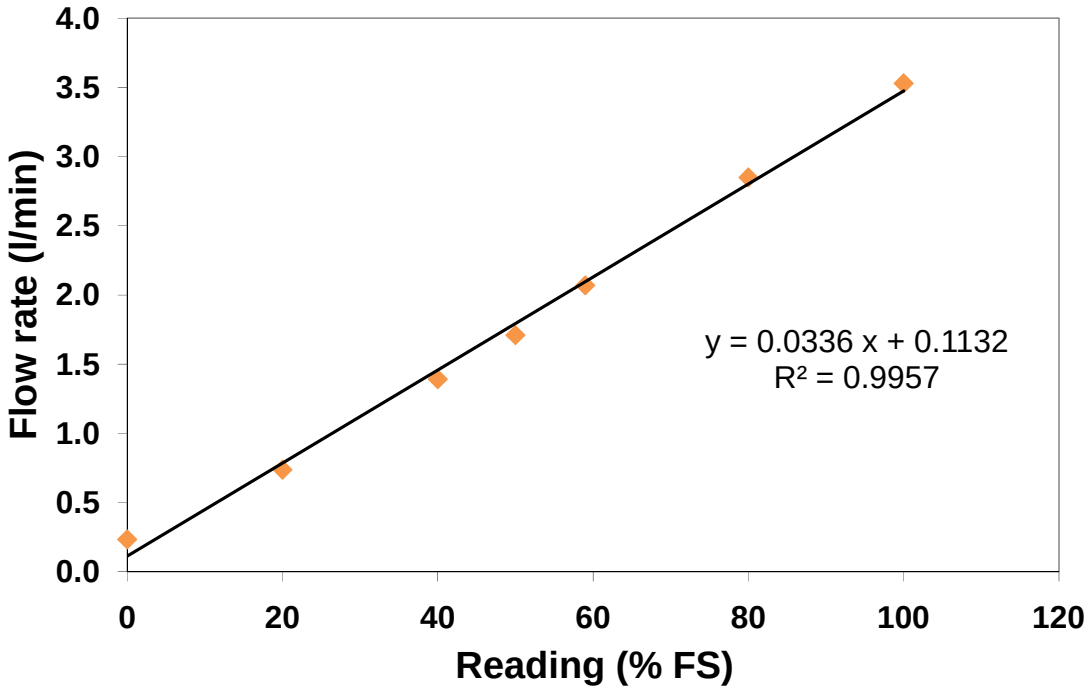

Figure 3.16 – Calibration curve of liquid flow rate for rotameter A.

The same procedure was applied for the rotameter B. The data is shown in Table 3.7 and the calibration curve is plotted in Figure 3.17.

Table 3.7 – Calibration tests for rotameter B.

Reading ***(l/h)***	**Time** ***(s)***	**Volume** ***(l)***	**Flow Rate** ***(l/min)***
20	55	0.5	0.545
40	65	1	0.923
60	47	1	1.276
80	36	1	1.667
100	30	1	2.0
120	25	1	2.4
140	22	1	2.727
160	20	1	3.0

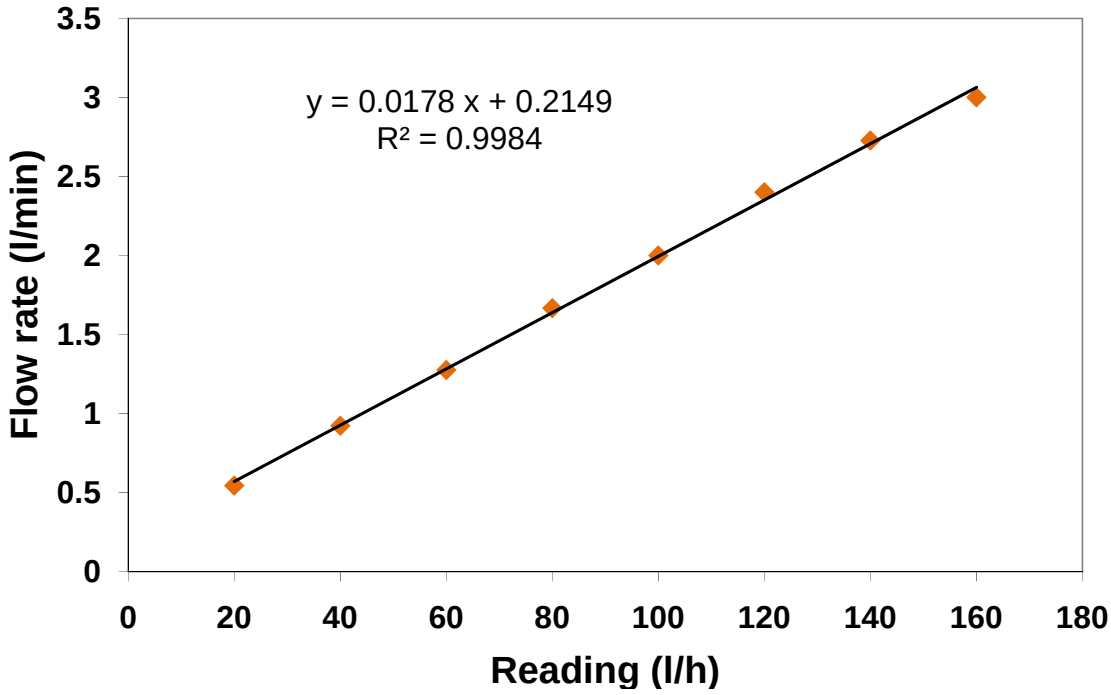

Figure 3.17 – Calibration curve of liquid flow rate for rotameter B.

In all the cases, the fitting follows a linear relationship with a high correlation coefficient.

The calibration for rotameter B shows that the expected flow rate is approximately 20% below the measured value. This may be due to the fact that this rotameter has been in use in the laboratory for a few years in various test rigs. Therefore some wear is expected. Nonetheless once this calibration is carried out the flow rate is accurately monitored.

3.3.3 Malvern 2600

The accuracy of the instrument has been extensively tested by direct comparison with a calibrated sample and discussed by Teixeira (1988), amongst others. It was concluded that it is efficient, giving results that differ within 3%, from a standard calibrated sample. The experimental tests were made in different days at various periods of the day and the results proved to be reproducible.

Chapter 4

Experimental Results and Discussion

In this chapter, the experimental pressure drop and droplet sizes are presented, as well as the test conditions.

The effect of the operating conditions such as gas velocity, liquid flow rates, liquid to gas ratio and droplet sizes on the pressure drop is investigated. The experimental pressure drop is tested against Cruz *et al.* (1997) model.

Droplet size distributions and droplet size data are reported and these data are tested against the most known droplet size correlations.

The most important trends in the experimental data are pointed out and the main conclusions are given.

4.1 Test conditions

In the present work, the gas flow rate is varied from 0.483 *kg/s* up to 0.987 *kg/s* and the water flow rate was within the range 0.013 *kg/s* to 0.075 *kg/s*. Table 4.1 shows the various flow rate combinations tested.

The current work extends the pressure data into lower liquid flow rates than previously available in the literature.

Table 4.1 – Volumetric flow rates and liquid to gas ratios tested.

Water (*l/h*)	**Air (m^3/h)**	**Volumetric L/G Ratio (l/m^3)**
Film and Spray Injection		
48	1445	0.033
48	2202	0.022
48	2575	0.019
48	2950	0.016
69	1445	0.048
69	2202	0.031
69	2575	0.027
69	2950	0.023
138	1445	0.096
138	2202	0.063
138	2575	0.054
138	2950	0.047
Film Injection		
270	1445	0.187
270	2202	0.123
270	2575	0.105
270	2950	0.092
Spray Injection		
210	1445	0.145
210	2202	0.095
210	2575	0.082
210	2950	0.071

4.2 Pressure drop

4.2.1 Experimental Data

Figure 4.1 shows the single phase gas flow gauge pressure along the experimental facility, for different flow rates. The inlet and outlet sections are at atmospheric pressure. The pressure drop that occurs in the bell mouth entrance (P_1-P_2) can be used to calculate the gas flow rate. Upstream of the venturi, the pressure recovery (P_3-P_4) is due to a small increase in the pipe diameter up to the nominal size of 250 *mm*, although this is below 0.8%.

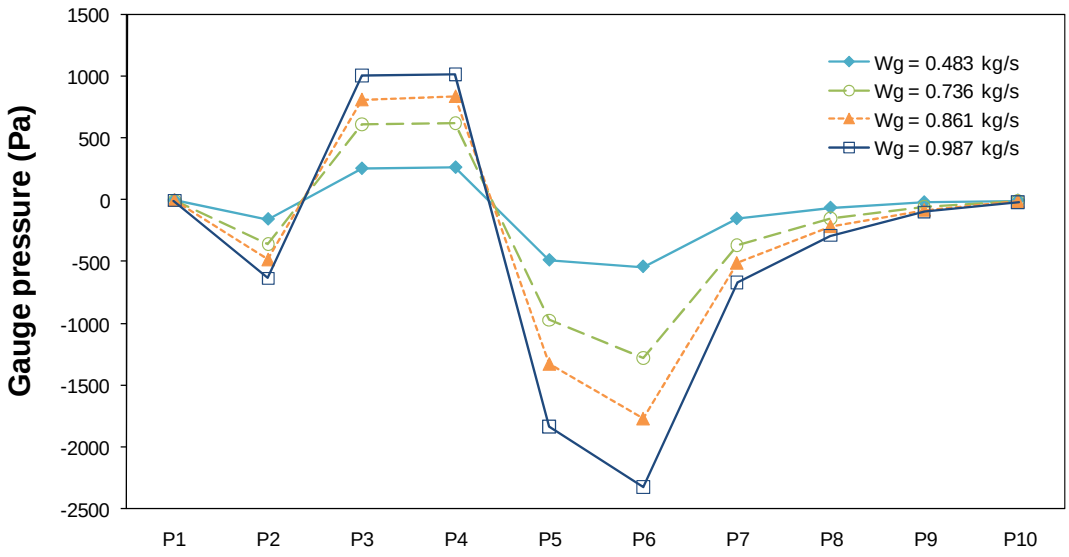

Figure 4.1 – Gauge pressure along the installation as a function of the air flow rate.

In the converging section of the venturi the pressure drop observed is mostly due to gas acceleration. In the throat, only the gas friction contributes to the pressure drop. Most of this pressure loss is recovered in the diverging section which can be as high as 70 %. The unaccounted energy is lost by friction.

The data show the expected characteristics of venturi geometry (Allen and Van Santen, 1996): the local pressure drop at each point is essentially proportional to the

square of the local gas velocity. Taking the throat as a reference, the factor is 0.6 $Pa/(m/s)^2$.

Figure 4.2 shows the pressure drop along the venturi, for various gas flow rates normalized by the pressure at the convergence inlet. The data refer to the lowest liquid flow rate tested here. Both forms of liquid injection (spray and film) are compared.

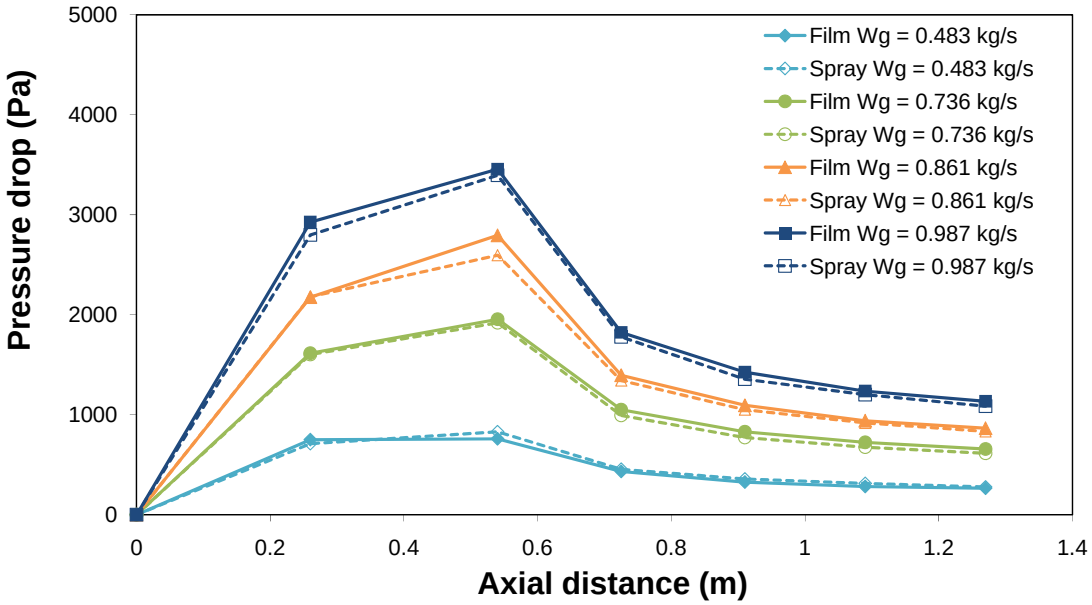

Figure 4.2 – Effect of gas flow rate upon the pressure along venturi, for different liquid injection systems. $W_L = 0.013\ kg/s$.

Small differences in the pressure drops are observed between the two liquid injection systems. Regarding the spray type injection, because the liquid nozzles are located upstream of the porous wall used for the film injection, droplets are at higher velocity at the first pressure tapping (P_4). Therefore, downstream of this position, they will not accelerate as much as those generated by a liquid film entrance and the total pressure drop will be lower than that with a film injection.

However, for the low liquid flow rate (Figure 4.2) the pressure drop profiles are not very dependent on the liquid injection used. The effect of the liquid injection method is more evident for higher liquid flow rates (Figure 4.3) because a larger number of droplets are accelerated. Therefore, the combination of the high gas and/or liquid flow rates favours differences between the two methods.

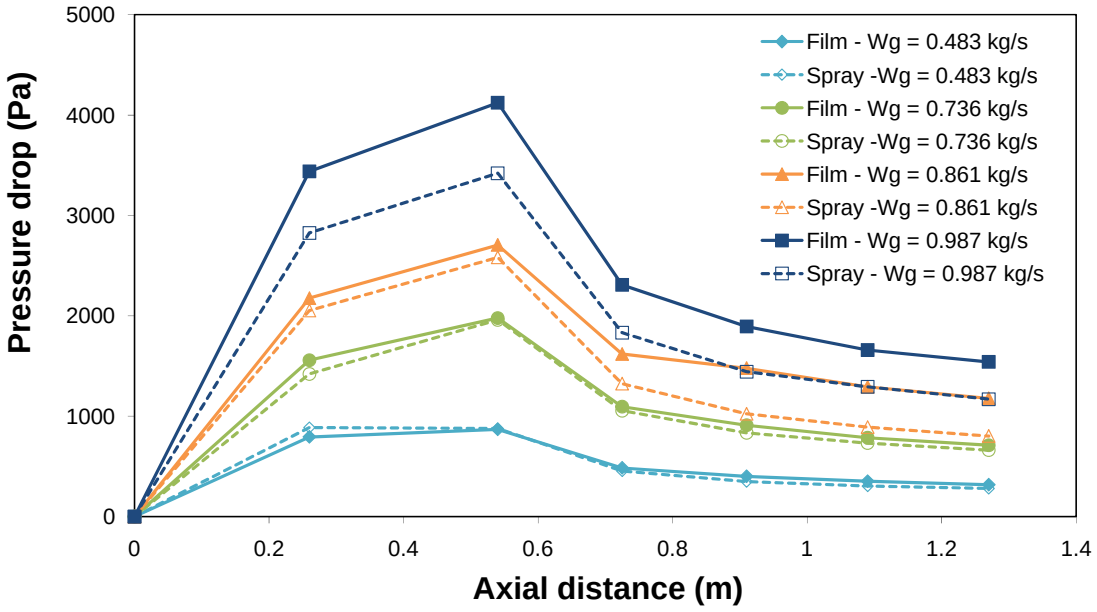

Figure 4.3 – Effect of gas flow rate upon the pressure drop along venturi for different liquid injection systems. $W_L = 0.038$ *kg/s*.

Figure 4.4 shows the influence of the gas throat velocity upon the total pressure drop inside the venturi. The data also show the effect of liquid loading, when compared with a single phase gas flow.

As expected, the pressure drop increases with the gas velocity, but the expected square relation between the two quantities is not apparent for low liquid flow rates. Allen and Van Santen (1996) reported that the total pressure drop in the venturi scrubber is more sensitive to variations in gas velocity than to those in liquid flow rate and that sensitivity increases with the throat length. The present data also shows similar behaviour.

For low gas flow rates, the effect of liquid flow is very small, but as the gas velocity increases the momentum exchange between phases increases and the liquid influence becomes more evident.

The differences between the injection methods may be due to the fact that for spray injection, a higher percentage of liquid is transported as droplets for a longer period of time. Due to their contribution to the total pressure drop, this may account for the difference between the two conditions. However, some influence may also be due to

the position of the liquid injection on the pressure drop because droplet acceleration in the early stages (upstream of P_4) is not taken into account in the pressure drop.

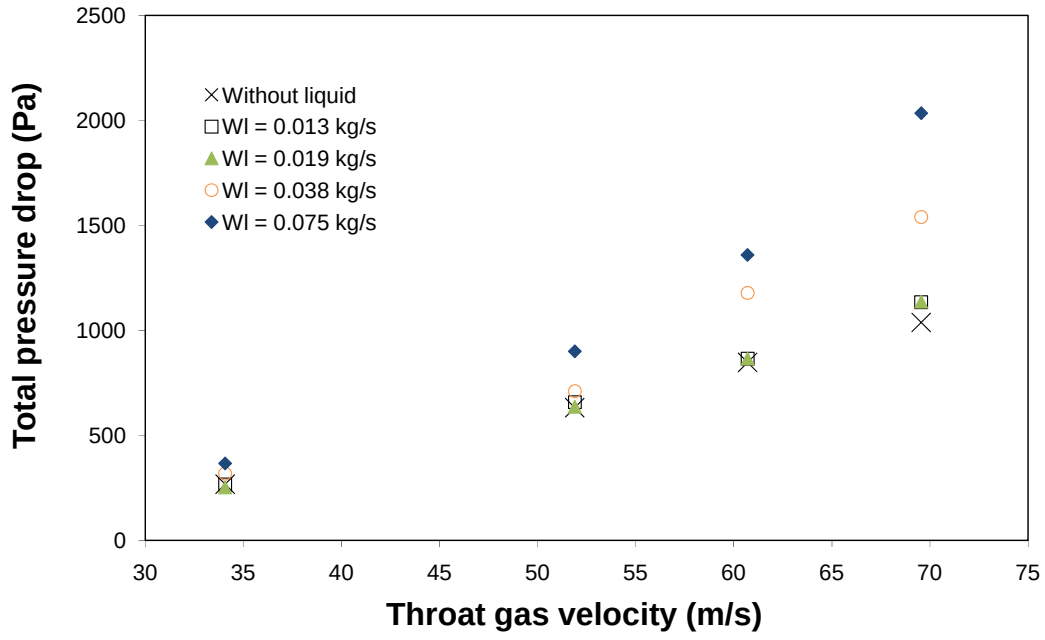

Figure 4.4 – Variation the total pressure drop in the venturi with gas velocity and liquid loading. Liquid injected as a film.

Figure 4.5 shows the influence of the liquid to gas ratio upon the total pressure drop for various gas throat velocities. Liquid is injected as a film. The data show that the pressure drop increases with increasing liquid to gasratio.

The influence of liquid to gasratio is greater with increasing the gas throat velocity due to a higher level of energy transfer from the gas to the liquid phase. This is a consequence of the long throat design, which results in a longer residence time and hence a higher droplet velocity in the exit of the throat. Because the liquid is injected as a low velocity film, the liquid acceleration by the gas along the venturi is an important fraction of the total pressure drop. Increasing the liquid flow rate, this component of the pressure drop, increases.

For higher gas flow rates, the influence of the liquid loading is stronger as shown in Figure 4.5.

This behaviour is not constant thought the data range and a minimum is observed for each gas flow rate. Allen and Van Santen (1996) did not report such

observation although they operate at higher liquid loadings, which are clearly beyond the occurrence of such minimum.

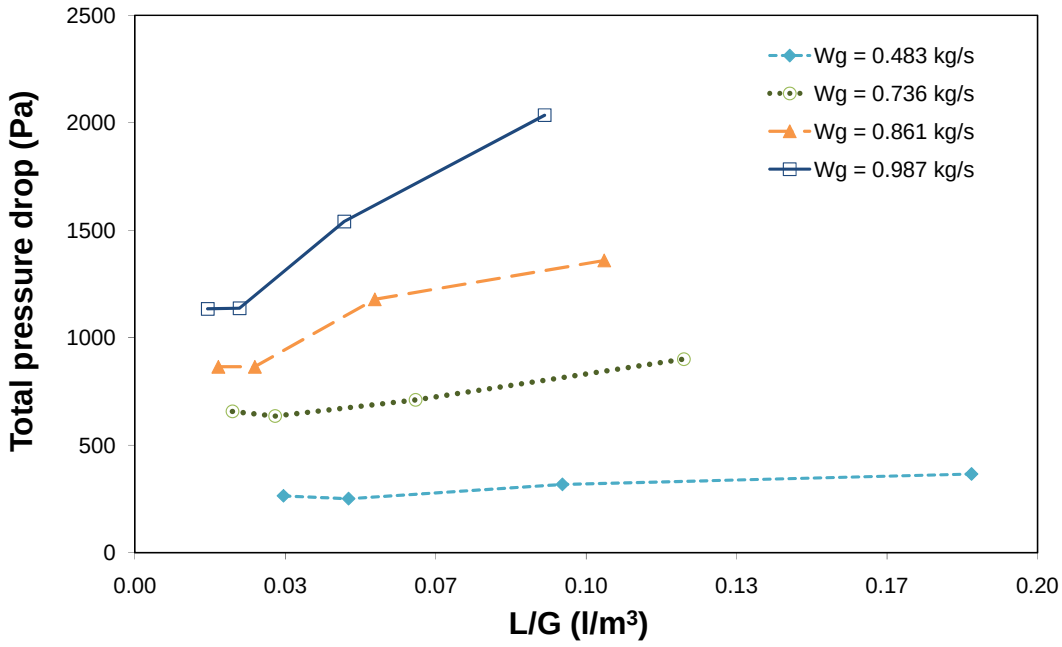

Figure 4.5 – Variation of the total pressure drop in the venturi with liquid to gas ratio and gas throat velocity. Liquid is injected as a film.

Teixeira (1988) observed that, in a two phase annular flow in a circular tube, there is an influence of the liquid flow rate on the droplet size, taking the gas velocity as constant. However this effect is not monotonic across the liquid flow rate range and a minimum in the mean droplet size is observed for each gas flow rate. Such minimum does not occur at a constant liquid flow rate but, in general, the higher the gas velocity the lower the liquid flow rate at which the minimum occurs. This observation was linked to the competing mechanisms in droplet formation: turbulent break up and droplet coalescence.

For low liquid loadings, coalescence is negligible and droplet size is mostly controlled by turbulent break up. Small increases in liquid droplet concentration enhance turbulence (Azzopardi and Teixeira, 1994a; Azzopardi and Teixeira, 1994b) and break up is induced. For higher liquid concentration, coalescence becomes dominant and an increase in droplet size is expected.

Because the droplet acceleration is the major term in the total pressure drop, variations in its size do affect the pressure drop. Therefore, the trends observed in the

pressure drop, may be related with the droplet formation mechanisms. These phenomena could explain the behaviour of the pressure drop with the liquid to gas ratio.

Figure 4.6 shows the influence of the liquid to gas ratio upon the total pressure drop for various gas throat velocities, with spray injection. The data show that the pressure drop increases with increasing liquid to gasratio.

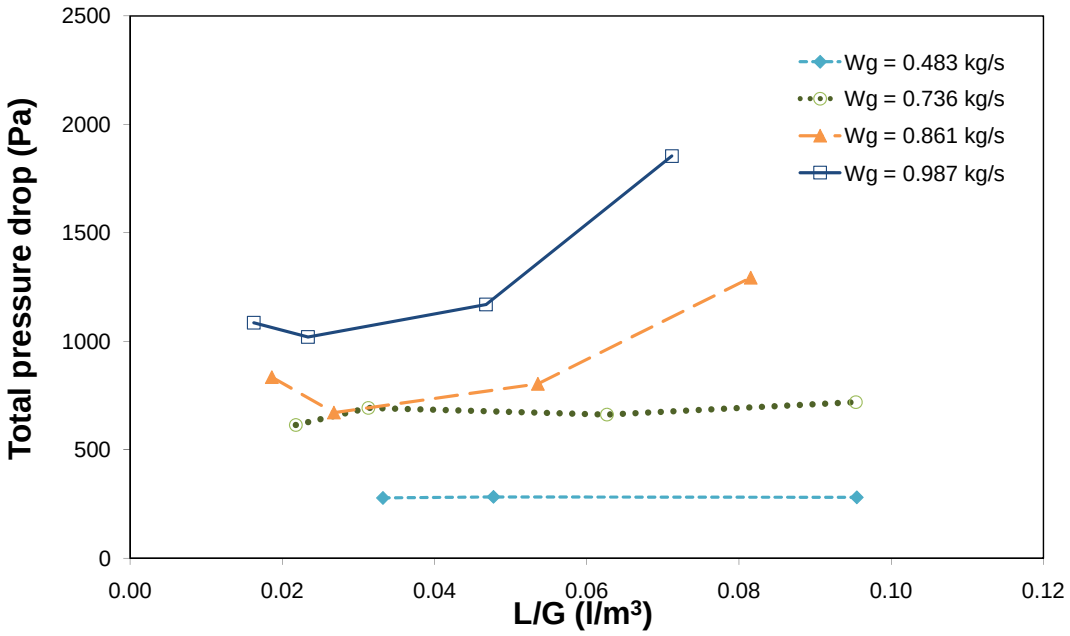

Figure 4.6 – Variation of the total pressure drop in the venturi with liquid to gas ratio and throat gas velocity. Liquid injected as a spray.

In order to better understand the total pressure drop measured, the profile for the axial pressure drop is investigated. Figure 4.7 shows the variation of the total pressure drop along venturi for different liquid flow rates and for a throat gas velocity of 70 *m/s*, when liquid is injected as a film. Figure 4.8 shows similar data, but with liquid injected as a spray.

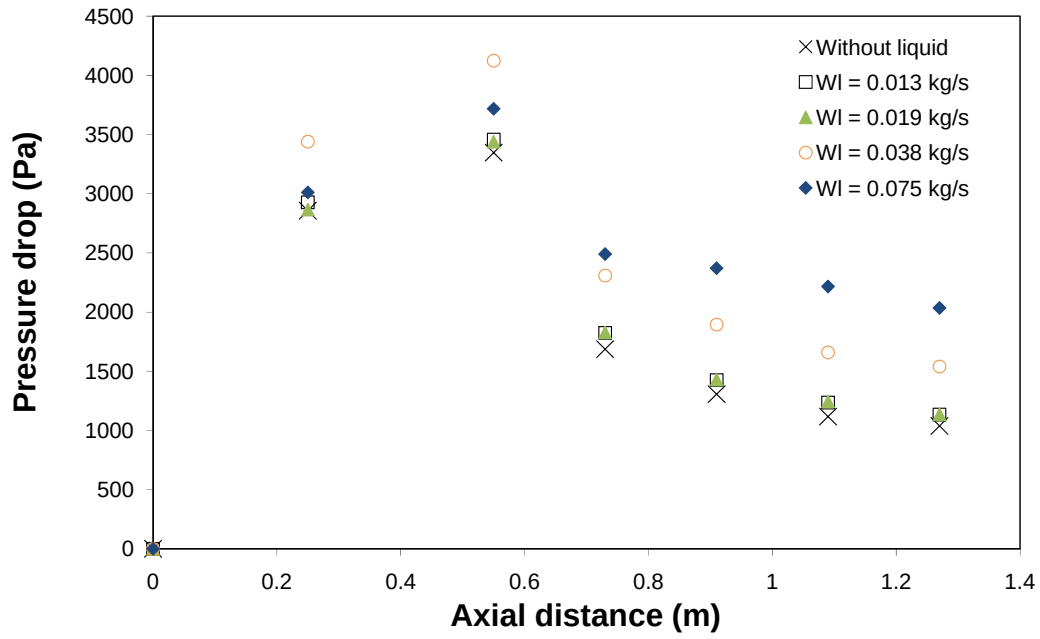

Figure 4.7 – Variation in the total pressure drop along the venturi with liquid flow rate. Liquid injected as a film. $U_{GT} = 70$ *m/s*.

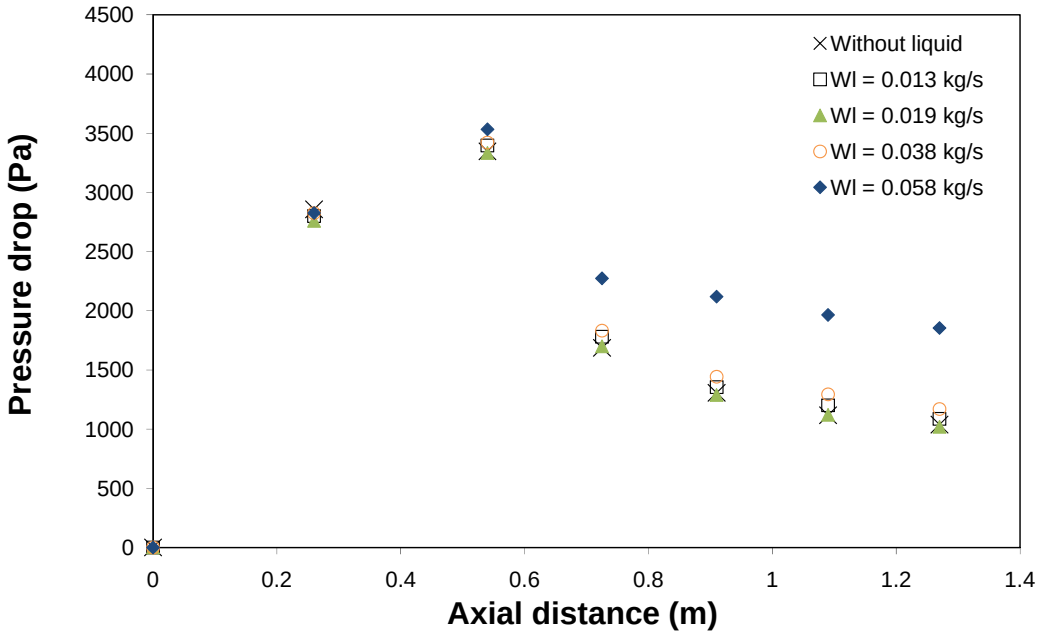

Figure 4.8 – Variation in the total pressure drop along the venturi with liquid flow rate. Liquid injected as a spray. $U_{GT} = 70$ *m/s*.

By comparing Figures 4.7 and 4.8, one observes that the influence of liquid flow rate upon the pressure drop in the converging section is negligible if the liquid is injected as a spray. This is due to the fact that in this layout the liquid inlet point is further upstream in the venturi. Therefore a significant fraction of droplet acceleration occurs upstream of the venturi. Furthermore, by increasing the liquid flow rate through the nozzles, the mean droplet size decreases yielding a spray that is easily accelerated and may compensate the increasingly liquid loading.

However, if the liquid is injected as a low velocity film, all the liquid has to be accelerated inside the converging section. Therefore, the more liquid is introduced, the higher the overall pressure drop.

4.2.2 Model validation

The experimental pressure drop data was compared with predictions resulting from the theoretical model described by Cruz *et al*. (1997).

As referred above, the model is also a variation of Azzopardi *et al*. (1991) model, with a more detailed description of the droplet distribution. The ability of the model to handle a large scale cylindrical venturi is now discussed, in terms of pressure drop and, in particular, the effect of liquid flow rate and the method of liquid injection.

A sensitivity analysis regarding the effect of the liquid flow rate upon the calculated pressure drop is shown in Figure 4.9. The gas velocity is kept constant. The results show that the pressure drop always increases with the liquid loading. This observation is not supported by experimental data (Figure 4.5) which show a minimum. This may be due to the fact that the experimental droplet size in annular flow shows a minimum as a function of the liquid flow rate. However, the droplet size model used in the hydrodynamic model is based on the portion of the data where coalescence is dominant and always shows an increase in the mean size with the liquid flow rate.

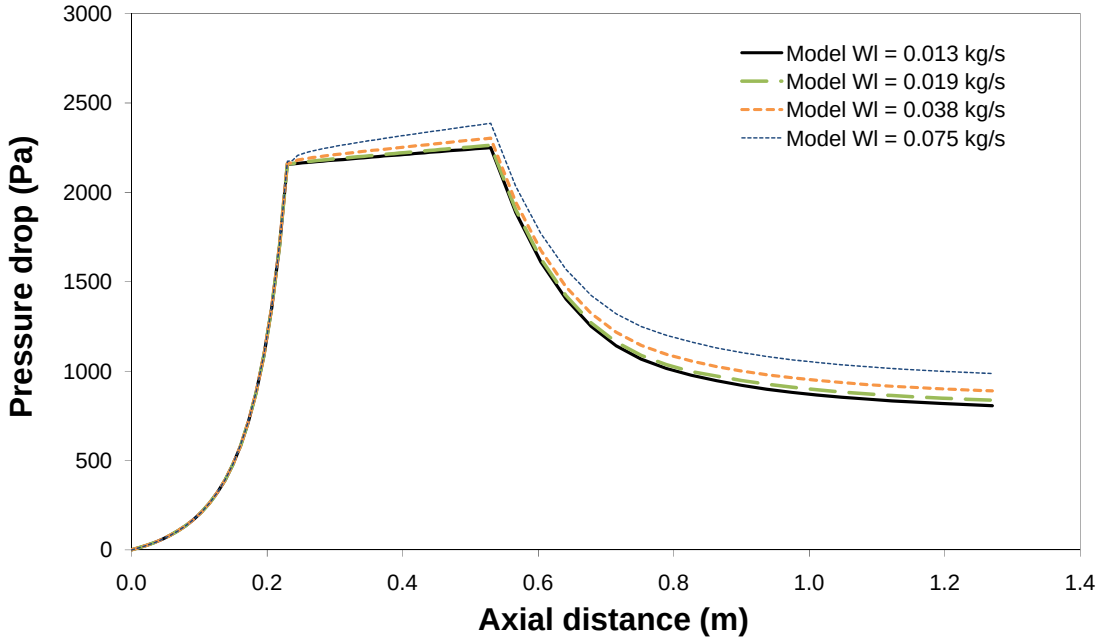

Figure 4.9 – Variation in the total pressure drop along venturi calculated by the model of Cruz (1997). $U_{GT} = 61\ m/s$.

Figure 4.10 compares the total pressure drop calculated by the model proposed by Cruz *et al*. (1997) with the experimental data, for the film injection case. As observed, most of the cases are well predicted, through its performance worsens for higher gas flow rates. The same trends can be observed in Figure 4.11, where the total pressure drop is presented and compared with the spray injection data. The results are apparently better in this case when the droplet size model influence is smaller.

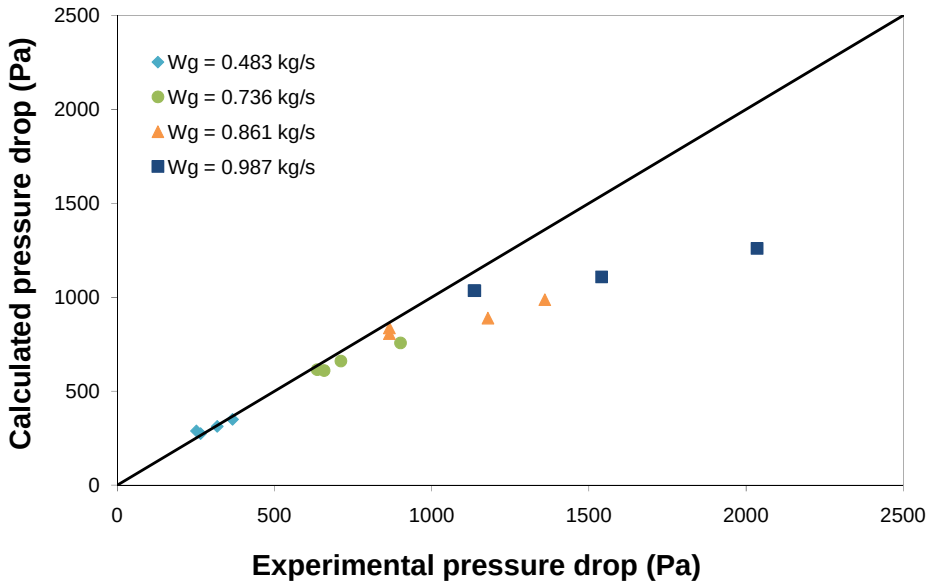

Figure 4.10 – Comparative total pressure drop predicted by Cruz (1997) model and experimental data. Liquid injected as a film.

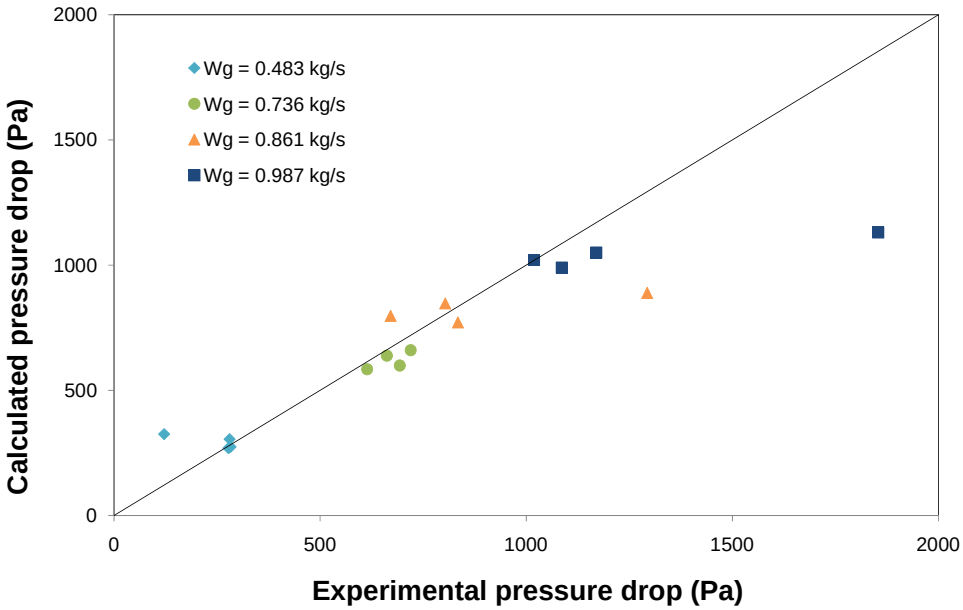

Figure 4.11 – Comparative total pressure drop predicted by Cruz (1997) model and experimental data. Liquid injected as a spray.

Figure 4.12 compares the model predictions with the experimental data for the pressure drop at the throat. The results do show that the major source of error in the model performance occurs in the throat which is in agreement with the pressure drop profiles shown in Figure 4.13.

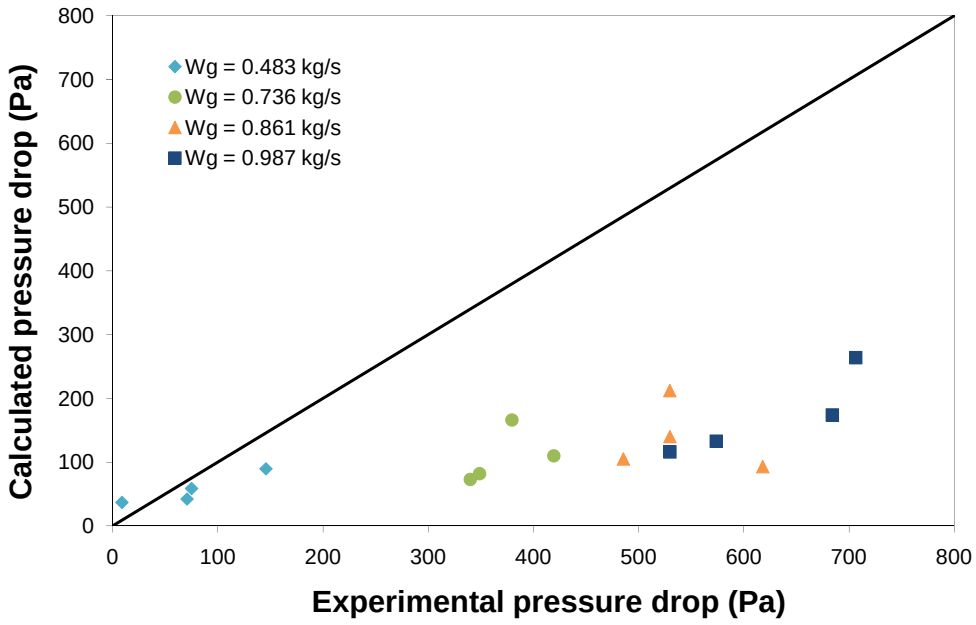

Figure 4.12 – Comparative pressure drop in the throat predicted by Cruz (1997) model and experimental data. Liquid injected as a film.

Even with the modifications introduced by Cruz *et al*. (1997) in the droplet distribution, a better estimative of the split of the liquid, into film and droplets, in the throat region, appears to be necessary (Gonçalves *et al*., 1999a). Also, the presence of the droplets in the boundary layer region should be taken into account.

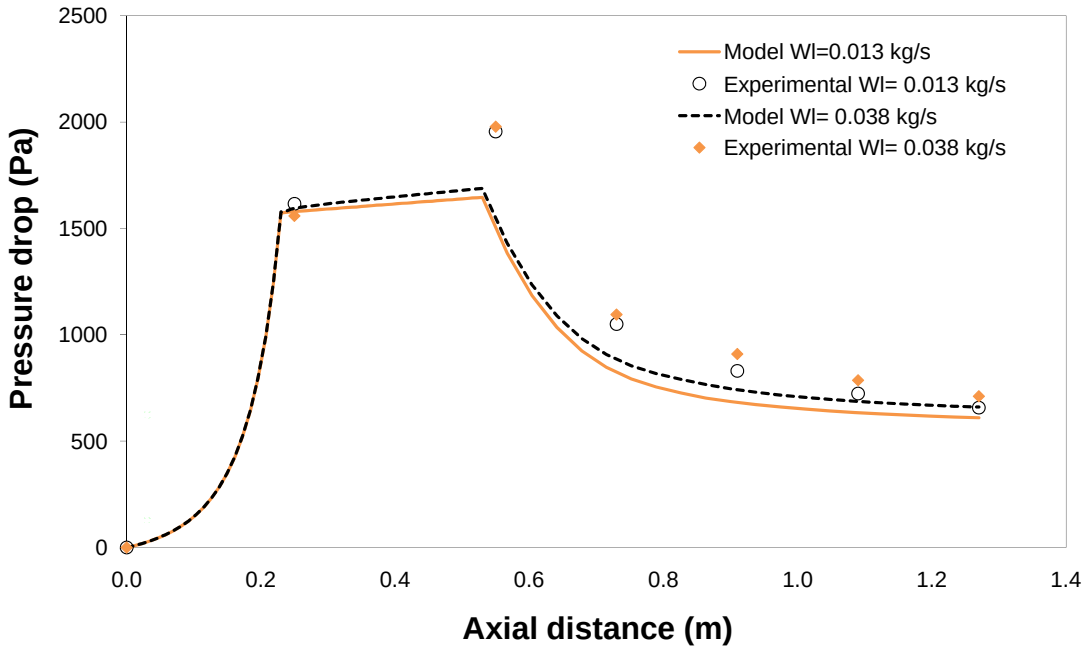

Figure 4.13 – Comparative example of pressure drop profiles predicted by Cruz (1997) model and experimental data. $U_{GT} = 52$ *m/s*.

4.2.3 Conclusions

Pressure drop measurements taken inside a large scale venturi have been presented. The effect of gas velocity and liquid flow rate has been investigated as well as two different types of liquid injection.

Water is introduced upstream of the convergence section either as film or as spray. The influence of the type of liquid introduction is only important at high liquid loading.

The total pressure drop is more influenced by gas velocity than by the liquid flow rate, which is in agreement with other published works. It was also found that the liquid to gasratio influence is stronger for high gas throat velocity although this behaviour is not constant and a minimum in pressure drop is observed for each gas flow rate. It is suggested that this observation may be linked with the droplet break up processes in annular two phase flow. Clearly, a better modelling of droplet size is required.

The model of Cruz *et al*. (1997) was validated against these set of data and the prediction for the total pressure drop found good, though the model performance is reduced for higher gas flow rates. The results also show that the inviscid model used in the convergence and throat section is clearly inadequate for predict experimental pressure drop in the throat region.

4.3 Droplet Size

4.3.1 Droplet size distribution

When using the laser diffraction technique for droplet sizing, the results are dependent upon the distribution model assumed. Therefore a brief discussion is necessary on the adequacy of the various options. In principle the best option to validate the fitness of any distribution would be the use of PDA technique. However the comparison is not straightforward because:

- The PDA is a point measurement technique;
- The dynamic range of a PDA is usually lower than that of a Malvern;
- The Malvern provides a measurement carried out over the volume of a beam which illuminates the spray.

Any spatial variation in the droplet size will make direct comparisons difficult. Nonetheless this approach has been used in the past. Viswanathan *et al.* (2005) has tested various functions with PDA data in a venturi with spray injection and found that depending upon the flow conditions some probability functions were more adequate than others. No single *pdf* would perform better over the entire data set. Castro (2002) tested various distribution functions with a wide range of data for sprays. These data were from sprays showing a very narrow spread, resulting in data confined within the dynamic range of the PDA. The author found that in some cases the RR would give a good approximation although for other conditions the Upper-Limit Log-Normal function would perform better. At any rate, both authors refer relatively simple atomization processes from a single source: spray nozzles.

Comparisons between the RR and the MI have been made in the past (Teixeira, 1988). For straight tubes both distributions provided similar mean diameters and *pdf*'s over the measuring range. However, if a multiple process of atomization is present, such as downstream of a venturi, Teixeira (1988) found that the width parameter (*n* in Equation 3.6) would decrease, suggesting the widening of the distribution. Comparisons with the MI fitting have shown that this spread was artificial due to the fitting of a multiple peak distribution by a unimodal function. Such complexities in the actual *pdf* can be identified by a polynomial fitting such as the MI. Alonso *et al*. (2001) have also observed a similar behaviour in a small scale venturi. Such phenomenon is more likely to occur downstream of the venturi throat where the droplet population is formed by various sources: entrainment film upstream the venturi, local entrainment at the throat inlet, secondary breakup.

From this, one may conclude that no single *pdf* appears to be a universal option for droplet distribution. Due to these uncertainties it was decided to measure all the data using the MI, in order to have a common reference. Furthermore, it was observed that for the majority of tests the MI gave a lower fitting error than the RR which suggests that over the entire range of flow conditions, liquid injection techniques and measuring location, the MI is a more adequate function.

For the present data, a direct comparison between the RR and MI functions can be observed in Figures 4.14 and 4.15 when liquid is injected both as a film and as a spray, respectively.

The polynomial fitting by the MI *pdf* enables the detection of multiple peak distributions, as opposed to the RR which smoothes the data through a single peak function.

It is also evident that further downstream of the liquid injection, the droplet probability distribution function mutates into a two peak function, which cannot be detected by the unimodal RR function. This suggests that two populations of droplets are present in the venturi: one that is basically the result of breakup of the spray droplets and another resulting from the atomisation of the liquid film. This effect is more evident when the liquid is injected as a spray. In fact, such conditions are more likely to create a two population spray.

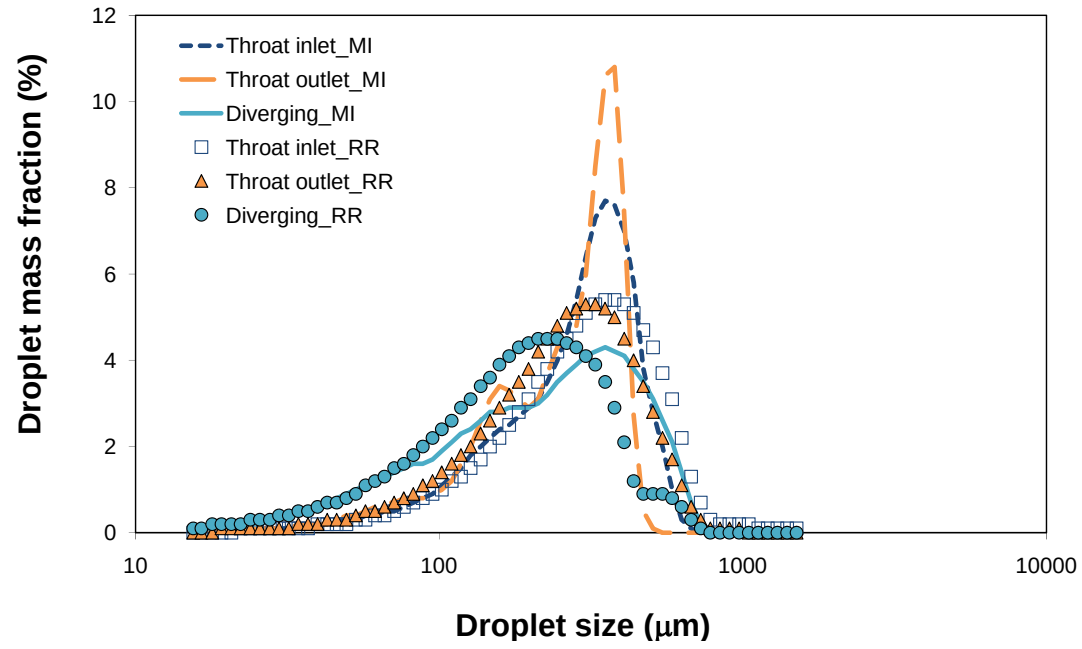

Figure 4.14 – Mass fraction droplet size distribution along the venturi axis (sections A, B and C). Liquid is injected as a film. $W_G = 0.861$ *kg/s* and $W_L = 0.075$ *kg/s*.

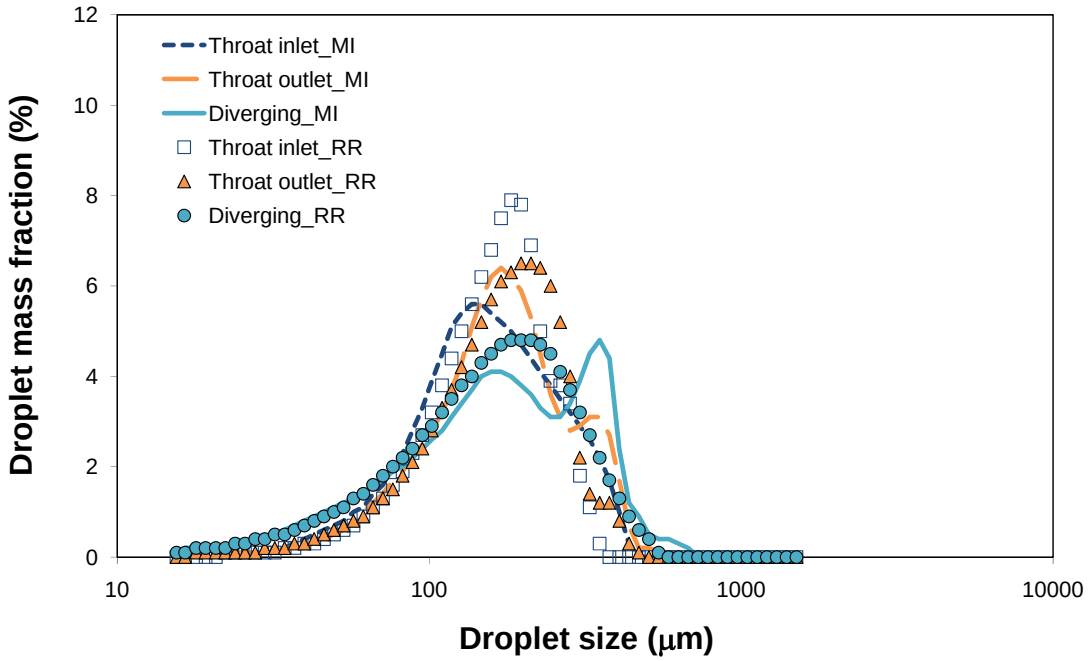

Figure 4.15 – Mass fraction droplet size distribution along the venturi axis (section A, B and C). Liquid is injected as a spray. $W_G = 0.861$ *kg/s* and $W_L = 0.058$ *kg/s*.

Figure 4.16 shows the droplet size distribution along venturi, when liquid is injected both as a film and as a spray. It can be observed that downstream the venturi the droplet probability functions are shifted to the lower end of the scale for spray injection, yielding a lower mean size. It is observed that the maximum droplet size frequency is within the range 200-300 μm.

This behaviour suggest that liquid breakup into stable droplets occurs along the venturi, as shown by the increase of the fraction of small droplets. Alonso *et al*. (2001) observed that the droplet *pdf* shows a shift towards larger droplets downstream of the venturi. However, their liquid loading (L/G ratios) is much higher (0.5 to 2.0 l/m^3) where coalescence should be much stronger. In the present data this phenomena should be less important as the L/G is between 0.016 and 0.187 l/m^3.

Teixeira (1988) has also observed a similar trend in annular flow in a 32 *mm* straight tube where the droplet size would decrease with the two-phase flow length if the liquid loading was small. For higher L/G ratios the opposite was observed.

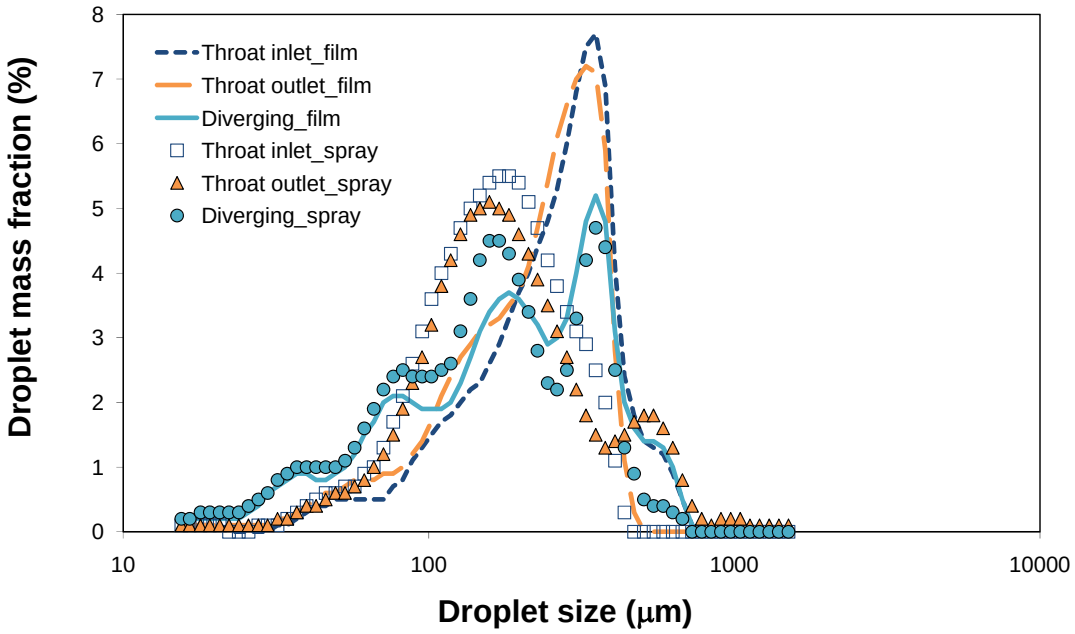

Figure 4.16 – Mass fraction droplet size distribution along the venturi axis (section A, B and C). Liquid is injected as film and spray. $W_G = 0.987$ *kg/s* and $W_L = 0.075$ *kg/s*.

Figure 4.17 depicts the effect of gas velocity upon the droplet size distribution considering two distribution functions. The data show that by increasing the gas

velocity, the RR function appears to be less adequate for describing the droplet *pdf*. In fact, a droplet coalescence mechanism is more likely to occur at higher gas flow rates, although the L/G ratio is of approximately 0.1 l/m^3. In such case, the occurrence of a multiple peak distribution may be related to the formation of various droplet populations resulting from their coalescence. Stochastic methods for droplet collision have predicted such occurrence in venturis (Cruz *et al*., 1997).

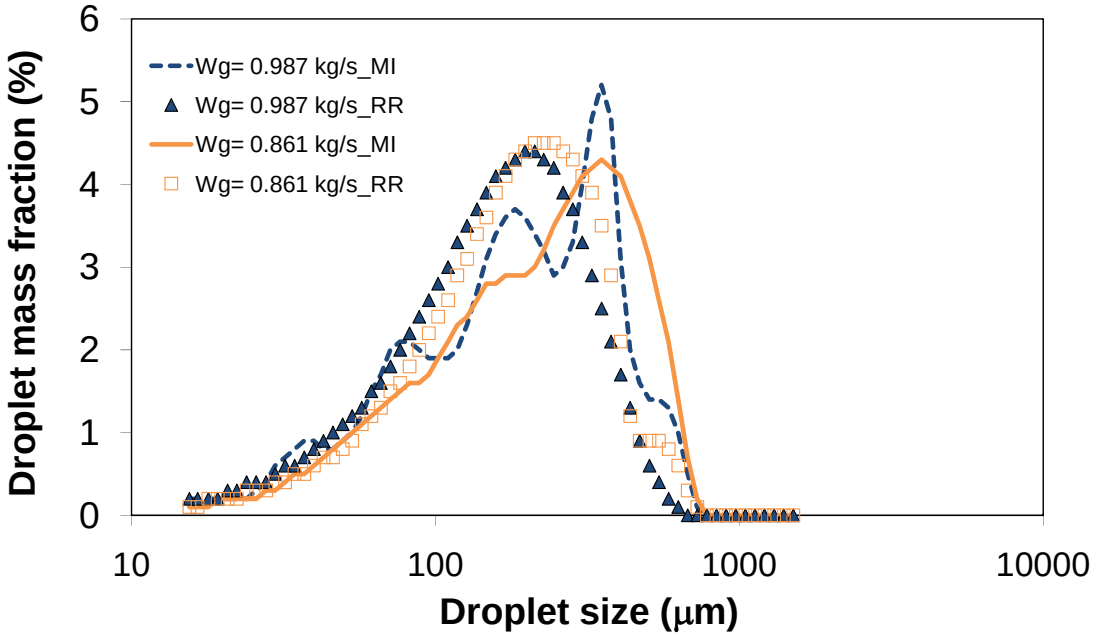

Figure 4.17 – Mass fraction droplet size distribution for different gas velocities in the diverging section. Liquid is injected as film. W_L = 0.075 *kg/s*.

Figure 4.18 shows the effect of liquid flow rate upon the droplet distribution. Coalescence results from the probability of droplets colliding with each others. Therefore, conditions that favour large number of droplets subject to changes in velocity are those most likely to induce coalescence. Liquid loading has a similar effect on the droplet probability distribution function as the gas velocity. The higher the droplet flow, the higher their coalescence and in such conditions the formation of various droplet populations is more likely. Again the RR distribution fails to detect such behaviour. The occurrence of multiple peak pdf's is accompanied by the increase of d_{32} from 92 up to 130 μm for the data reported in Figure 4.18.

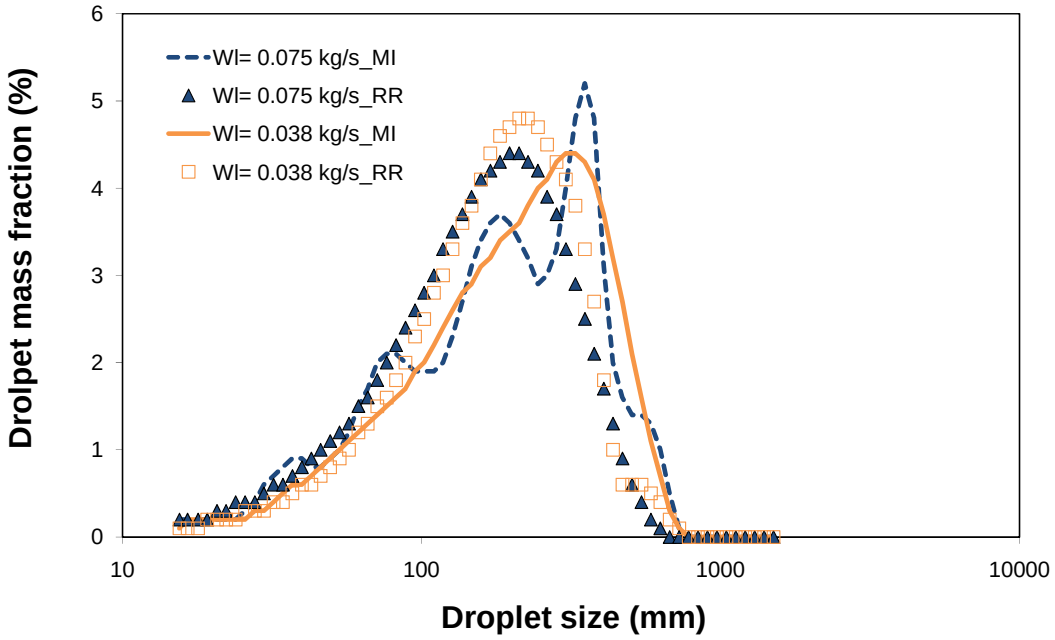

Figure 4.18 – Mass fraction droplet size distribution for different liquid loading in the diverging section. Liquid is injected as film. $Wg = 0.987$ *m/s*.

4.3.2 Droplet size data

In processes governed by mass and surface phenomena, the Sauter mean is often employed as the characteristic mean diameter of a droplet distribution. This mean represents the ratio between the volume and the surface area of the entire droplet population and is defined by:

$$d_{32} = \frac{\sum_{i=1}^{I}\left(n_i d_i^3\right)}{\sum_{i=1}^{I}\left(n_i d_i^2\right)} \tag{4.1}$$

Figure 4.19 shows the effect of the gas velocity and liquid injection method upon the mean droplet size along the venturi. The data on the left hand side of the graph reports measurements at the end of the converging section (location A, Figure 3.3). When liquid is injected as a spray, the initial droplet size is determined by the nozzle dynamics and for a constant liquid flow rate, this initial droplet diameter should remain

unchanged. Therefore the data observed at location A is virtually independent of the gas flow rate. A characterization of the spray nozzles has been carried out on a separate rig and the results are shown in Figure 4.20. It is observed that the initial droplet size, for the liquid flow rate reported in Figure 4.19, is below 300 μm. From the injection point to location A, a reduction in droplet size is observed due to subsequent breakup of droplets. At any rate, the droplet size in location A is approximately constant across the gas velocity range which shows that the initial atomization is paramount to the droplet size. On the other hand, if the liquid is injected as a film, there is a strong influence of the gas flow rate because the liquid atomization is controlled by the gas shear upon the liquid film. In this case, the mean droplet size in location A is strongly dependent upon the gas flow rate.

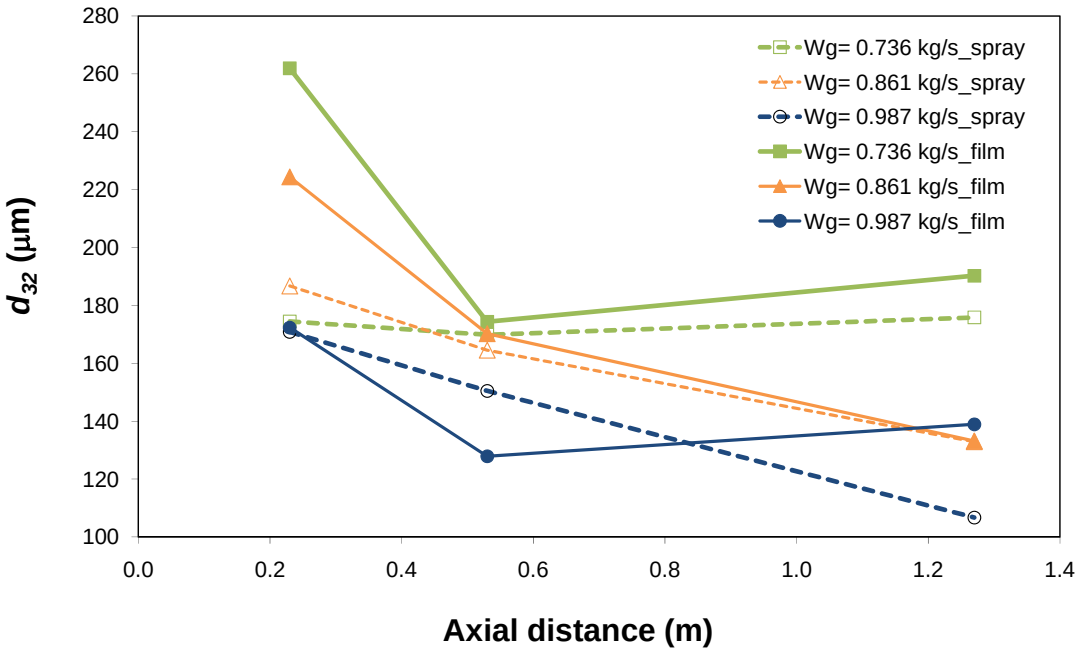

Figure 4.19 – Mean droplet size along the venturi comparisons between two methods for liquid injections. $W_L = 0.038$ *kg/s*.

Along the throat the droplet size shows further decrease. Although the local gas velocity is constant, the reduction in size suggests that secondary breakup occurs downstream the venturi for liquid being injected both as a spray and a film. This observation is in agreement with those reported in Figures 4.14 and 4.15. Such effect may continue through the entire length of the venturi as observed in Figure 4.19, particularly for higher gas velocities (lower residence time) where a continuous

reduction in size is observed. This behaviour is more evident for spray injection. In this configuration, most of the droplets are formed upstream of the venturi and the population downstream of the venturi is less influenced by droplets entrained from the liquid film. Any effect of the increase in droplet size due to the lower local gas velocity is less effective. However for film injection, droplet formation close to the venturi outlet yields a larger mean diameter due to the lower local gas velocity. Droplets formed at this section represent a larger fraction of the total population.

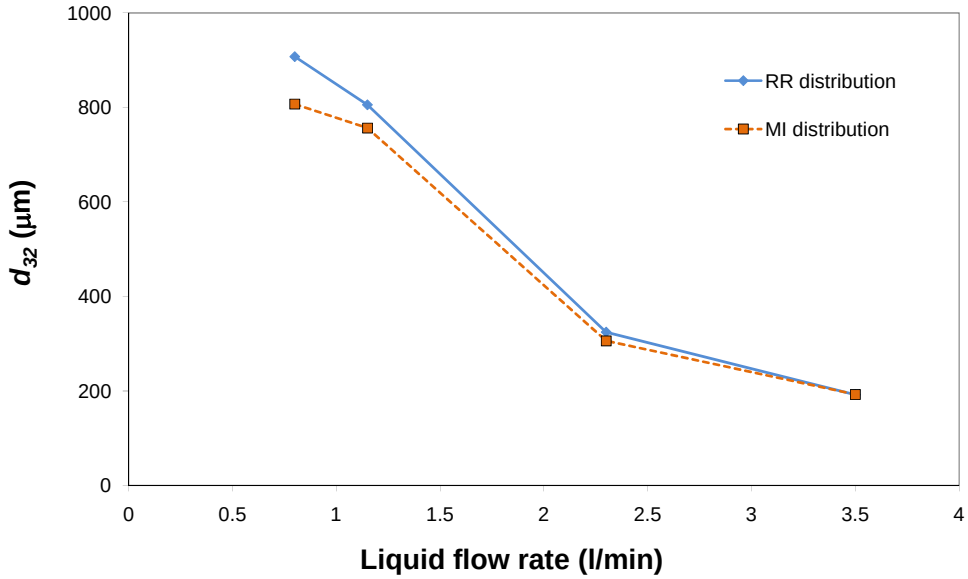

Figure 4.20 – Influence of the liquid flow rate on the mean droplet size for the spray nozzles.

In their experiments, using a spray injection, Costa *et al*. (2004) observed that the droplets usually increase with the distance from the liquid injection point, as also referred by Alonso *et al*. (2001). The authors suggest that the droplet size distribution shifts toward to larger diameters along venturi.

The present data show an opposite behaviour as the droplet size decreases in the throat section and shows a small increase in the diverging section. This difference should be due to the venturi size, as the experiments of Costa *et al*. (2004) and Alonso *et al*. (2001) were carried out in laboratory scale venturis. On the contrary, in the present work, the long throat favours the droplet breakup into smaller sizes.

The effect of gas velocity on droplet size can be observed in Figure 4.21 when liquid is injected as a spray. In general terms, an increase in gas velocity correlates the decrease in droplet size. This effect is in agreement with other authors such Nukiyama e Tanasawa (1938) and Boll *et al*. (1974), and more recently with Costa *et al*. (2004) and Viswanathan *et al*. (2005). This effect can be explained by the fact that with the increase in the gas velocity, the higher inertial forces must be balanced by the surface forces through droplets of smaller size.

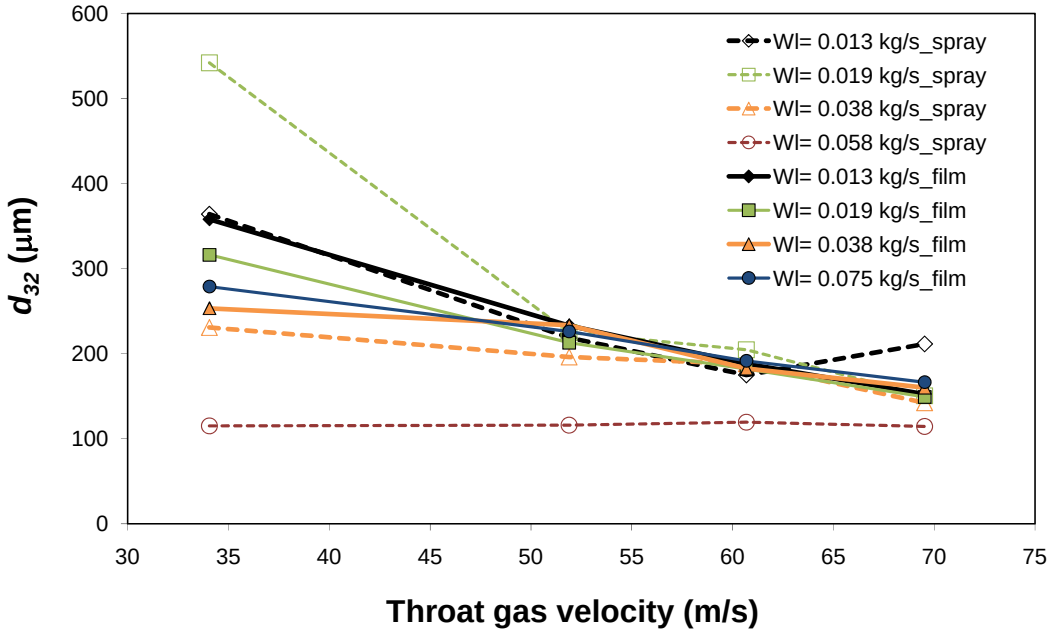

Figure 4.21 – Effect of the gas velocity upon the mean droplet size at the end of the converging section (A). Liquid introduced as a film and as a spray.

The data show that, for a combination of low liquid and high gas flow rates, the droplet size increases. This behaviour is observed for just one data set and the reasons are not clear. One may speculate that coalescence can occur although the liquid flow rate is at the lowest value. However coalescence is a very complex phenomenon and such hypothesis may be valid. Most of the droplets are formed at the venturi inlet and for the lowest liquid flow rate; the mean droplet size is very large (Figure 4.20). Although droplet concentration is low, such large droplets are more likely to accelerate at different rates throughout the venturi increasing the likelihood of the droplet coalescence.

Figure 4.22 shows the effect of liquid flow rate on droplet size at the end of the converging section (point A). It is observed that when liquid is introduced as a spray, an increase in liquid flow rate caused a decrease in droplet size. On the other hand, when the liquid in injected as a film the influence is not very important.

Because the nozzle orifices are of fixed diameter, the increase in liquid flow rate increases the injection velocity yielding a reduction in the droplet size (see Figure 4.20). Such initial diameter controls the droplet size throughout the venturi particularly in the upstream sections. On the other hand, injecting the liquid as a film increases the film thickness and the corresponding length scales for the liquid ligaments that are atomized into droplets.

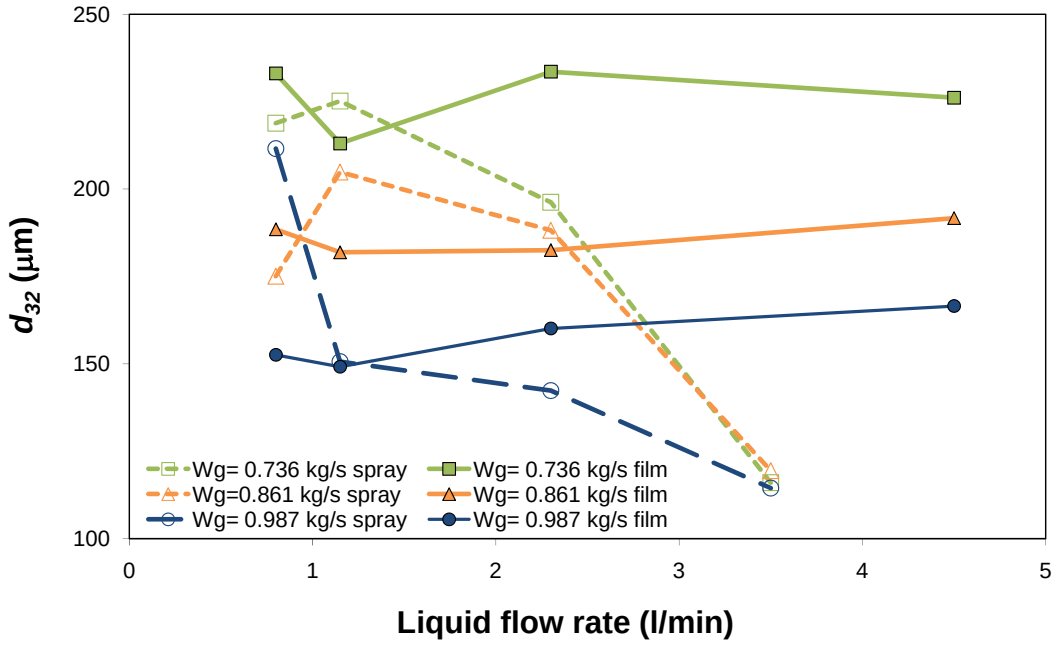

Figure 4.22 – Influence of the liquid flow rate upon the mean droplet size. Liquid injected as a spray and as a film for various gas flow rates.

Both Nukiyama and Tanasawa (1938) and Boll *et al*. (1974) found that droplet size increases slightly with liquid to gas ratio. The work of Alonso *et al*. (2001) reported no significant influence of the liquid flow rate on the mean droplet diameter, for higher liquid to gas ratios (0.5 – 2.0 l/m^3) in a laboratory scale venturi.

Viswanathan *et al*. (2005) reported higher liquid to gas ratios (0.4–1.8 l/m^3) in a rectangular large scale venturi scrubber. In this, water was introduced at the top of the

throat section of the venturi (downward flow, throat length 76 *mm*) through 34 orifices (17 of them on each side) perpendicularly to the air flow. They observed that the Sauter mean diameter increases with the liquid to gasratio at a constant throat gas velocity. This method of injection is closer, in concept, to the liquid film technique.

The present experiments extend the data for a very low liquid to gas ratios. In such circumstances the effect of liquid flow rate for film injection may show more complex interactions between the droplets and the gas core. In annular flow, Teixeira (1988) observed that for low liquid flow rates, the droplet size decreases with the liquid flow rate and suggested that droplet size could be controlled by turbulent breakup in the gas stream. Increased turbulence induced by a higher concentration of the dispersed phase would enhance droplet break-up. On the other hand at high liquid flow rates, the higher loading favours an increase in droplet size because of droplet-droplet interaction. The current data suggests a similar behaviour.

Reporting lower liquid to gasratios (0.01 to 0.17 l/m^3), in a laboratory scale venturi, Costa *et al*. (2004) found that an increase in liquid to gas ratio caused a decrease in droplet size and reported that for small liquid to gas ratios, droplet size is strongly influenced by liquid to gas ratios such behaviour is not predict by available correlations. The liquid is also injected as a spray and the trend observed is in agreement with the present work.

4.3.3 Droplet size correlations

The present experimental data was used to test three of most used correlations (Boll *et al*, 1974; Azzopardi and Govan, 1984; Nukitama and Tanasawa, 1938).

Based on experimental data with spray injection, Boll *et al*. (1974) proposed the following correlation for an air/water system:

$$d_{32} = \frac{4.22 \times 10^{-2} + 5.77 \times 10^{-3} (1000 Q_L / Q_G)^{1.922}}{U_r^{\,0.58}} \tag{4.2}$$

For annular flow in straight tubes, Azzopardi and Govan (1984) proposed a correlation based on the experimental data in small diameter pipe taking the form:

$$\frac{d_{32}}{\lambda} = \frac{15.4}{\mathrm{We}^{0.58}} + \frac{3.5\rho_G W_{LE}}{\rho_L W_G} \tag{4.3}$$

where $\lambda = \sqrt{\sigma/\rho_L g}$ is a length scale. The first term accounts for the liquid break-up due to the gas shear and the second accounts for the droplet coalescence. This correlation is mostly appropriate for high liquid loadings.

The correlation of Nukiyama and Tanasawa (1938) has been used extensively over many years. Their correlation is:

$$d_{32} = \frac{0.585}{U_r}\sqrt{\frac{\sigma}{\rho_L}} + 1.683\times10^{-3}\left(\frac{\mu}{\sqrt{\sigma\,\rho_L}}\right)^{0.45}\left(\frac{1000Q_L}{Q_G}\right)^{1.5} \tag{4.4}$$

Of these correlations, only that of Boll *et al*. (1974) (Equation 4.2) has been derived for venturi. The others are based on data taken in annular flow in plain tubes (Equation 4.3) and sprays (Equation 4.4).

Figures 4.23 through 4.25 compare the present experimental data on droplet size with these available correlations often used in such applications. The tests were carried out for all the measuring sections: A, B and C (Figure 3.3).

As observed, all the correlations systematically under predict data by a wide margin. This may be due to the fact that such correlations have been derived from data measured in tubes of small diameter, where the correlations proved to be adequate. However, in large diameter pipes, as found in annular two phase flow in straight tubes, there is an effect of pipe diameter upon the droplet size (Gibbons, 1985). Another factor is the range flow conditions which, for the liquid to gas ratio, are much lower in the present work, than that used in the correlation fitting. Experiments in annular two phase flow in straight pipes suggest that the competing mechanisms in droplet formation may not apply to both the conditions used for correlation fitting and those present in the current work.

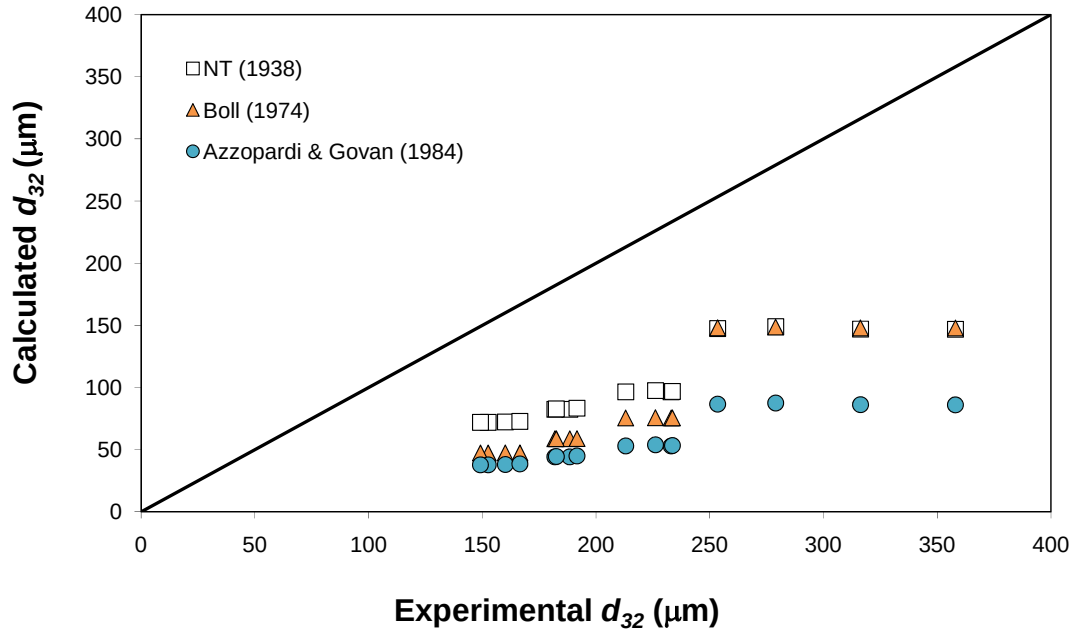

Figure 4.23 – Comparison between experimental and predicted droplet size in the converging section of the venturi (A). Droplet size is predicted using the throat velocity. Liquid is injected as a film.

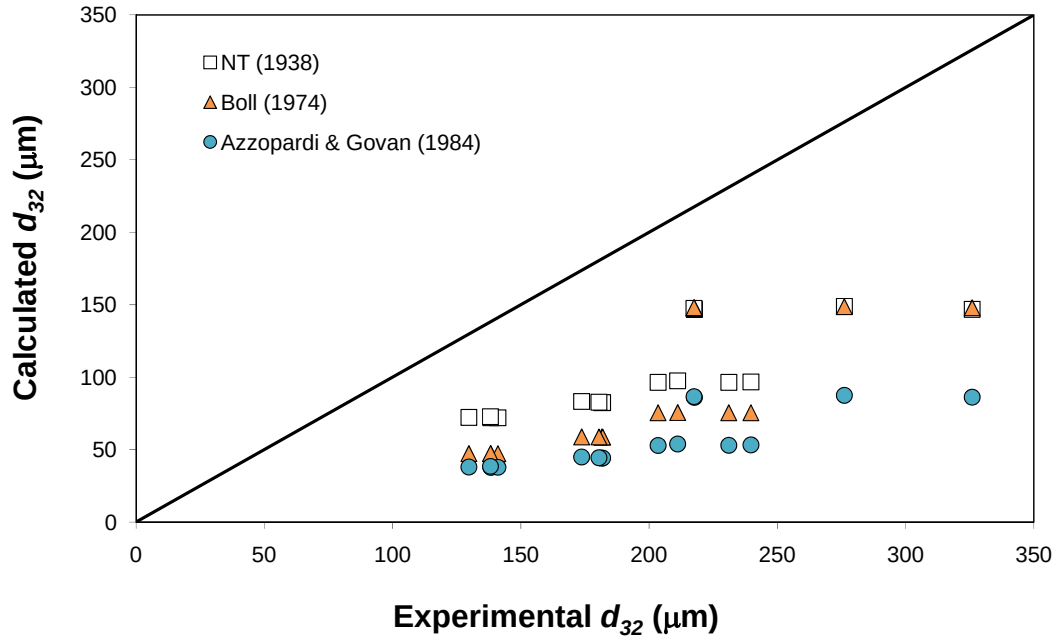

Figure 4.24 – Comparison between experimental and predicted droplet size in the throat section of the venturi (B). Droplet size is predicted using the throat velocity. Liquid is injected as a film.

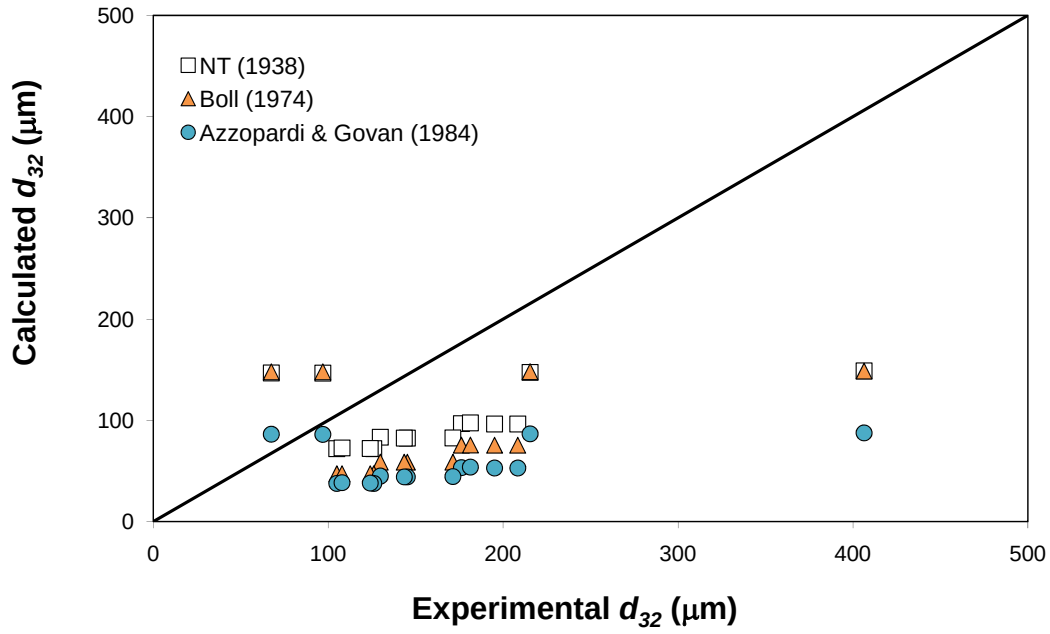

Figure 4.25 – Comparison between experimental and predicted droplet size in the divergent section of the venturi (C). Droplet size is predicted using the throat velocity. Liquid is injected as a film.

In their work, Viswanathan *et al.* (2005) observed that the Sauter mean diameters are systematically lower than those predicted by the Nukiyama and Tanasawa (1938) equation for all operating conditions, although they are in agreement with the equation of Boll *et al.* (1974) for all liquid to gasratios at a throat gas velocity of 45 *m/s*. However, as the throat gas velocity increases progressively to 75 *m/s*, the agreement becomes poor.

In a rectangular small scale venturi, Costa *et al*. (2004) compared their experimental results with the predictions of Nukiyama and Tanasawa (1938) and Boll *et al*. (1974) and neither correlation represented these results satisfactorily. Alonso *et al*. (2001) has shown that the experimental Sauter mean diameter of the spray can be well correlated by the equation of Boll *et al*. (1974).

The under prediction of droplet size at the venturi exit may be due to the use of the throat velocity in the correlations. This is not appropriate because the local velocity is reduced.

Figure 4.26 shows the droplet size predictions when using the local gas velocity in the correlations. The correlation of Boll *et al*. (1974) is not included because it was derived using the throat velocity as the gas velocity. It is observed that droplet size is

over predicted by a factor of up to 3. In this approach one is assuming that all the droplets are formed under conditions typically of the venturi divergence. In reality droplets are formed along the venturi, and under complex processes of atomization and coalescence, the resulting population combines such phenomena. Therefore neither the throat velocity nor the local velocity should represent accurately the gas momentum. Nonetheless, the Azzopardi and Govan (1984) correlation (Equation 4.3) appears to give the best results and may be used to predict the local droplet size distribution.

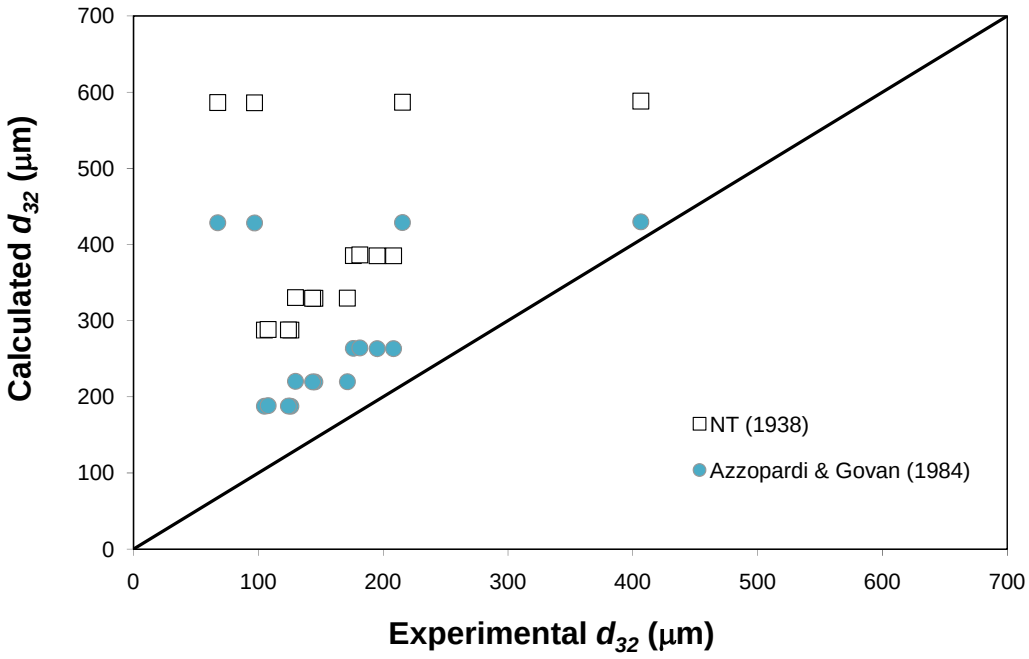

Figure 4.26 – Comparison between experimental and predicted droplet size in the divergent section of the venturi (C). Droplet size is predicted using the local velocity. Liquid is injected as a film.

4.3.4 Conclusions

From the work reported here the following conclusions may be drawn:

- The data suggest that in large scale venturis, two competing mechanisms control droplet size: turbulent breakup and coalescence.
- The available correlations show a significant deviation from the experimental data. This observation is particularly evident in the

converging and throat sections. In the diverging section, a better correlation is observed.

- The method for liquid injection is a major parameter for droplet formation. If liquid is injected as spray, droplet size is mostly controlled by the nozzle characteristics and the interaction with the gas in the upstream in the venturi.
- Neither the throat nor the exit velocities are suitable for predicting the mean droplet size from available correlations. The complexity of droplet interactions may not be properly taken into account.
- Evidence of droplet coalescence is found with the data. Spray injection and high gas and liquid flow rates are the most favourable conditions.
- The droplet distribution may show multiple peaks, particularly downstream in the venturi. Spray injection favours such occurrence.

Chapter 5

CFD Model

This chapter details the numerical model used in the present work. The fundamentals of CFD modelling are pointed out as well as the main aspects regarding multiphase flow modelling. This discussion includes both the governing equations for the gas and droplet phases and the numerical procedure.

5.1 Fundamentals of CFD Modelling

CFD is the analysis of systems involving fluid flow, heat transfer and associated phenomena such as chemical reactions by means of computer-based simulation. The technique is very powerful and spans a wide range of industrial and non-industrial application areas (Versteeg and Malalasekera, 1995).

In the past, the high computing costs have been a major factor in limiting the widespread use of such tools. The availability of high performance computing hardware and the user-friendly interfaces have led to recent increase of interest on using the CFD technique into a wider industrial environment.

There are several advantages of CFD over experimental approaches to the study of fluid system:

- substantial reduction of lead times and cost of new designs;

- ability to study large systems where controlled experiments are difficult or impossible;
- ability to study systems under hazardous conditions;
- practically unlimited level of detail of results.

The CFD codes can produce large volumes of results when compared with experimental work, being more economical both in time and effective cost.

A CFD code contains three main parts:

- *a pre-processor* – input of a flow problem to a CFD program by an operator using friendly interface and subsequent transformation of this input into a form suitable for use by the solver (definition of the geometry, grid generation, definition of fluid properties, etc);
- *a solver* – selection of the software parameters such as discretization schemes, physical models and numerical solution methods of the conservation equations;
- *a post-processor* – visualisation of the results.

The basic equations in all mathematical models for CFD are balances for momentum and mass determining velocity, pressure and density field. Depending on the case considered, they are supplemented by mass balances for single species and an energy balance. Additional models may be required to describe, e.g. turbulence, multiphase flows, chemically reactive systems and other special cases.

The starting point for the solving of any conservation equation is the discretization of a space also known as grid generation. Certain requirements concerning grid structure have to be fulfilled to get stable convergence and an accurate solution. There are three distinct streams of numerical solution techniques: finite difference, finite element and finite volume methods. Traditionally, most CFD codes use finite volume discretization for the conservation equations, as the software used in the present work - Fluent.

The finite volume method was originally developed as a special finite difference formulation and the numerical algorithm consists of the following steps:

- integration of the governing equations of fluid flow over all the control volumes of the solution domain;
- discretization involves the substitution of a variety of finite-difference-type approximations for the terms in the integrated equation representing

flow processes such as convection, diffusion and sources. This converts the integral equations into systems of algebraic equations;

The first step, the control volume integration, distinguishes the finite volume method from all the other CFD techniques. The resulting statements express (exact) conservation of relevant properties for each elemental cell. This clear relationship between the numerical algorithm and the underlying physical conservation principle forms one of the main attractions of the finite volume method and makes its concepts much simpler to understand (Versteeg and Malalasekera, 1995).

Finally, the numerical results have to be graphically presented and interpreted. Because of the huge amount of numerical data provided by each simulation this cannot be done with a general method. It must always be analyzed in reference to a certain research question. Errors caused by the model formulation and by the numerical scheme have to be analyzed in order to judge the accuracy of a simulation.

A commercial CFD code, Fluent, is used to perform the numerical analysis of the two-phase flow.

Fluent provides comprehensive modelling capacities for a wide range of incompressible and compressible flow, laminar and turbulent fluid problems. Steady-state or transient analyses can be performed. A broad range of mathematical models for transport phenomena is combined with the ability to model complex geometries (Fluent 6.2, User's Guide, 2005).

5.2 Eulerian-Lagrangian Approach

A large number of flows encountered in nature and technology are a mixture of phases. Multiphase flow can be classified:

- Gas-liquid or liquid-liquid flows
- Gas-solid flows
- Liquid-solid flows
- Three-phase flows

Advances in computational fluid mechanics have provided the basis for further insight into the dynamics of multiphase flows. Currently there are two main approaches

for the numerical calculation of multiphase flows: the Euler-Euler and the Euler-Lagrange approach.

In the Euler-Euler approach, the different phases are treated mathematically as interpenetrating continua. Since the volume of a phase cannot be occupied by the other phase, the concept of phase volume fraction is introduced. These volume fractions are assumed to be continuous functions of space and time and their sum is equal to one. Conservation equations for each phase are derived to obtain a set of equations, which have similar structure for all phases. These equations are closed by providing constitutive relations that are obtained from empirical information by applications of kinetic theory. It is a very useful approach for separated flows.

In Fluent, three different Euler-Euler multiphase models are available: the volume of fluid model, the mixture model and the Eulerian model.

The major drawback of the Eulerian-Eulerian approach is the inability to capture the polydispersion in size of the spray (different diameters, density …). One should therefore treat every class of particles diameter as a separate phase. Thus the advantage of less computational costs becomes not realistic, due to the fact that every class of particles has to be treated separately (Fluent 6.2, User's Guide, 2005).

In the Euler-Lagrange approach, the fluid is treated as a continuum by solving time-averaged Navier-Stokes equations, while the dispersed phase is solved by tracking a large number of particles, bubbles, or droplets through the computed flow field. The dispersed phase can exchange momentum, mass and energy with the fluid phase.

The Lagrangian discrete phase model in Fluent assumes that the second phase is sufficiently dilute and so, droplet-droplet interactions and the effects of the droplet volume fraction on the gas phase are negligible. The particle or droplet trajectories are computed individually at specified intervals during the fluid phase calculations. This makes the model appropriate for modelling spray dryers, coal and liquid fuel combustions and some particle laden flows, but inappropriate for the modelling of liquid-liquid mixtures, fluidized beds or any application where the volume fraction of the second phase is not negligible.

The first step in solving any multiphase problem is to determine which of regimes best represents the flow in study, and, based on that, select the most suitable model to use.

In the venturi scrubber, the flow is defined as annular flow, considered as a gas core with droplets surrounded by a wall film. Based on guidelines proposed by Fluent

(Fluent 6.2, User's Guide, 2005) to select the appropriate model, for bubbly, droplets and particle-laden flows in which the dispersed phase volume fraction are less than or equal to 10%, the Euler-Lagrange approach should be used. Fluent uses the discrete phase model to apply this approach.

Discrete-phase model

Fluent allows the simulation of the discrete phase in a Lagrangian frame reference, in which the second phase are spherical particles (which may be taken as droplets or bubbles) dispersed in the continuous phase. The trajectories of these discrete entities as well as heat and mass transfer to/from them, are computed. The coupling between the phases and its impact on both the discrete phase trajectories and the continuous phase flow can be included.

The dispersion due to the turbulence in the fluid phase can be predicted using the stochastic tracking model or the particle cloud model. The stochastic model includes the effect of instantaneous turbulent velocity fluctuations on the particle trajectories through the use of stochastic methods. The particle cloud model tracks the statistical evolution of a cloud of particles through an average trajectory. For the stochastic tracking a model is available to account for the turbulence generation or dissipation in the continuous phase.

The general procedure for setting up and solving a steady-state discrete-phase problem is:

- Solve the continuous phase;
- Create the discrete-phase injections;
- Solve the coupled flow, if desired;
- Track the discrete-phase injections, using plots or reports.

Limitations of the discrete phase model

The discrete phase model has a few limitations. The most important are:

- Assumption that the second phase is sufficiently dilute that particle-particle interactions and the effects of the particle volume fraction on the gas phase are negligible;

- Does not effectively model flows in which the particles are suspended indefinitely in the continuum;
- The second phase consists of spherical particles;

5.3 Governing Equations

The governing equations of fluid flow represent mathematical statements of conservation laws of physics. The mass of a fluid is conserved, the rate of change of momentum equals the sum of the forces on a fluid particle, and the rate of change of energy is equal to the sum of the rate of heat addition to and the rate of work done on a fluid particle (White, 2003).

The CFD model used in the present work is 3D, two-phase flow (air with liquid droplets) considered incompressible, Newtonian, in steady state and turbulent, for isothermal conditions.

5.3.1 Continuous phase description

The gas flow field is solved as turbulent steady-state flow and so the governing equations of mass conservation, momentum, energy, and species are solved with appropriate modelling procedures to describe the effects of turbulence fluctuations.

For the resolution of the velocity field, the Navier-Stokes equations are solved. The momentum equation for turbulent flows is obtained through the laminar flows equation using the Reynolds averaging method (Hinze, 1975).

In Reynolds averaging, the solution variables in the instantaneous (exact) Navier-Stokes equations are decomposed into the mean (ensemble-averaged or time-averaged) and fluctuating components. For the velocity components:

$$u_i = \overline{u}_i + u_i' \tag{5.1}$$

These equations describe the momentum conservation for turbulent flow at steady state conditions (droping the over bars):

$$\rho u_j \frac{\partial u_i}{\partial x_j} = -\frac{\partial p}{\partial x_i} + \frac{\partial}{\partial x_j}\left[\mu\left(\frac{\partial u_i}{\partial x_j} + \frac{\partial u_j}{\partial x_i} - \frac{2}{3}\delta_{ij}\frac{\partial u_l}{\partial x_l}\right)\right] + \frac{\partial}{\partial x_j}\left(-\rho\overline{u_i' u_j'}\right) + S_D \tag{5.2}$$

where p is the static pressure, μ is the air viscosity, the term $(-\rho\overline{u_i' u_j'})$ is called the turbulent stresses and S_D represents the source term due to the presence of particles/droplets.

The Reynolds-averaged approach to turbulence modelling requires that the Reynolds stresses be appropriately modelled. A common method employs the Boussinesq hypothesis (Hinze, 1975) to relate the Reynolds stresses to the mean velocity gradients:

$$\rho\overline{u_i' u_j'} = \rho\frac{2}{3}k\delta_{ij} - \mu_t\left(\frac{\partial u_i}{\partial x_j} + \frac{\partial u_j}{\partial x_i}\right) + \frac{2}{3}\mu_t\frac{\partial u_i}{\partial x_i}\delta_{ij} \tag{5.3}$$

where μ_t, the turbulence viscosity is described by the expression:

$$\mu_t = \rho C_\mu \frac{k^2}{\varepsilon} \tag{5.4}$$

where C_μ is a constant.

The Boussinesq hypothesis is used in the Spalart-Allmaras model, the k-ε models, and the k-ω models. The advantage of this approach is the relatively low computational cost associated with the computation of the turbulent viscosity, μ_t.

Turbulence Modelling

Turbulent flows are characterized by fluctuating velocity fields. These fluctuations mix transported quantities such as momentum, energy, and species concentration, and cause these quantities to fluctuate as well. Since these fluctuations can be of small scale and high frequency, they are computationally too expensive to simulate directly in practical engineering calculations. Instead, the instantaneous (exact) governing equations can be time-averaged, ensemble-averaged, or otherwise manipulated to remove the small scales, resulting in a modified set of equations that are computationally less expensive to solve. However, the modified equations contain

additional unknown variables, and turbulence models are needed to determine these variables in terms of known quantities (Fluent 6.2, User's guide, 2005).

There are several turbulence methods, each of them has its advantages and limitations and there is no single turbulence model able to predict all kinds of turbulent flows. Due to the importance and difficulty of the turbulence flow properties modelling, an appropriate turbulence model must be chosen (Ananthanarayanan and Viswanathan, 1999).

The most used models of turbulence are two-equation models in which the solution of two separate transport equations allows the turbulent velocity and length scales to be independently determined.

The standard k-ε model in Fluent falls within this class of turbulence model and has become the workhorse of practical engineering flow calculations even since it was proposed by Launder and Spalding (1972). Robustness, economy, and reasonable accuracy for a wide range of turbulent flows explain its popularity in industrial flow and heat transfer simulations. It is a semi-empirical model, and the derivation of the model equations relies on phenomenological considerations and empiricism.

As the strengths and weaknesses of the standard k-ε model have become known, improvements have been made to the model to improve its performance. Two of these variants are available in Fluent: the Renormalization Group (RNG) k-ε model (Yakhot and Orszag., 1986) and the realizable k-ε model (Shih *et al*., 1995).

The RNG is used to simulate gas flow for faster numerical tests. This model is derived by more rigorous statistical technique and is particularly beneficial for separate and recirculating flows (Fluent 6.2 User's Guide, 2005). The RNG model was already been used for other authors (Ananthanarayanan and Viswanathan, 1999) simulating a pilot-scale venturi scrubber.

The RNG-based k-ε turbulence model is derived from the instantaneous Navier-Stokes equations, using a mathematical technique called "renormalization group" (RNG) methods. The analytical derivation results in a model with constants different from those in the standard k-ε model, and additional terms and functions in the transport equations for k and ε.

The turbulence kinetic energy, k, and its rate of dissipation, ε, are obtained from the following transport equations (Yakhot and Orszag., 1986):

$$\rho \frac{\partial}{\partial x_i}(ku_i) = \frac{\partial}{\partial x_j}\left[\alpha_k \mu_{eff} \frac{\partial k}{\partial x_j}\right] + G_k - \rho\varepsilon \tag{5.5}$$

and

$$\rho \frac{\partial}{\partial x_i}(\varepsilon u_i) = \frac{\partial}{\partial x_j}\left[\alpha_\varepsilon \mu_{eff} \frac{\partial \varepsilon}{\partial x_j}\right] + G_{1\varepsilon}\frac{\varepsilon}{k}G_k - C_{2\varepsilon}\rho\frac{\varepsilon^2}{k} - R_\varepsilon \tag{5.6}$$

where the effective viscosity, μ_{eff} is defined as the sum of the molecular and the turbulent viscosity (Equation 5.4):

$$\mu_{eff} = \mu + \mu_t \tag{5.7}$$

The quantities α_k and α_ε are the inverse effective Prandtl numbers for k and ε, respectively and could be approximate by $\alpha_k = \alpha_\varepsilon \approx 1.393$.

$$G_k = \mu_t\left(\frac{\partial u_j}{\partial x_i} + \frac{\partial u_i}{\partial x_j}\right)\frac{\partial u_j}{\partial x_i} \tag{5.8}$$

is the generation term. In the present study, the turbulence generation due to buoyancy is neglected.

The model constants have the following default values derived analytically by the RNG theory (Yakhot and Orszag., 1986):

$$C_{1\varepsilon} = 1.42 \qquad C_{2\varepsilon} = 1.68$$

The main difference between the RNG and standard k-ε models lies in the additional term in the ε equation given by:

$$R_\varepsilon = \frac{C_\mu \rho \eta^3 \left(1 - \eta/\eta_0\right)}{1 + \beta\eta^3}\frac{\varepsilon^2}{k} \tag{5.9}$$

where $\eta \equiv Sk/\varepsilon$, $\eta_0 = 4.38$, $\beta = 0.012$.

There are two approaches for modelling the near-wall region: the wall-function approach and the near-wall modelling approach. In the first, the viscous sublayer is not resolved and semiempirical formulas are used to "bridge" this inner viscosity-affected region between the wall and the fully turbulent region. In the latter approach, the viscosity-affected region is resolved with a mesh all the way to the wall, including the viscous sublayer. The wall function approach is economical, robust and reasonably accurate and is a practical option for industrial flow simulations (Ananthanarayanan and Viswanathan, 1999) as opposed to the near-wall formulation where very fine grids are required in the wall vicinity.

Energy equation

If the evaporation of the second phase is taken into account, equations for the exchange of mass and heat between phases are solved in the calculations.

Fluent solves the energy equation in the form of a transport equation for static enthalpy, *h*:

$$\frac{\partial}{\partial x_i}\left(\rho u_i h\right) = -\frac{\partial}{\partial x_i}\left(\rho \overline{u'_i\, h'}\right) + \frac{\partial}{\partial x_i}\left(k + k_t\right)\frac{\partial T}{\partial x_i} + S_h \tag{5.10}$$

where the source term, S_h, includes heat transfer between the continuous and dispersed phase. The viscous dissipation terms and the effect of enthalpy transport due to species diffusion have been negligible in the present application.

The vaporisation of the liquid droplets is taken into account into the source term, S_m, (mass added to the continuous phase from the dispersed phase) in the mass conservation equation:

$$\frac{\partial u_i}{\partial x_i} = S_m \tag{5.11}$$

Boundary Conditions

The boundary conditions available in Fluent for the continuous phase are classified as follows:

- Flow inlet and exit boundaries: pressure inlet, velocity inlet, mass flow inlet, inlet vent, intake fan, pressure outlet, pressure far-field, outflow, outlet vent, exhaust fan;
- Wall, repeating, and pole boundaries: wall, symmetry, periodic, axis;
- Internal cell zones: fluid, solid (porous is a type of fluid zone);
- Internal face boundaries: fan, radiator, porous jump, wall, interior.

The turbulence model requires estimated k and ε values at the inlet and outlet of the domain. In Fluent, it is possible to specify the turbulence quantities in terms of more convenient quantities such as: turbulence intensity, turbulent viscosity ratio, hydraulic diameter, and turbulence length scale.

The turbulence intensity is predicted using the relation for fully developed flow:

$$I \equiv \frac{u'}{u_{average}} = 0.16\left(\mathrm{Re}_{D_h}\right)^{-1/8} \tag{5.12}$$

5.3.2 Discrete phase description

The dispersed second phase is introduced in the computational domain at a certain position (with initial conditions) and its trajectory is then computed along the continuous gas flow field.

In Fluent, the dispersed phase droplet trajectory is determined by solving its equation of motion. A force balance on the droplet immersed in a turbulent gas flow equates the particle inertia with the forces acting on the droplet (Clift *et al.*, 1978) and can be written (for the x-direction in Cartesian coordinates) as:

$$\frac{du_D}{dt} = F_D(u - u_D) + g_x \frac{\rho_D - \rho}{\rho_D} + F_x \tag{5.13}$$

where, u is the fluid phase velocity, u_D is the particle (droplet) velocity, μ is the molecular viscosity of the fluid, ρ is the fluid density ρ_D is the density of the droplet.

The first term in the right side of Equation (5.13) accounts for the drag force, the second one for the gravity effects and F_x includes additional forces such as

thermophoretic force, Brownian force, Saffman's lift force which can be important only in certain circumstances. However, provided that the particles meet the condition that $\rho_D \geq \rho$, these terms can be neglected.

In the first term,

$$F_D = \frac{18\mu}{\rho_D d_D^2} \frac{C_D \,\mathrm{Re}}{24} \tag{5.14}$$

where d_D is the droplet diameter and Re is the Reynolds number, which is based on the relative velocity:

$$\mathrm{Re} = \frac{\rho d_D \left| u_D - u \right|}{\mu} \tag{5.15}$$

The drag coefficient, C_D is a function of Re:

$$C_D = a_1 + \frac{a_2}{\mathrm{Re}} + \frac{a_3}{\mathrm{Re}^2} \tag{5.16}$$

where the constants (a_i) apply to smooth spherical particles over several ranges of Reynolds number given by Morsi and Alexander (1972).

Fluent allows changes in the drag coefficient Equation (5.16) through user defined subroutines, which can be compiled and linked with the main code, as well as, additional forces that can also be defined in the user code.

The inclusion of the gravity force term on the droplet equation is an option in Fluent and it is neglected in the present study.

Assuming that the term containing the body force remains constant over small discrete time steps, and linearizing any other forces acting on the droplet, the trajectory equation (Equation 5.13) is rewritten in simplified form:

$$\frac{du_D}{dt} = \alpha\left(u - u_D\right) \tag{5.17}$$

to be integrated analytically:

$$u_D(t+\Delta t) = u_D(t) + (u - u_D(t))\left(1 - e^{-\alpha(t+\Delta t)}\right) \tag{5.18}$$

The trajectory of the droplet itself is then predicted by integration of:

$$\frac{dx}{dt} = u_D \tag{5.19}$$

Small steps have to be used to integrate the equations of motion for the droplet and Fluent allows the user to control the integration time step when the equations are analytically solved.

Turbulence effects

When the gas flow field is turbulent, Fluent can predict the trajectories of the second phase using only the mean fluid phase velocity in the trajectory equation or optionally it can include the instantaneous value of the fluctuating gas flow velocity in order to predict the dispersion of the droplets due to turbulence.

In the present application, the inclusion of the turbulence effects on droplets has been considered important. By computing the droplets trajectories for a sufficient number of representative droplets the stochastic nature of turbulence can be modelled. In Fluent, the Discrete Random Walk model is used. This model is based on the eddy lifetime concept. The droplets trajectory equation can be integrated analytically over small time steps in which the instantaneous fluid velocity and the droplet relaxation time ($\tau_d = 1/F_D$) are assumed to be constant. To determine the fluctuating fluid velocity component, the model accounts for the eddy-droplet interaction. The droplet is assumed to interact with a succession of random eddies as it moves in the computational domain. Each eddy is characterized by a velocity (fluctuating) and a time scale (lifetime).

The fluctuating fluid velocity is assumed to obey a Gaussian probability distribution:

$$u' = \zeta\sqrt{u'^2} \tag{5.20}$$

where ζ are a normally distributed random number and the remainder of the right-hand side is the local r.m.s value of the velocity fluctuations. When the k-ε model is used

(assuming isotropy) these values of the r.m.s. fluctuating components can be obtained by:

$$\sqrt{u'^2} = \sqrt{v'^2} = \sqrt{w'^2} = \sqrt{2k/3} \tag{5.21}$$

The eddy lifetime needed at each droplet location to determine the next interaction time can be obtained from the local turbulence properties (k and ε). Fluent offers two choices to calculate the characteristics lifetime of the eddy: can be either a constant ($\tau_e = 2T_L = 0.3k/\varepsilon$) or a random value ($\tau_e = -T_L \log(r) = -\log(r)0.15k/\varepsilon$) where r is an uniform random number between 0 and 1.

The droplet is assumed to interact with the fluid phase eddy over this eddy lifetime. When the eddy lifetime is reached, a new value of the instantaneous velocity is calculated.

Heat and mass transfer calculations

When the water is injected in the gas flow field, the droplets can heat (or cool) and evaporation may occur. Fluent allows for the simulations of these heat and mass transfer phenomena in the dispersed second phase calculations. The available heat and mass transfer relationship are named as "laws" and for the water droplets in the present application the inert heating and cooling (Law 1) and droplet vaporization (Law 2) has been considered.

The inert heating or cooling law is a transfer relationship and it is active while the droplet temperature is less than the vaporization temperature. The vaporization temperature is defined by the user as a constant value (usually the initial temperature of the second phase) and so it defines the onset of vaporization.

Law 1 uses a simple heat balance to relate the droplet temperature to the convective heat transfer (the absorption of radiation at the droplet surface can also be included as an option):

$$m_D c_p \frac{dT_D}{dt} = h_c A_D \left(T_\infty - T_D\right) \tag{5.22}$$

where the heat transfer coefficient, h_c, is calculated using the Ranz and Marshall correlation (Ranz and Marshal, 1952)

$$\mathrm{Nu} = \frac{h_c d_D}{K_\infty} = 2.0 + 0.6\,\mathrm{Re}^{\frac{1}{2}}\,\mathrm{Pr}^{\frac{1}{3}} \tag{5.23}$$

It is assumed that the droplet temperature is uniform.

As the droplet trajectory is computed (Equations 5.17 and 5.19), this equation is also integrated analytically assuming that the droplet temperature changes slowly in the integration time step.

When the droplet temperature reaches the vaporization temperature, Law 2 becomes active. This law includes mass transfer and heat transfer effects.

The mass of the droplet is reduced taking into account the vaporization effect according to

$$m_D(t + \Delta t) = m_D(t) - N_{i'} A_D M_{i'} \Delta t \tag{5.24}$$

where $N_{i'}$, the molar flux of vapour is given by:

$$N_{i'} = k_c\left(C_{i',s} - C_{i',\infty}\right) \tag{5.25}$$

The rate of vaporization is governed by gradient diffusion, with the flux of droplet vapour into the gas phase related to the gradient of the vapour concentration between the droplet surface and the bulk gas. The mass transfer coefficient, k_c is calculated from the correlation (Ranz and Marshall, 1952):

$$\mathrm{Sh} = \frac{k_c d_D}{D_{i',m}} = 2.0 + 0.6\,\mathrm{Re}^{\frac{1}{2}}\,Sc^{\frac{1}{3}} \tag{5.26}$$

The droplet temperature is also updated according to a heat balance that relates the sensible heat change in the droplet to the convective and latent heat transfer between the droplet and the gas:

$$m_D c_p \frac{dT_D}{dt} = h_c A_D\left(T_\infty - T_D\right) + h_{fg}\frac{dm_D}{dt} \tag{5.27}$$

This equation is solved in Fluent using an adaptive time step Runge-Kutta technique.

Initial conditions

The dispersed second phase is introduced in the computational domain at a certain position (with initial conditions) and its trajectory is then computed along the continuous gas flow field.

Fluent provides different ways for input of the initial conditions for the dispersed phase. These initial conditions provide the starting values for all of the dependent discrete phase variables that describe the instantaneous conditions of an individual particle/droplet:

- (x, y, z) droplet position in a reference frame;
- (u_D, v_D, w_D) droplet velocities;
- d_D , droplet diameter;
- T_D, droplet temperature;
- m_D, mass flow rate of the particle stream that will follow the trajectory of the individual particle/droplet (required only for coupled calculations).

Each set of these initial conditions represents an "injection" of particle/droplet identified in Fluent by a label "injection number". Each injection or parcel means thousands of droplets assumed to have the same size, diameter, temperature, starting at the same spatial position with the same velocity components. The mass flow rate indicates the amount of liquid that will follow the same calculated droplet trajectory.

The user can define any number of different sets of initial conditions for dispersed phase droplets provided that sufficient memory has been allocated.

Boundary conditions

When the droplet reaches a physical boundary (like a wall or an inlet boundary), Fluent applies a discrete phase boundary condition to determine the fate of the trajectory at that boundary. These boundary conditions are defined by the user at each cell-type and they can be:

- reflection via an elastic or inelastic collision – rebounds the particle/droplet off the boundary with a change in its momentum defined by a coefficient of restitution;
- escape through the boundary - the particle is lost from the calculation at the point where it impacts the boundary;
- trap at the wall – terminates the trajectory calculation and if it is a case of an evaporating second phase, their entire mass is converted into vapour phase;
- passing through an internal boundary zone, such as radiator or porous jump;
- slide along the wall depending on the particle properties and impact angle.

For droplets of water, it was decided to simplify the simulation of the droplet trajectory at the boundary. Because the wall temperature was the same of the gas flow in the adjacent cells, the droplets are assumed to escape through all boundaries.

5.3.3 Coupling Procedure

As described above, the second phase trajectory calculations are based on the local gas flow field conditions (velocity, turbulence parameters, temperature, vapour concentration...). Fluent can include the direct effect of the droplets on turbulence generation or dissipation in the continuous phase and it is able to keep track of heat, mass, momentum gained or lost by each droplet injection, as its trajectory is calculated. These quantities can be incorporated in the subsequent continuous phase calculations and, in this way, to study the effect of dispersed phase on the continuous gas flow field.

This two-way coupling is essential to calculate an accurate solution for the two-phase flow.

The momentum transfer from the continuous phase to the discrete phase, S_D (Equation 5.2), is computed in Fluent by examining the change in momentum of a particle as it passes through each control volume in the Fluent model. This momentum change is computed as

$$S_D = \sum \frac{18\mu C_D \,\mathrm{Re}}{\rho_D d_D^2 24}(u_D - u)W_D \Delta t \tag{5.28}$$

This momentum exchange appears as a momentum sink in the continuous phase momentum balance in any subsequent calculations of the continuous phase flow field (Equation 5.2).

The mass flow rate of each injection, which has no impact on the droplet trajectory calculations, is now used in the calculation of the effect of second phase on the gas phase. It must be noted that when different trajectories are calculated for the same injection, in order to simulate the turbulence effects of the gas phase, the mass flow rate of that injection is divided equally by the number of stochastic tracks computed for that injection and so the exchange terms of momentum, mass and heat are calculated using the divided mass flow rate.

Similar calculations are made in each control volume to quantify the exchange of heat and mass between the two phases. The heat exchange appears as a source term or sink of enthalpy in the continuous phase energy balance and the mass exchange appears as a source of mass in the continuous phase continuity equation and as a source of a chemical species.

The coupling between the both phases can be automatically simulated in Fluent by solving alternatively the dispersed phase and the continuous phase equations (Figure 5.1), until the solution in both phases have stopped changing. Usually, the second phase calculations are made after a certain number of gas phase iterations.

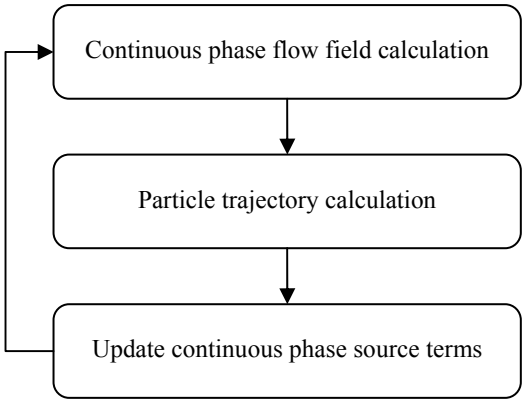

Figure 5.1 - Overview of the two-way coupling (Adapted from Fluent 6.2 User's guide)

5.4 Numerical Procedure

As mentioned before, Fluent uses a control volume based technique to solve the conservation equations for mass, momentum, energy, species and turbulence quantities. The domain is divided into discrete control volumes where the governing equations are integrated to obtain the algebraic equations for the unknowns (velocities, pressure and scalars). The integration of the differential equations in each control volume yields a finite-difference equation that conserves each quantity on a control-volume basis.

Because Fluent defines the discrete control volumes using a non-staggered storage scheme (all variables are stored at the control volume cell centre), interpolation schemes are needed to determine the face values of the unknowns from the stored values at the cell centre. Only the Power-Law Differencing Scheme (Patankar, 1980) has been used in the present application.

Fluent allows the choice between two numerical methods that employ the same discretization process (finite volume), but different approaches to linearize and solve the discretized equations: the segregated solver and the coupled solver.

The coupled solver solves the governing equations of continuity, momentum and energy and species transport simultaneously. Governing equations for additional scalars will be solved sequentially using the procedure described for the segregated solver.

The segregated was selected in the numerical simulations of this study and since the inflow is coming from a stationary domain, the absolute velocity formulation was used, which means that the governing equations are solved sequentially during several iterations before converged solution is obtained according to the sequence in Figure 5.2. In the momentum and turbulence equations discretization, the second order implicit method was applied.

The segregated solver was chosen rather than the couple approach due to the fact that this method is more appropriate for incompressible flow (which is the case in study) and the coupled approach was originally designed for high speed compressible flows (Fluent 6.2, User's Guide, 2005).

In the segregated solver the momentum and continuity equations are solved sequentially (Figure 5.2). In this sequential procedure, the continuity equation is used as an equation for pressure. However for incompressible flows, the density is not directly related to pressure. In this case, coupling between pressure and velocity introduces a constraint on the solution of the flow field: if the correct pressure field is applied in the momentum equations the resulting velocity filed should satisfy continuity. The SIMPLE

(Semi-Implicit Method for Pressure-Linked Equations) is used as a pressure-velocity coupling algorithm.

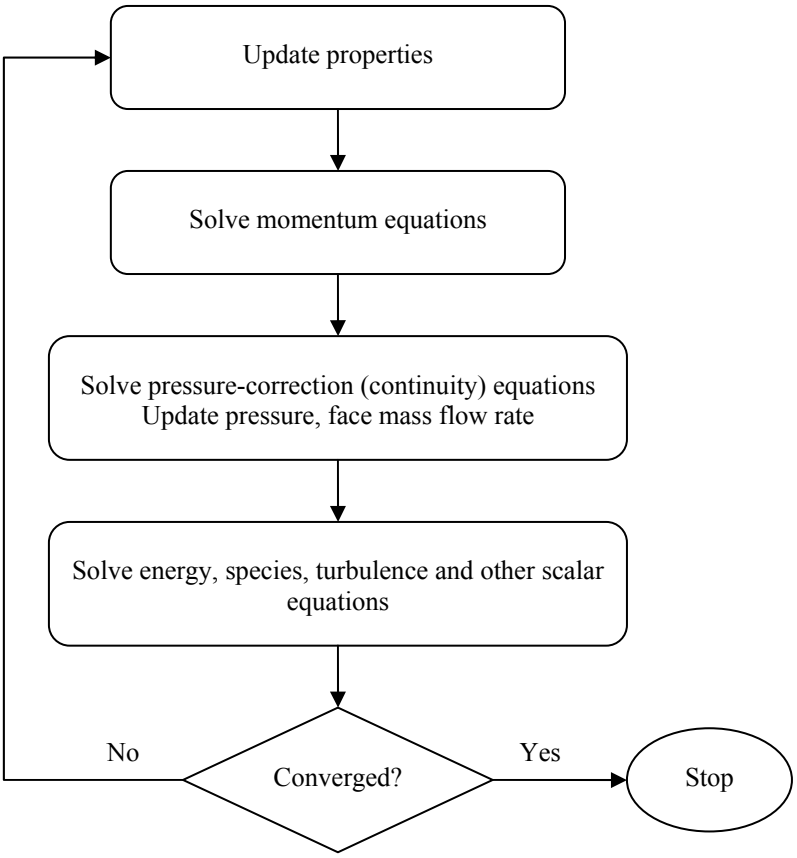

Figure 5.2 - Overview of the Segregated Solution Method (Adapted from Fluent 6.2 User's guide)

The SIMPLE algorithm is essentially a guess-and-correct procedure for the calculation of pressure by closing the discretized momentum equations with the continuity equations in a sequential manner (Versteeg and Malalasekera, 1995; Norton and Sun, 2006).

A good understanding of the numerical solution algorithm is crucial to achieve and optimize of the solution. But it is also important to infer about the success of such algorithms and prove conclusively that a numerical solution scheme is convergent. Convergence is the property of a numerical method to produce a solution which approaches the exact solution as the grid spacing; control volume size or element approch zero (Versteeg and Malalasekera, 1995).

During the solution process one can monitor the convergence dynamically by checking residuals, statistics, force values, surface integrals, and volume integrals. At

the end of each solver iteration, the residual sum for each of the conserved variables is computed and stored, thus recording the convergence history (Fluent 6.2, User's guide, 2005).

The algebraic equation for each variable is solved using a Line Gauss-Seidel procedure (LGS) and the user can specify the direction in which the lines are solved and the number of times the lines are solved in order to update a given variable within each global iteration cycle. To speed up the convergence achieved by the LGS procedure, Fluent uses a Multigrid acceleration technique (Hutchinson and Raithby, 1986).

The relaxation factors field defines the explicit relaxation of variables between sub-iterations. The relaxation factors can be used to prevent the solution from diverging. If the solution diverges, it should first try to stabilize the solution by lowering the relaxation factors and by reducing the time step.

It is good practice to start a calculation using the default under-relaxation factors. If the residuals continue to increase after the first 4 or 5 iterations, you should reduce the under-relaxation factors (Fluent 6.2, User's guide, 2005).

5.5 Output Results from Fluent

Fluent provides both graphical and alphanumeric reporting facilities for the gas flow field calculations and for the simulation results of the dispersed second phase.

After a converged solution have been obtained in the two-way coupling (this means that no major changes are occurring in both phases), the user has available information on the main dependent variables in the computational domain for continuous phase, namely, the velocity field, the temperature distribution and the turbulence parameters. Also, of some interest, is the mass fraction distribution of the species and the exchange terms of mass, momentum and heat between the phases.

For the dispersed phase itself, the main facilities available include: graphical display of the droplets trajectories and a step-by-step report of the droplet position, velocity, temperature, and diameter which can be stored in a file (droplet history file) for post processing. From this information for each injection, Fluent can generate a quantitative plot of these variables versus time.

Chapter 6

Numerical Simulation and Experimental Validation

This chapter presents the numerical results covering the simulation of multiphase flow in a venturi scrubber. The numerical parameters, the boundary conditions for the continuous and dispersed phases are presented.

The numerical results are then compared with available experimental data in the large scale venturi scrubber. Firstly, the single phase pressure drop results are discussed and the main discrepancies pointed out.

The most important trends on the pressure profile results for two-phase are discussed and the main conclusions are given. Finally, some comparisons has been made between the phenomenological model and the present results.

6.1 Grid Generation

Successful computations of turbulent flows are strongly dependent upon the grid generation. Because of the strong interaction of the mean flow and turbulence, the numerical results for turbulent flow tend to be more dependent of the grid than those for laminar flows. Hence, it is recommended to solve, with appropriatly fine meshes, the regions of high velocity gradients. Moreover, the flow is wall-bounded and requires appropriate resolution of the grid in the near-wall region, which is dependent upon the

combination of a wall function and the turbulence model (Ananthanarayanan and Viswanathan, 1999).

In this way, a sufficiently dense hexahedral mesh with near wall boundary layer is used. Grid refinements were also applied at the venturi inlet and at the transitions upstream and downstream of the throat section. The mesh was refined into a level that the results proved to be independent of further refinements.

Flow symmetry is assumed along the cross section of the scrubber. Hence only one-fourth of the scrubber volume is modelled, in order to reduce the computational time. The grid for this geometry is built using an available grid generation package – Gambit with the Hexahedral/Wedge Cooper mesh generation algorithm. The 3D final mesh is made of 15229 hexahedral elements (Figure 6.1).

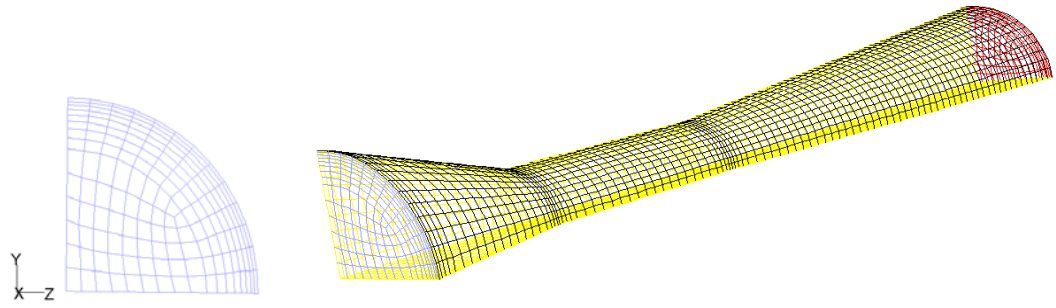

Figure 6.1 – Computational mesh of the circular venturi scrubber.

The Gambit package quantifies the quality of the grid by a dimensionless parameter: the skewness that represents the difference between the shape of the cell and the shape of an equilateral cell of equivalent volume. Highly skewed cells can decrease accuracy and destabilize the solution (Fluent, User's Guide, 2005). The lower the value the better the grid. By analysing the quality of the mesh, values of equivolume skewness within the range 0–0.25 are considered excellent, 0.25–0.5 are good and 0.5–0.75 are fair.

In this case, and in terms of equivolume skewness values, 96.14% of the control volumes were considered excellent and 3.86% could be described as good. The worst element of equivolume skewness is 0.45.

6.2 Numerical Simulation

The simulations were performed assuming atmospheric pressure and the gas flow was considered to be at the same temperature as that of dispersed phase and the solid walls.

Tests were made with different gas velocities, the same used in the experiments to allow a direct comparison between both the experimental and numerical data. The throat gas velocities were tested at: 34, 52, 61 and 70 *m/s*. In these conditions the air flow is highly turbulent, as the Re varies between 1.4×10^5 and 2.85×10^5.

The air velocity is used as a constant inlet condition, and an outflow condition is considered at the venturi outlet. Outflow boundary conditions are used to model flow exits where the details of the flow velocity and pressure are not known prior to solution of the flow problem. They are appropriate where the exit flow is close to a fully developed condition, as the outflow boundary condition assumes a zero normal gradient for all flow variables except pressure. They are not appropriate for compressible flow calculations (Fluent 6.2, User's Guide, 2005), which is not a key limitation for this problem. The turbulence intensity and the hydraulic diameter quantities are used to specify k and ε at inlet and outlet of the domain.

The geometry is modelled as a rigid wall with a no-slip velocity condition. The liquid mass flow rate was introduced through the spray nozzles at the venturi inlet. The liquid is injected into the gas core and is atomised into drops of varying size by the air stream. The droplet size distribution, following the RR distribution, is within the range from 15 to 1504 μm for all the simulated operating conditions. The initial liquid droplet velocity was assumed to be 1 *m/s* in the radial direction, towards the centre of the pipe.

Two injections as a group of 16 particle streams (representing a set of droplets having the same initial conditions, with the same minimum, mean and maximum diameter) were considered in the numerical tests. The mean diameter value was taken from the experimental measurements of the water spray (Figure 4.20). The injection points for the dispersed phase are: (0.001, 0.12, 0.001) and (0.001, 0.001, 0.12). These refer to the coordinate system described in Figure 6.1.

The liquid flow rate was set as those tested experimentally. Because only a fourth of the volume of the geometry is simulated, the total water flow rate is divided by four and equally distributed by the two injections.

The dispersion of the droplets due to the turbulence in the gas phase is predicted by using the stochastic particle tracking. This model requires two parameters that

control the time integration of the particle trajectory equations: the length scale and the maximum number of time steps used to abort trajectory calculations when the droplet never exits the flow domain. This is important for small particles that, due to the gas diffusion, may be under a Brownian motion. The values used for these parameters are 5 and 50000, respectively.

To account for the turbulence effect of the gas phase on the droplet trajectory calculations, each injection was calculated 30 times (tries) yielding a total of 960 trajectories. This value is not very high to be statistically representative of the turbulence fluctuations, but it was a compromise to allow a wide variety of tests, covering various parameters, at a reasonable computational time.

The boundary condition at the wall allows the droplets to escape from the flow domain as they reach the wall.

The two-way coupling between the phases was included in the simulation procedure: given the initial conditions for the gas flow field, a converged solution was determined for the continuous phase. At this stage, the dispersed phase calculations were performed and after this, every 10 iterations of the continuous phase the droplet trajectories were again calculated. For most of the cases, the steady-state solution was obtained with less than 1000 iterations.

In the present study, the convergence criterion is that residuals should drop to 10^{-6} for single-phase and 10^{-4} for two-phase flow simulations and the default under-relaxation factors are used which are 0.3 for the continuity equation, 0.7 for momentum equation and 0.8 for the turbulence kinetic energy and turbulence dissipation rate.

6.3 Single Phase Results

The turbulence inside the venturi determines droplet mixing in the two-phase flow. Hence, it is important to predict the single-phase gas flow as accurately as possible, as a step to solve the more complex air-liquid flow.

6.3.1 Numerical results

Two different *k-ε* turbulence models were tested and compared for the maximum throat air velocity, *70 m/s*: the standard and the renormalization-group (RNG). The axial velocity along venturi is presented at Figure 6.2, for those two models.

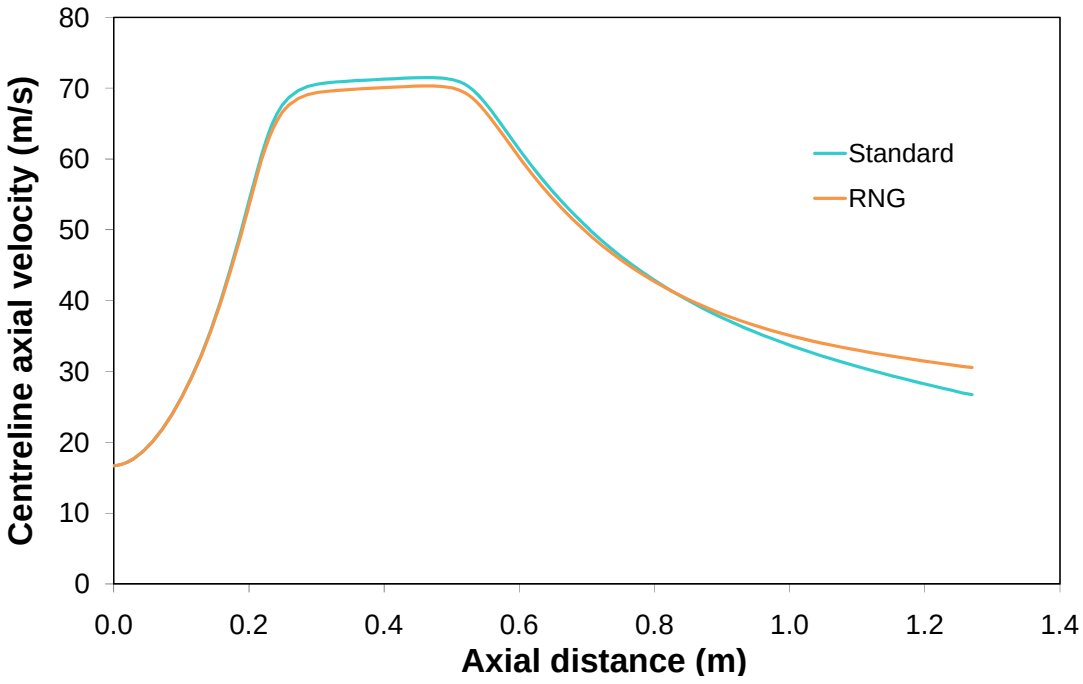

Figure 6.2 – Axial velocity along the venturi centreline.

The results are very similar for the two *k-ε* models, being within 14% of each other at the venturi outlet.

As explained before, the RNG model has been used in the subsequent numerical simulations which has proved appropriate by other authors (Ananthanarayanan and Viswanathan, 1999).

In Figure 6.3 the axial velocity profile at the centreline is presented for different throat gas velocities and the velocity vectors along venturi, at the medium *y* plan, are presented in Figure 6.4.

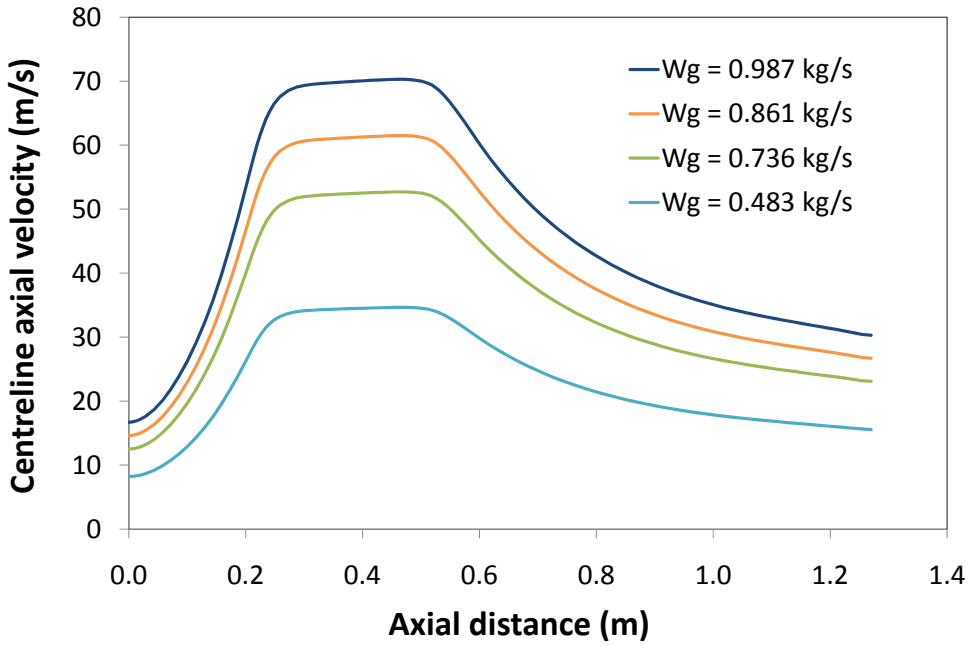

Figure 6.3 – Axial velocity along the venturi as function of gas flow rate.

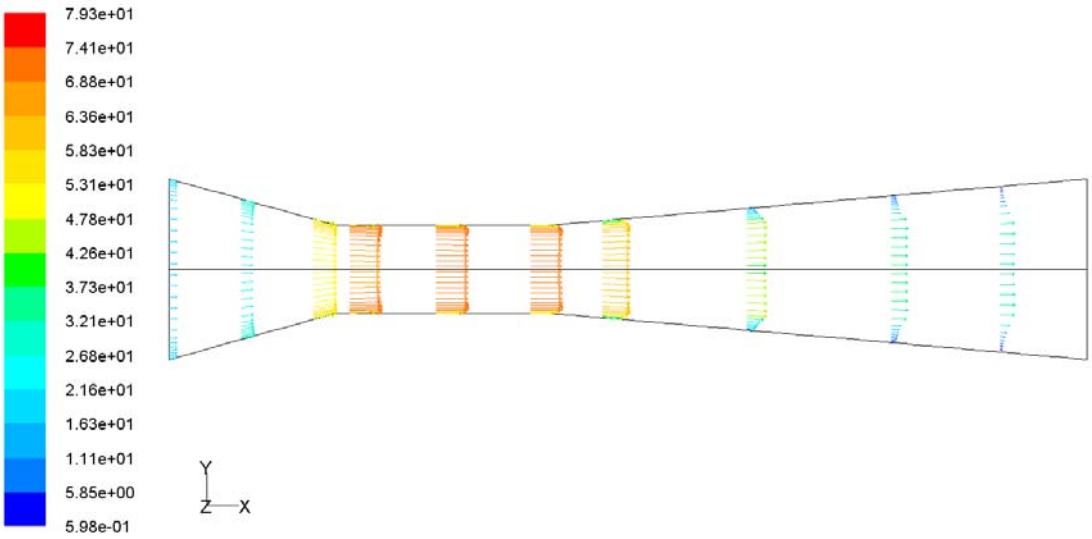

Figure 6.4 – Velocity vectors profiles at medium *z* plan (throat velocity 70 *m/s*).

The boundary layer growth in the divergence section can be observed. In the converging section the flow is of favourable pressure gradient and this is close to zero in

the throat. At the expanding-area diffuser a reduction in the velocity is observed, along a steep increase of the boundary layer thickness.

The wall pressure drop along venturi, relative to the inlet pressure, for single phase flow cases, is presented in Figure 6.5. The effect of gas velocities on the pressure drop can be observed and it seems correctly predicted.

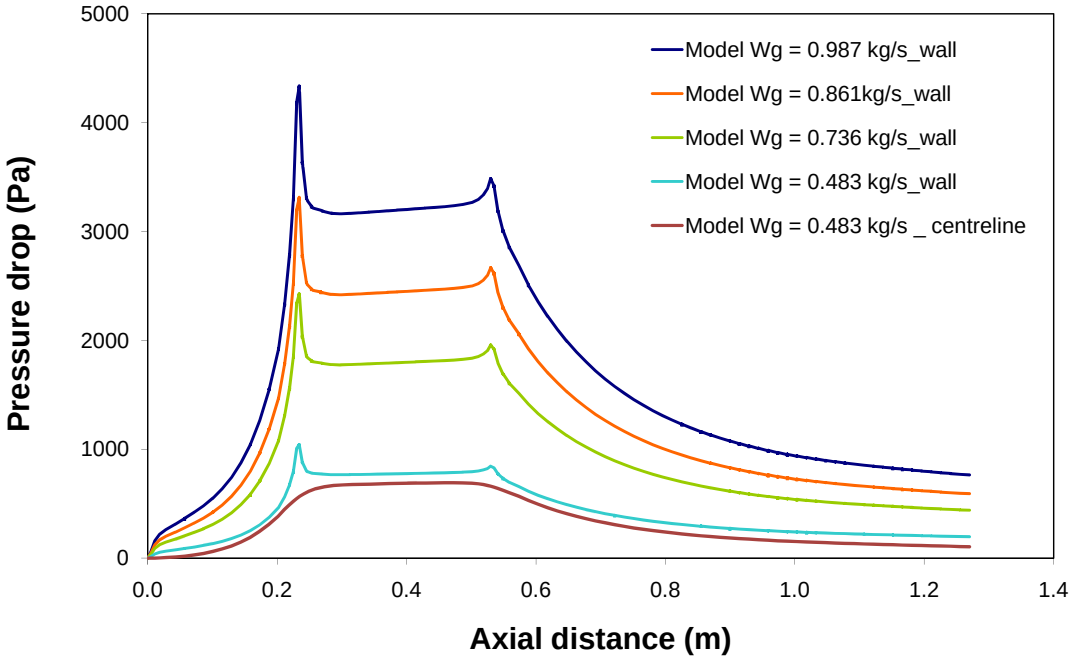

Figure 6.5 – Effect of the gas velocity on pressure drop.

The sharp peaks in the predicted pressure drop are representative of losses at the sudden transitions at the intersection between the throat and the converging or diverging sections. These effects are not presented on the centreline pressure drop profile also presented in Figure 6.5, to the lowest gas velocity.

6.3.2 Comparison with experimental data

The variation of the total pressure drop along the venturi, for the maximum throat air velocity, 70 *m/s*, is shown in Figure 6.6 with the experimental data for the large scale venturi scrubber. Small discrepancies can be observed at the end of convergent section. But the total pressure drop upstream of the divergence is well predicted.

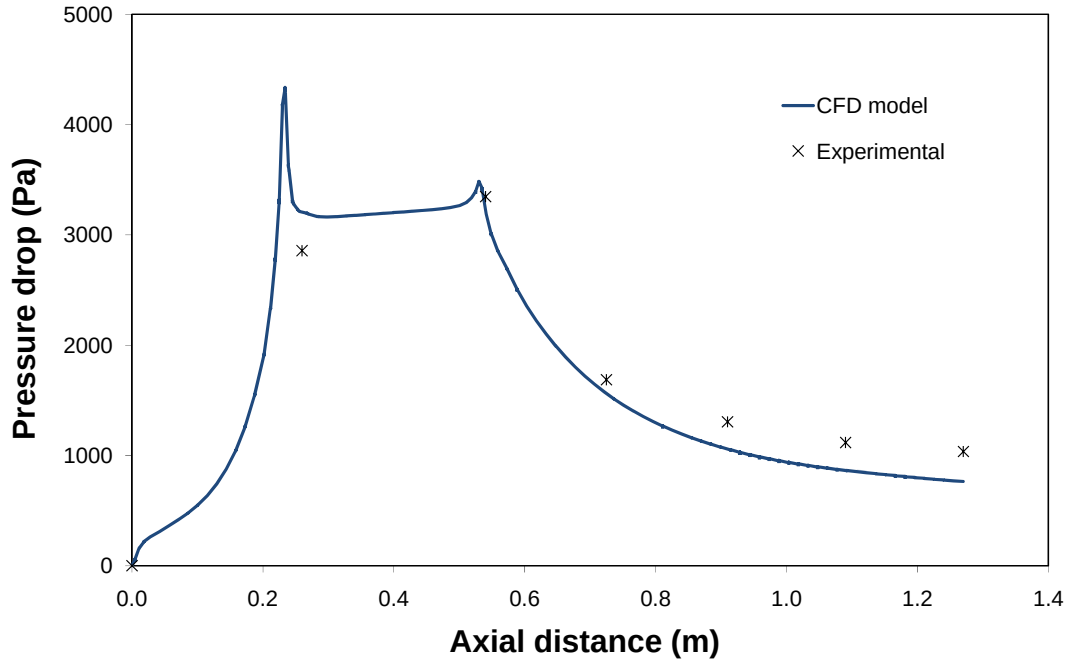

Figure 6.6 – Comparisons between experimental and predicted pressure drop. $U_{GT} = 70$ *m/s*.

Figure 6.7 shows the wall pressure drop along the venturi, refered to that at the venturi inlet, for various gas velocities.

The discrepancies between the experimental data and the model simulations are more evident for higher velocities.

The predicted pressure drop up to the throat and the total pressure drop are plotted against the gas throat velocity in Figure 6.8. The results are very encouraging, considering the uncertainties associated with the experimental data. This is highlited in Figure 6.8 when the pressure drop up to the throat and the total pressure loss are plotted against the gas throat velocity.

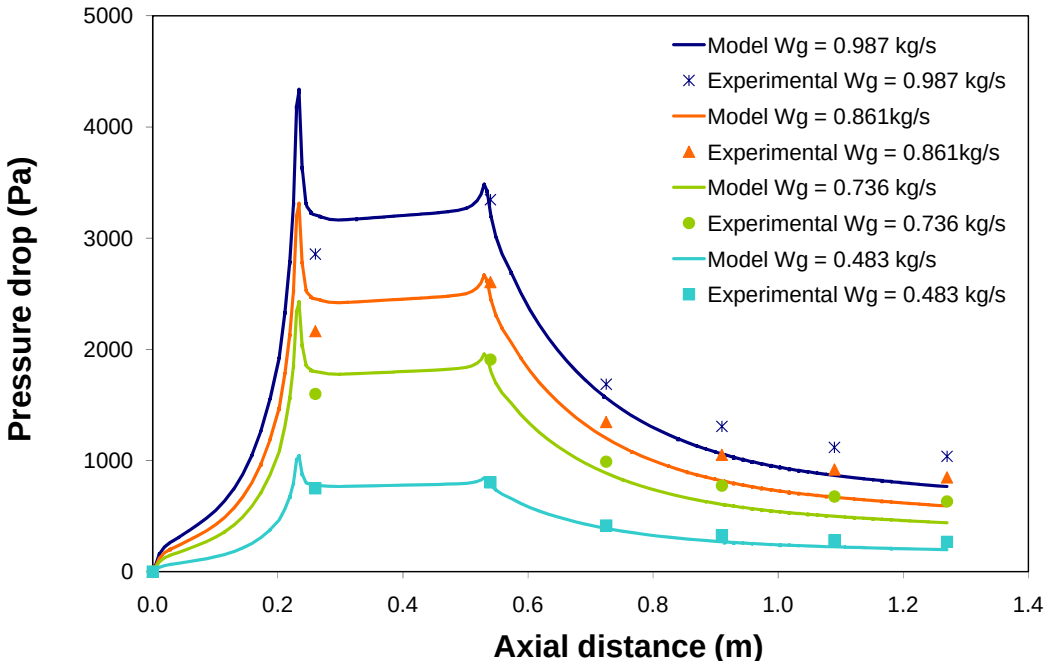

Figure 6.7 –Experimental and numerical pressure drop comparison for various air flow rates.

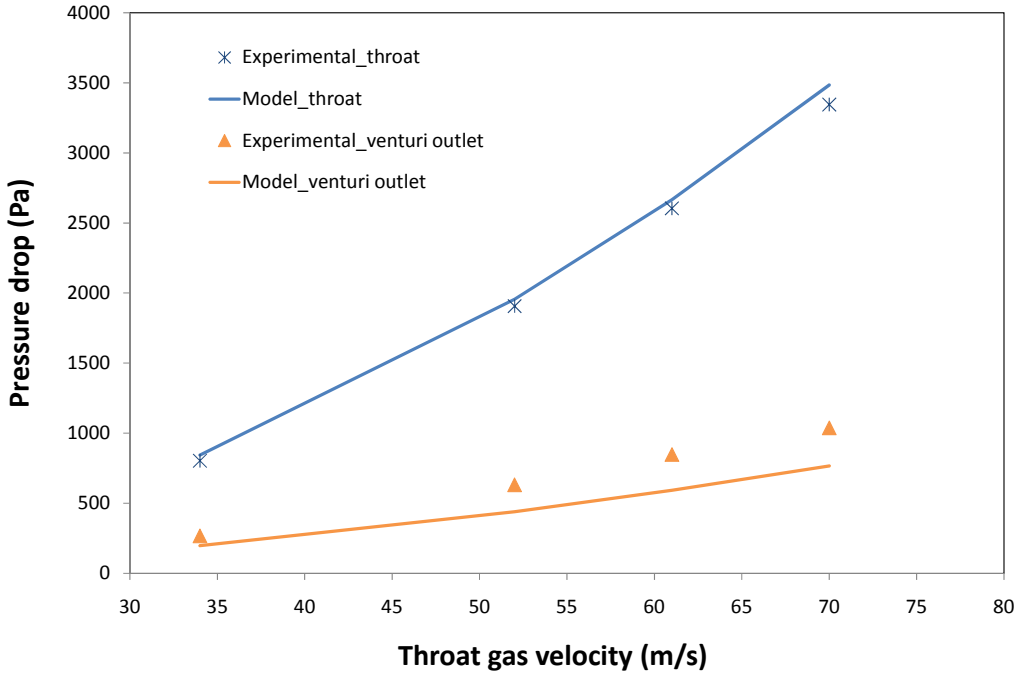

Figure 6.8 – Experimental and numerical total pressure drop as a function of the throat gas velocity.

In Figure 6.9, the pressure drop for each one of the sections of the venturi (convergence, throat and divergence) is compared with the experimental data.

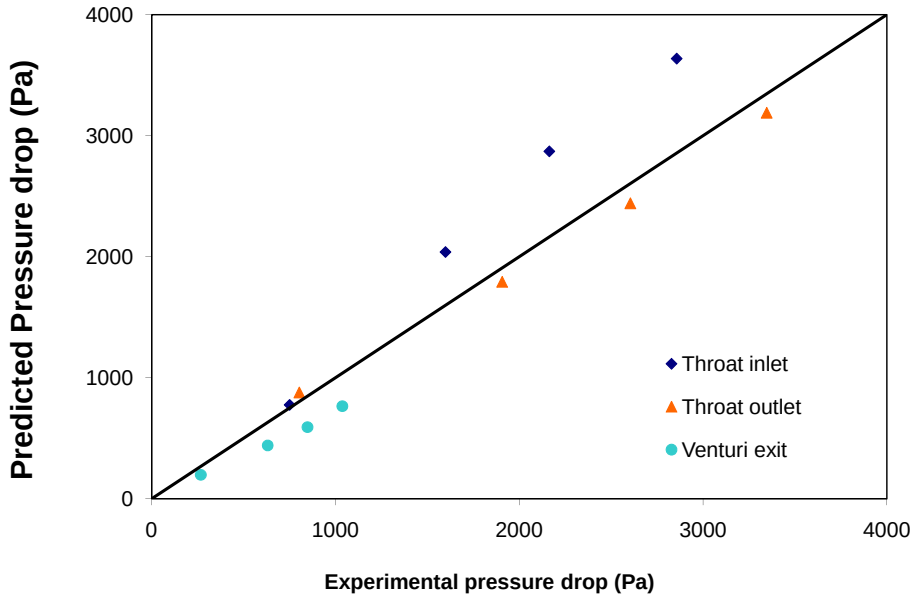

Figure 6.9 – Comparative pressure drop predicted by CFD and experimental data, for each section

The effect of the sudden bend between convergence and throat can explained the differences in the pressure drop upstream of the throat.

Because no other experimental measurements (such as velocity vectors and turbulent kinetic energy, k) are available on the single-phase flow, a more comprehensive validation of the model predictions is not possible.

6.3.3 Discussion

The 3D computational model used to describe the flow inside a venturi scrubber has assessed the application of various turbulence models and the results have been compared with experimental data for a large scale venturi scrubber.

The results show that the turbulence models show similar results for a wide variety of flow conditions.

The predicted pressure drop along the venturi follows the experimental data, including the pressure recovery in the diverging section. The model shows some

discrepancies with the experimental data in the convergent section regarding the prediction of the pressure drop.

The velocity profiles predict a boundary layer of reduced thickness in the converging section and a substantial growth in the diverging region. Flow separation is not observed.

6.4 Two-Phase Flow Steady State

The effect of the dispersed phase was then simulated and the results are presented separately for both the continuous and dispersed phases. Experimental validation of the pressure drop results is then presented.

6.4.1 Continuous phase

The influence of the second phase is well illustrated in Figures 6.10 and 6.11, for two gas throat velocities (70 and 34 *m/s*). For each one, the effect of the liquid loading is also studied. This effect is stronger for the lowest gas velocity and the highest liquid flow rate. The reduction of the gas velocity at the centreline (Figure 6.11) can be explained by the momentum losses due to the droplet acceleration in the throat. In fact, the higher momentum of the liquid jets means that most of gas droplet interactions occur in the centre of the tube, reducing there gas momentum as droplets are accelerated. The velocity vectors in Figure 6.12 also ilustrate this behaviour.

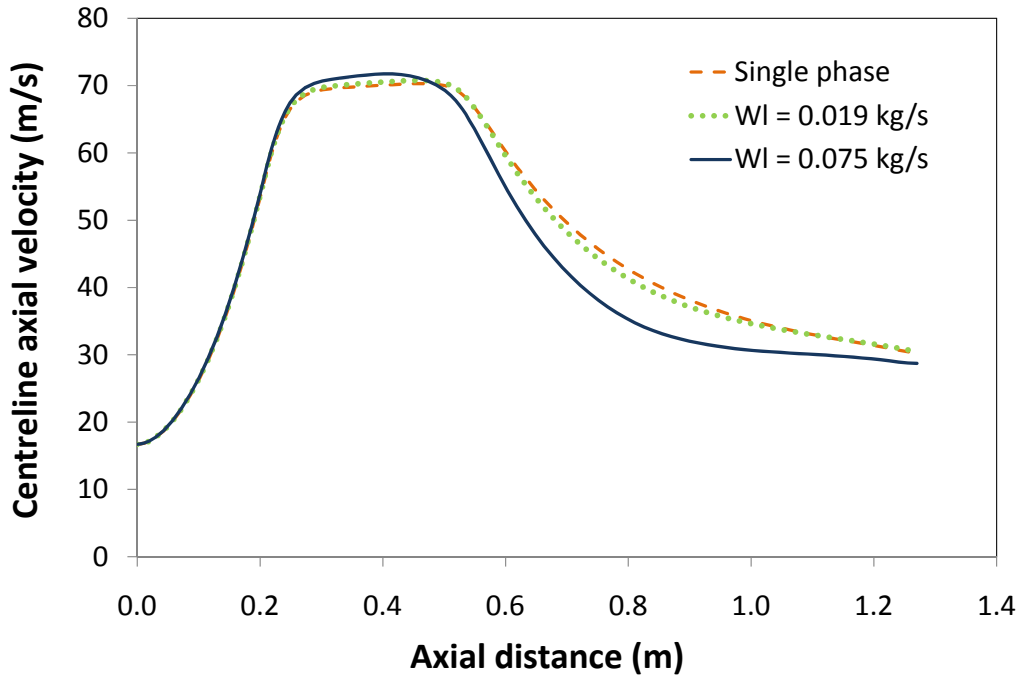

Figure 6.10 – Influence of the liquid upon the velocity along the venturi. U_{GT} = 70 *m/s*.

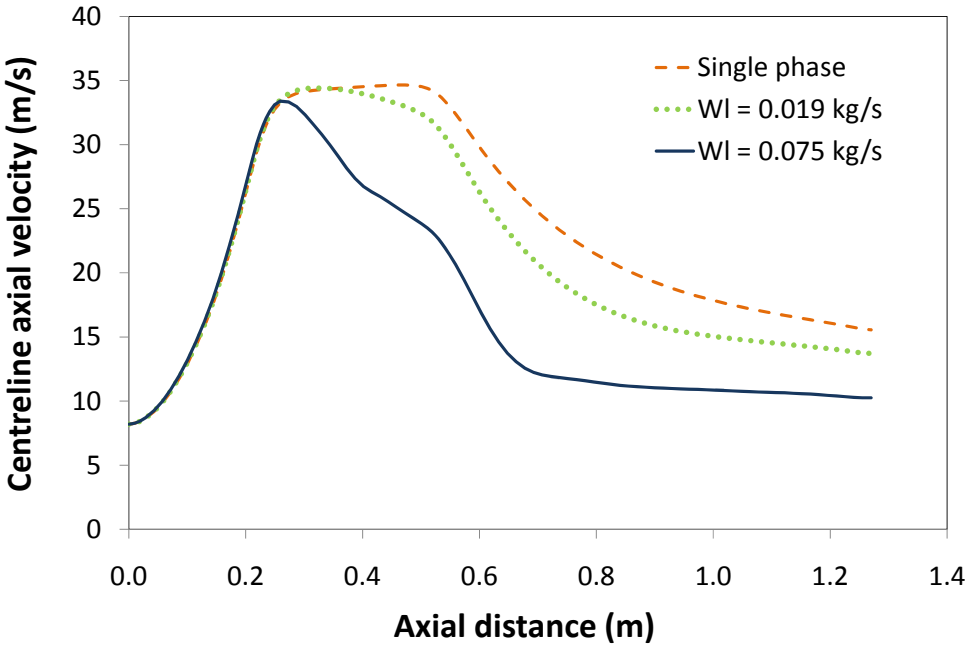

Figure 6.11 – Influence of the liquid loading upon the velocity at the venturi axis U_{GT} = 34 *m/s*

Simulations carried out with a different code (KIVA), of a spray in a small diameter (0.07 *m*) venturi (Pak and Shang, 2006), also show that the liquid droplets reduce the gas velocity in the vicinity of the spray core.

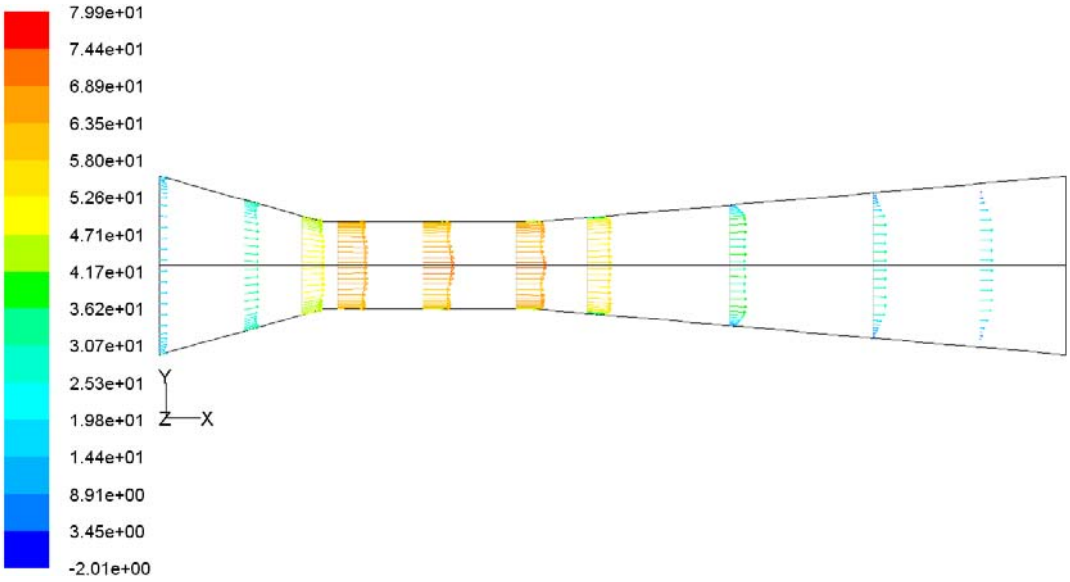

Figure 6.12 – Velocity vectors for the continuous phase. W_G = 0.987 *kg/s* and W_L = 0.075 *kg/s*.

Of interest are the simulation results for the turbulence parameter *k* (Figure 6.13) when the single and two-phase continuous field are compared.

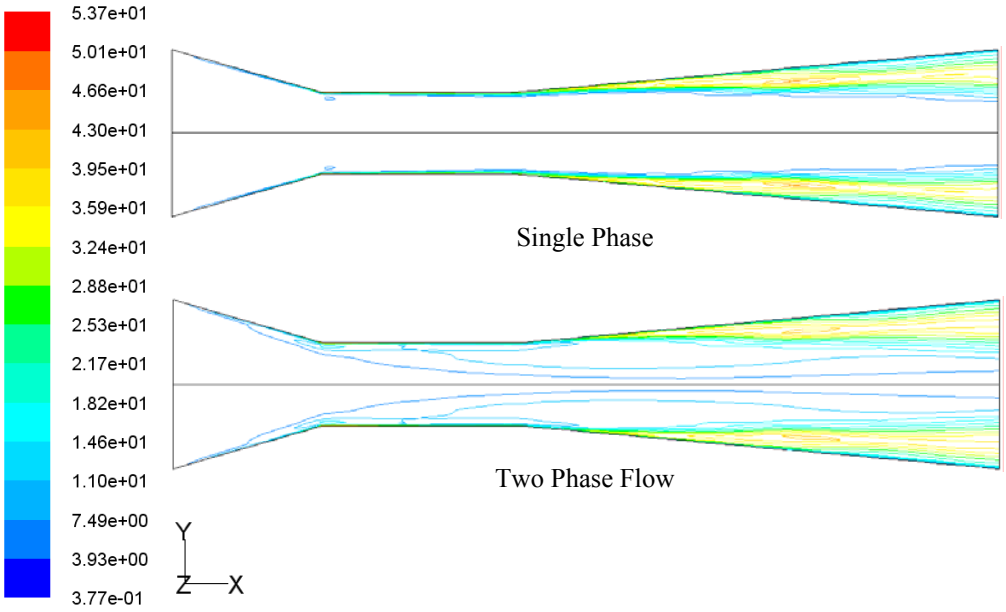

Figure 6.13 – Influence of the discrete phase onthe continuous phase kinetic turbulence (*k*).

The results shows that while in a single phase flow, turbulence kinetic energy is higher in the boundary layer, the presence of a dispersed phase increases the k in the core of the flow. This feature may be associated with the momentum interchange between the gas and the droplets downstream of the injection point.

In fact, this is illustrated in Figure 6.14 where the source term in Equation 5.2 is plotted as contours of constant S_D. The results show a close relashionship with those from Figure 6.13: the increase in k in the gas core matches the patterns of momentum interchange between the phases.

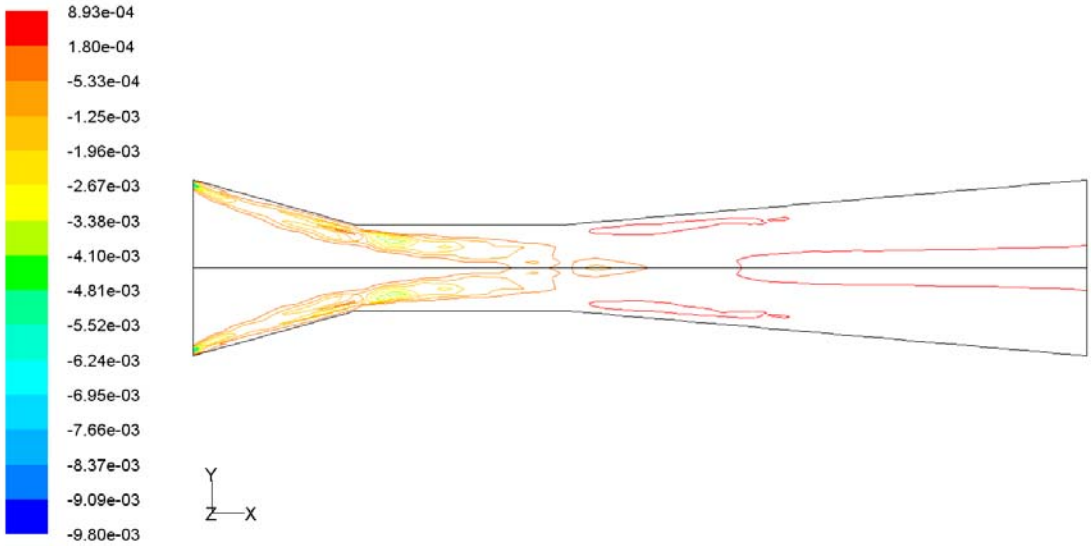

Figure 6.14 – Interphase momentum exchange ($kg.m/s^2$).

The liquid concentration is plotted in Figure 6.15. The location of the liquid injection and its subsequent dispersion is clearly observed. Also, this behaviour is in accordance with the momentum interchange between the phases (Figure 6.14).

It also show that, except in the region very close to the nozzle exit, the liquid concentration is very low, which validates the assumption of a dilute liquid phase.

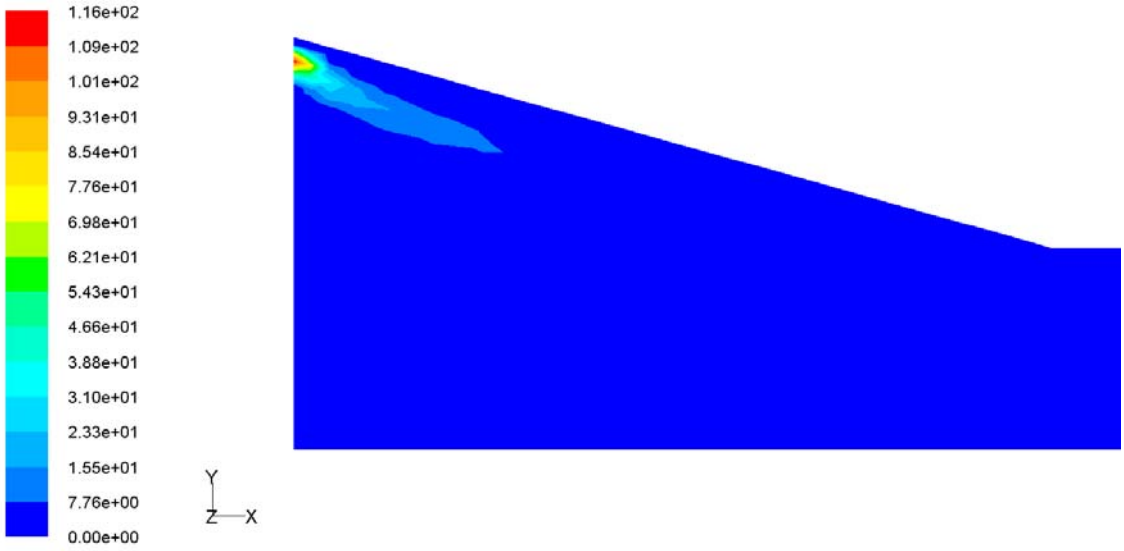

Figure 6.15 – Discrete phase concentration (kg/m^3). W_G=0.987 *kg/s* and W_L=0.075 *kg/s*.

6.4.2 Dispersed second phase

The study of the droplets behaviour is presented for throat gas velocity of 70 *m/s* and total liquid flow rate 0.075 *kg/s*. The particles trajectories are represented in Figures 6.16 through 6.20.

Figure 6.16 depicts the particles trajectories and their residence time. It could be observed that in the diverging section, virtually all the particles flow outside the boundary layer, in the core of the gas. This vindicates the option of restricting the two-phase boundary layer model (Cruz, 1997) to the region outside the boundary layer. Obviously this does not take into account the fact that droplets are also entrained from the wall film although this may be of lesser relevance if the liquid is injected as droplets from a nozzle. In addition the Brownian type of motion for the few particles that are transported into regions close to the wall, suggests that only the smaller particles may travel inside the boundary layer.

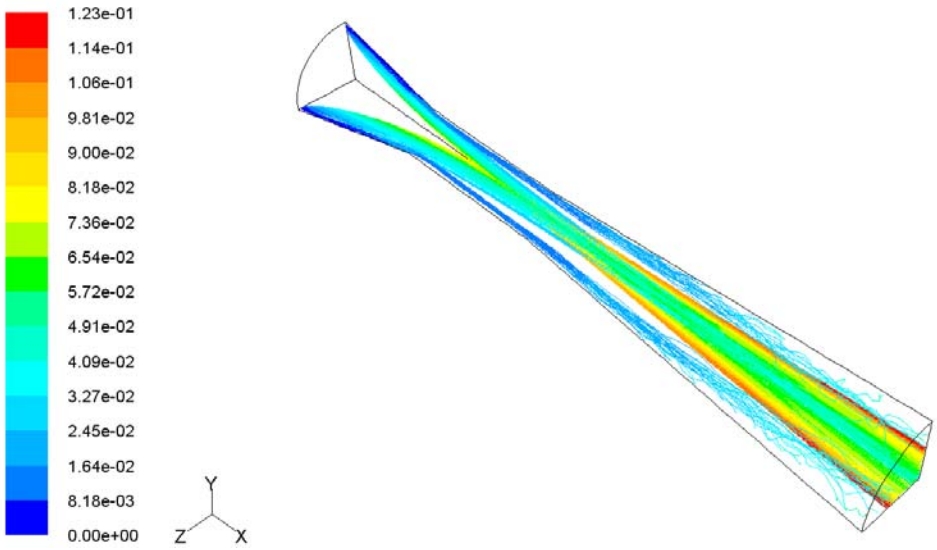

Figure 6.16 – Particle Trajectories identified by particle residence time (*s*)

The hypothesis that smaller particles may travel inside the boundary layer can be observed in Figure 6.17 which shows the trajectories for the particles of 15.5 μm in diameter.

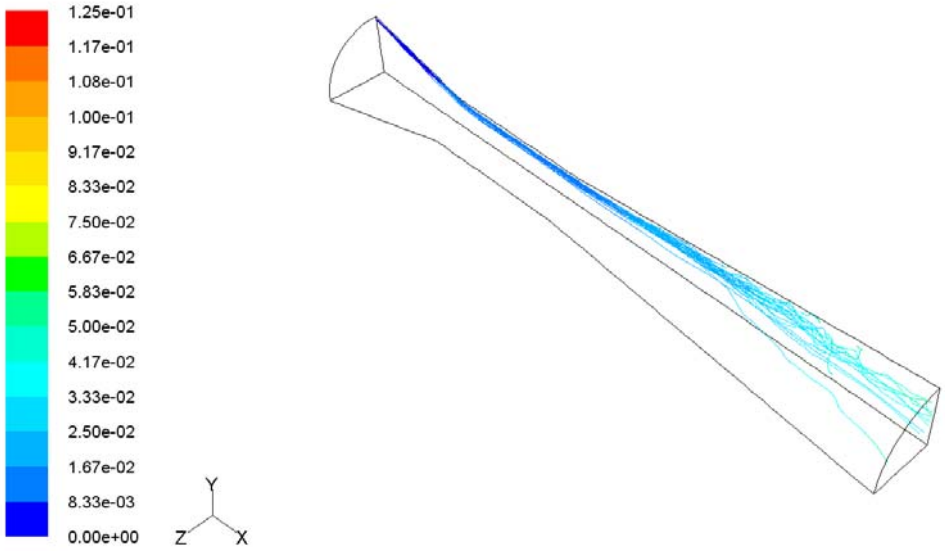

Figure 6.17 – Particle Trajectories for the smaller droplets (15.5 μm) identified by particle residence time (*s*)

However, larger particles do show a trajectory dominated by inertia which prevents them to be transported into the boundary layer in the divergent section as shown in Figure 6.18.

In addition, due to their higher inertia, large particles have longer residence times inside the venturi (Figure 6.17 and 6.18).

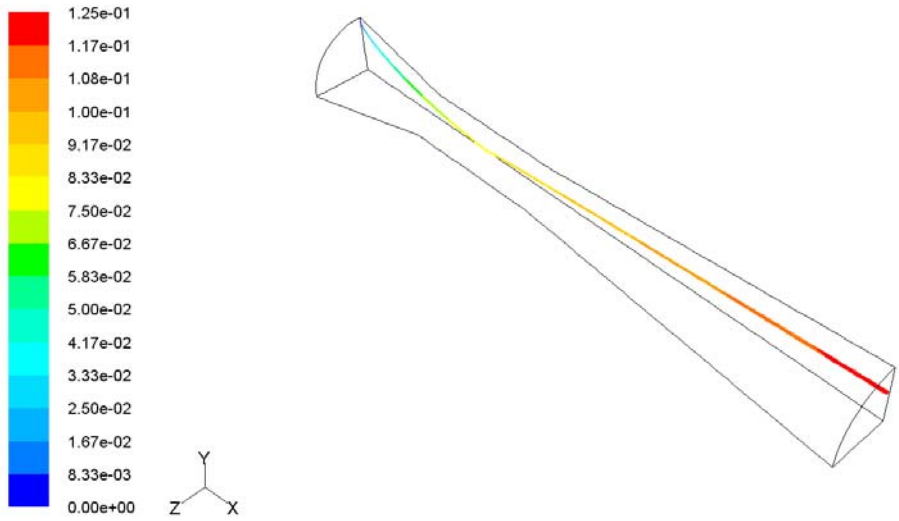

Figure 6.18 – Particle Trajectories for the larger droplets (1504 μm) identified by particle residence time (s)

The x component of the particles velocity can be visualized in Figure 6.19. This figure shows that particles accelerates to its maximum velocity in the throat, as expected. By comparing the trajectories in Figure 6.19 with those from Figures 6.17 and 6.18, one can also conclude that the smaller particles are accelerating to the higher velocity faster then the larger ones. In addition they also show a corresponding deceleration in the diverging section.

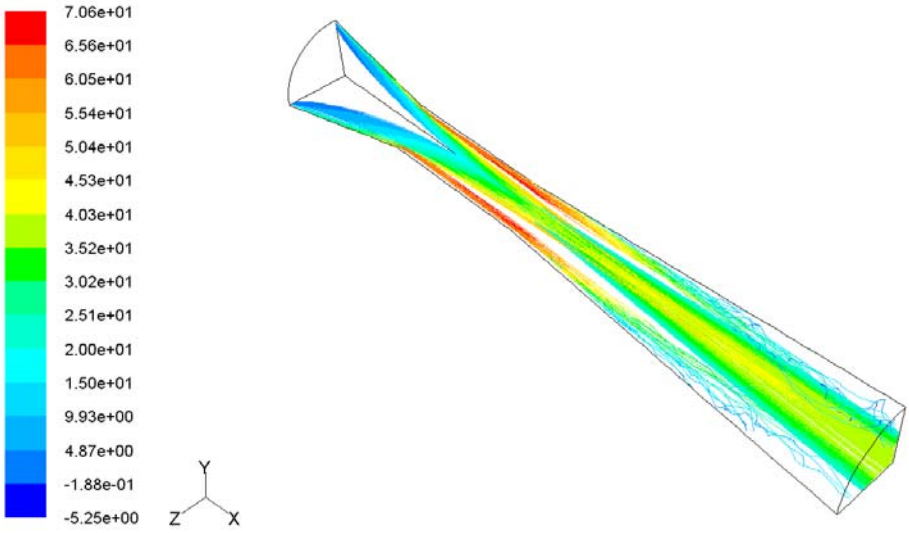

Figure 6.19 – Particle trajectories identified by particle x velocity (m/s)

Figure 6.20 shows the particle trajectories identified by the diameter of the particles. The largest particles tend to flow in the center of the air stream when the smaller ones are spread over the cross section of the tube, with a small number of them flowing inside the boundary layer.

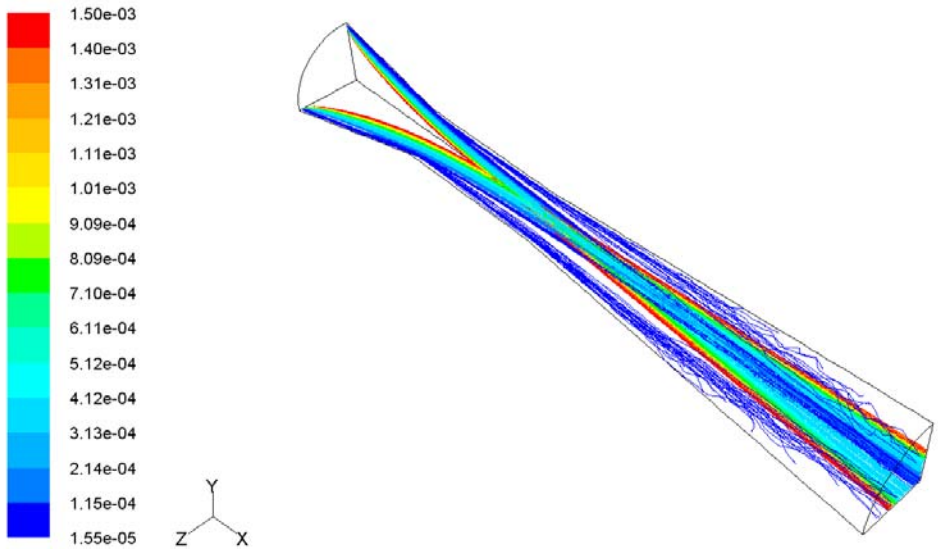

Figure 6.20 – Particle trajectories identified by particle diameter (*m*)

6.4.3 Experimental validation

The numerical results obtained are validated against the experimental data with liquid injected as a spray since this is the condition closer to those simulated. As discussed in chapter four, the comparisons refer to the pressure drop.

Figure 6.21 shows the pressure drop along the venturi and the comparisons with the computational model for both single and two-phase flows. These are compared for all the flow combinations tested in laboratory (Figure 6.22). The overall agreement is very good except for the highest gas and liquid flow rates (points at the right hand side of the graph).

The experimental pressure drop values are always higher then those calculated, which is in agreement with the pressure drop profiles shown in Figure 6.21. However, the results are apparently better for the lower gas flow rates.

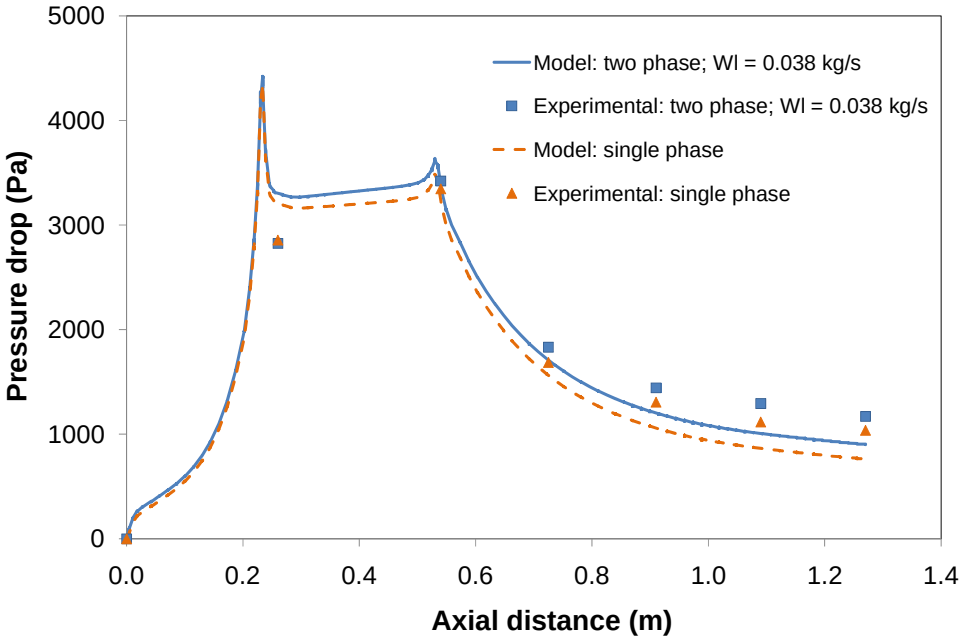

Figure 6.21 – Comparison of pressure drop profiles predicted by the CFD model and experimental data. $U_{GT} = 70\ m/s$.

The cause for the poor agreement in some of the tested cases can be further investigated in Figure 6.23 which compares the pressure drop in each one of the sections of the venturi with the local pressure drop. The results show that it is in the throat that most of the discrepancies are observed.

The small discrepancies observed in all the sections can be due to the poor description of the liquid phase.

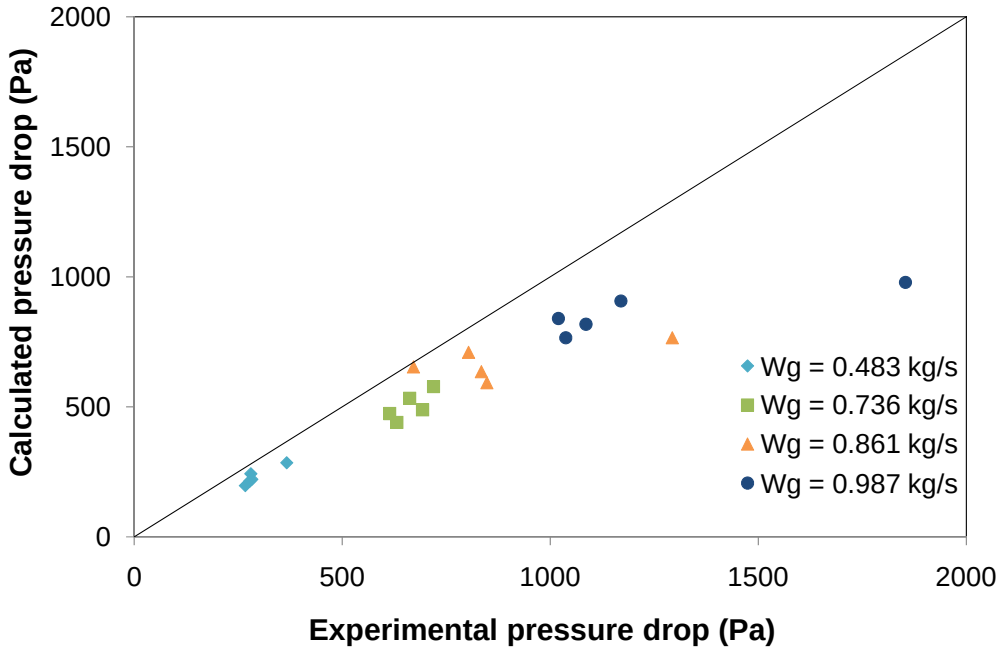

Figure 6.22 – Comparative total pressure drop predicted by CFD model and experimental data.

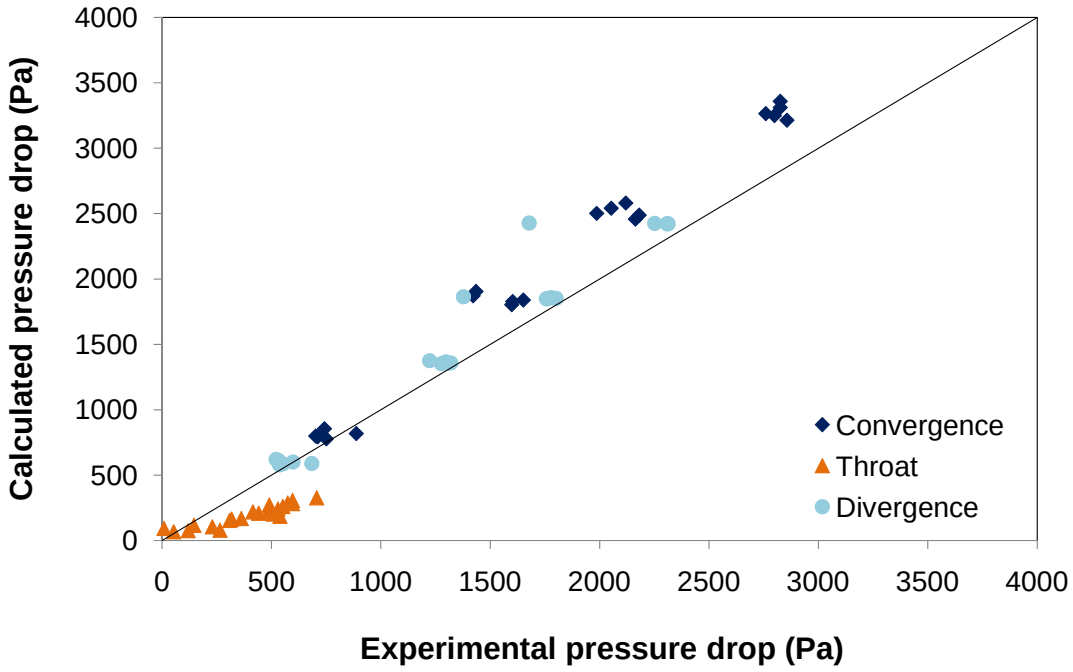

Figure 6.23 – Comparative total pressure drop predicted by CFD model and experimental data for each section.

6.4.4 Discussion

Figure 6.24 compares the CFD model and the model by Cruz (1997) with the experimental pressure drop along the venturi. With the CFD model the experimental results can be directly compared with, because information at the wall is readly available.

In fact, pressure is measured at the wall and the CFD results can describe the sudden transitions in geometry at the converging/throat and throat/diffuser intersections. In addition the 1D Bounday Layer model is in good agreement with the centreline pressure calculated with the CFD model and compares favourably with the experimental data regarding the pressure recovery in the diffuser. One reason is that even for liquid spray injection, downstream of the venturi the liquid is deposited and entrained from the film. This feature is the basis for the 1D model, which appears to be relevant in annular flow. Therefore, fully dispersed phase flows may not be limited in describing the physics of the flow.

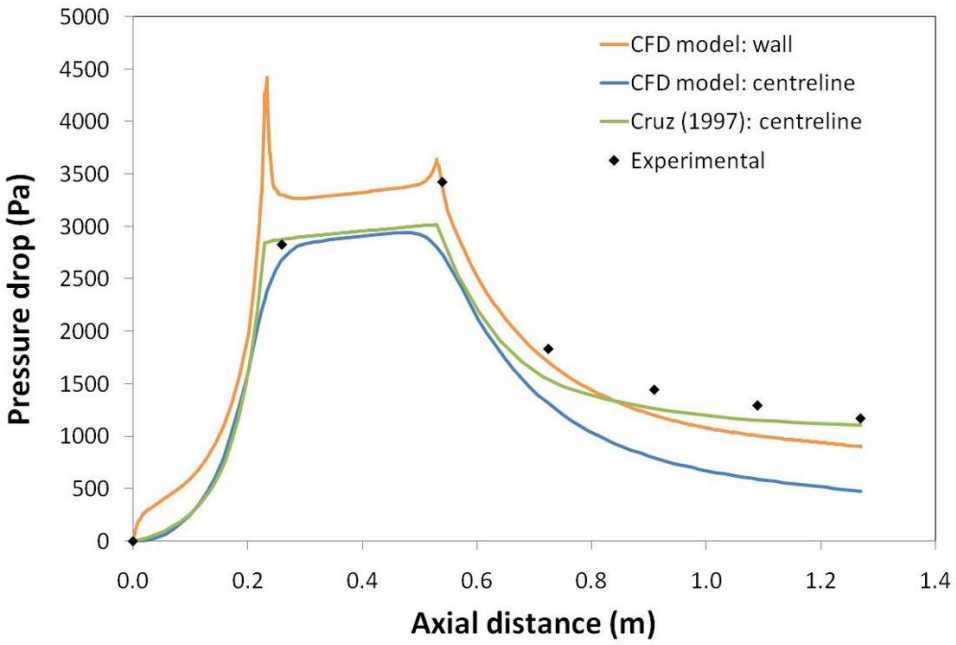

Figure 6.24 – Comparison of pressure drop profiles predicted by the CFD model, the Cruz (1997) model and experimental data. $W_G = 0.987$ *kg/s* and $W_L = 0.038$ *kg/s*.

Chapter 7

Conclusions and Future Work

The conclusions that may be drawn from the current work and suggestions into how future work could be developed are a direct outcome of the present thesis. Here they are outlined.

7.1 Conclusions

Concluding remarks have been detailed throughout the thesis. In here, the main conclusions of the present work are put forward.

A comprehensive review of published work shows that experimental data in a large scale venturi are very scarce. In this way, and in order to fulfil this gap, an experimental rig with a large scale venturi scrubber, closer to the industrial size, has been built at the University of Minho. An extended set of data in pressure drop and droplet size can be obtained. The experimental apparatus has also been modified to get preliminary results of collection efficiency.

The experimental data also cover different types of liquid injections and extend the available data to lower ranges of liquid to gas ratio.

The liquid to gasratio influence on the total pressure drop, although smaller than that of the gas velocity, is stronger for high gas throat velocities. In addition, within this range of flow conditions, a minimum is observed for each gas flow rate. This

observation was linked to the competing mechanisms in droplet formation in annular two phase flow: turbulent break-up and droplet coalescence.

The droplet size measurements have highlighted their deep contribution to the venturi performance. However the data have shown that the existing correlations are not appropriate to model the dispersed phase in large scale facilities, particularly in the convergence and throat sections.

When the correlations are applied, neither the throat nor the exit velocities are suitable for predicting the mean droplet size. One should point out that most of them were developed for straight tubes which do not capture the complexities of the gas droplet interactions in a venturi scrubber. Evidence of droplet coalescence is found with the data. Spray injection and high gas and liquid flow rates are the most favourable conditions.

The droplet size is strongly affected by the method for liquid injection. When liquid is injected as spray, the nozzle characteristics (type and orifice) and the upstream interactions with the gas are the most relevant variables. The effect upon the overall pressure drop was clearly identified.

The droplet distribution may show multiple peaks, particularly downstream in the venturi. Furthermore, the long length of the venturi favours the occurrence of secondary droplet break up as the mean droplet size decreases. Spray injection favours such occurrence.

These new set of data has been used to validate some improvements made in the research group to a phenomenological model (Cruz *et al*., 1997). The prediction for the total pressure drop was found good in special, the recovery pressure in the diffuser. The results also show that the inviscid model used in the convergence and throat section is clearly inadequate for predicting experimental pressure drop in the throat region.

In addition, a 3D CFD multiphase model has been developed using the Fluent code. The model uses an Eulerian/Lagrangian approach and a two-way coupling between the phases has been included. The overall agreement is very good except for the highest gas and liquid flow rates.

The work also suggests that the liquid exchange between droplets and the film plays an important role in the flow dynamics, particularly in the divergent section. Most of the discrepancies regarding the pressure drop result from a less than good ability to describe the flow inside the throat. Liquid interchange between the film and the

dispersed phase and the high liquid concentration in the gas core are not properly accounted for by both models.

7.2 Future Work

Based on the above conclusions and in order to develop the research further, some suggestions are now given:

- in order to get a complete validation of the CFD Fluent code, it will be interesting to obtain the velocity profiles along the venturi using the Laser Doppler Anemometer technique;
- additional measurement points of pressure drop along the convergence and throat will get some useful information, in order to better understand the two-phase flow physics in especial interchange between the film and droplets, in these two sections of the venturi;
- establish new droplet size correlations, applicable for large scale venturis, based on the experimental data presented. Some steps have been taken and preliminary results have been presented (Silva *et al.*, 2008);
- improve the method for collection efficiency and collect data using the large scale test facility;
- the test facility should be improved in order extend the liquid flow rate into higher fluxes;
- other combinations of throat length could be useful in order to better understand the flow dynamics and droplet interaction;

Appendix A

Collection System

This appendix describes an experimental setup that was developed for measuring the collection efficiency in venturi scrubbers. Some preliminary results are also presented.

A.1 Solid Particle Introduction System

In the industrial applications dust particles are already airborne but in the laboratory they have to be introduced into the flow. Their introduction could, on a first approximation, appear to be very straightforward but due to the nature and the features of the particles involved that proved not to be the case. Finally, they have to be fed at a controlable rate in order to make the results meaningful and reproducible. They also must have known characteristics (density and size) in order to assess the influence of such variables in the collection efficiency inside the venturi. Finally, the compaction of the powder is a possibility. Early tests with aluminium oxide (Al_2O_3) proved to be prone to colmatation (Espaze, 2005).

Figure A.1 represents the system that was developed to introduce the dust particles. Their introduction takes place upstream of the water droplets injection (Figure 3.2).

In order to have a constant flow rate of particles, the best option was to agitate the particles in order to break the adhesion forces. This mechanical agitation will allow the particles to move under their own weight.

The particles are introduced into the gas flow through a small venturi centred with the axis pipe, as depicted in Figure A.1. This induces a pressure reduction below atmospheric pressure that improves the suction of particles into the main flow.

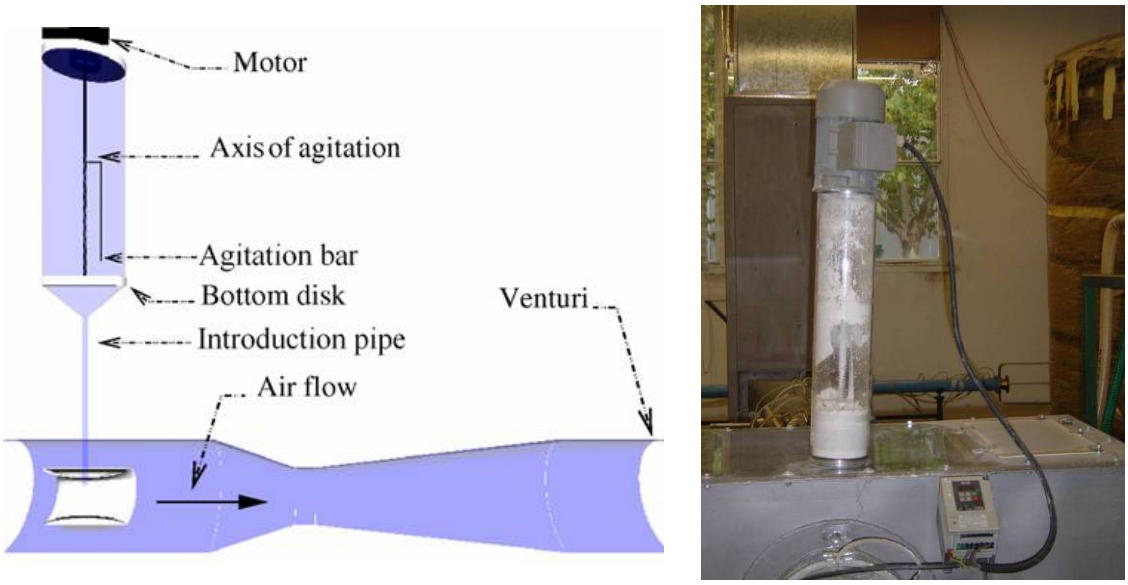

Figure A.1 – Schematic representation of solid particle introduction system

The test rig was built with a $180W$ motor which was controlled by a dimmer switch to change the electrical frequency supplied to the motor. The agitation level was always low. Various tests were carried out by changing the values on the switch which led to different rates of particle supply (Figure A.2).

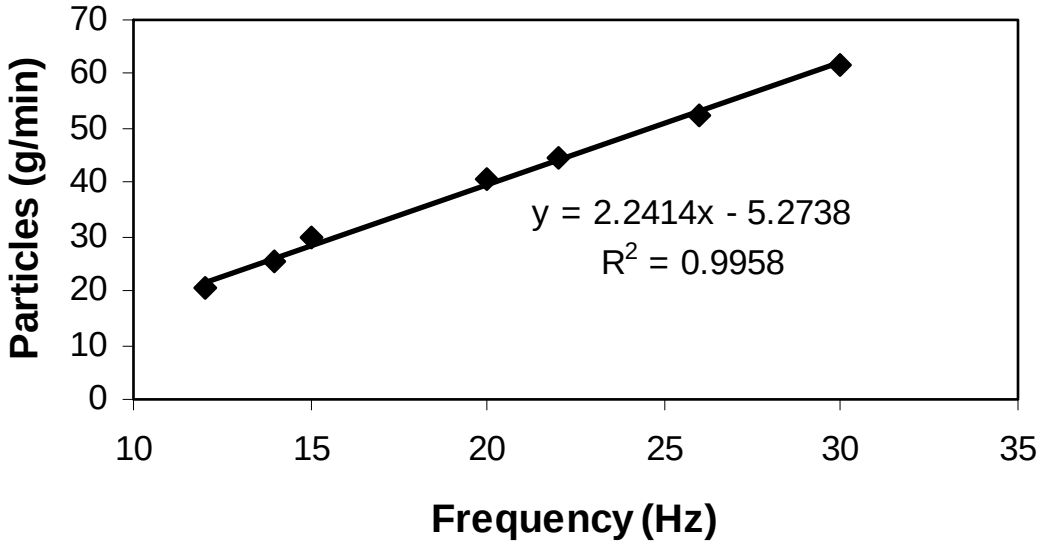

Figure A.2 - Calibration curve for mass flow rate of dust particles.

A.2 Solid Particle Measurement

Once the particles are introduced and interact with the two phase flow through the venturi they must be removed in order to assess the efficiency of the venturi scrubber as a collection device. A system was especially design for that purpose (Figure A.3).

Throughout the venturi, part of the particles will collide with the water droplets and are most likely to be collected while some of them will not be collected. The objective is to focus only on these dry, uncollected, particles.

Figure A.3 – Solid particle collection system

The droplets are heavier than dry dust, so their inertia is higher. In that way, it may be possible to catch the dry particles from the flow by creating a local suction which will affect their motion sufficiently for them to be sucked into a probe. On the other hand, the water droplets are heavier and will not be affected enough and will miss the suction probe. For this purpose, a turbine with a dimmer switch is used in order to adjust the suction velocity to that of the main flow. The particles drawn up are collected by a wet filter, as illustrated in Figure A.4.

The details of the suction system have been tuned by running a flow simulation of a two phase flow split into a side arm. In this way, the diameter of the section pipe, flow rate and the orientation to the main flow were adjusted. A 30º orientation was decided upon and the aperture is located closer to the venturi axis in order to avoid interference by the liquid film.

The suction flow rate is specific for each measurement. The procedure consists in increasing the suction velocity up to the point that droplets are removed. This run is carried out without dust particles. Once this level is determined, dust particles are introduced into the main flow.

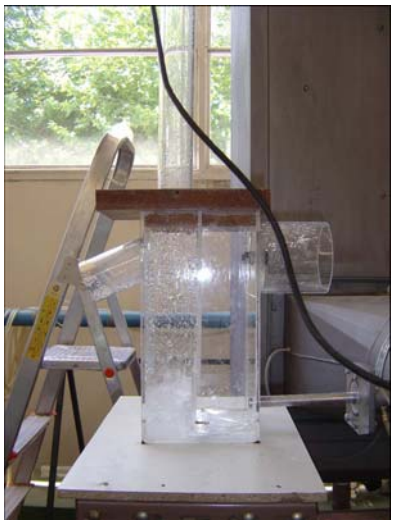

Figure A.4 – Wet filter in the suction probe.

A.3 Collection Efficiency Preliminary Results

Once the equipment was assembled a few tests were carried out. These were mainly to test the consistency of the introduction and collection systems; to assess the operating limits for the system and improve the experimental procedure.

For the experimental data obtained with the collection system, the air flow is fixed to 0.987 *kg/s*, which is the maximum air flow possible in the test rig and two different liquid flow rates are used, 0.019 and 0.038 *kg/s*.

Alumina (Al_2O_3) with a 10μm size with a density of 3970 kg/m^3 is used as dust.

For measuring the quantity of particles inside the filter of water the method used is to extract the particles by evaporating the contaminated water in an oven at 105 ^{o}C.

The preliminary results of the collection efficiency are presented in Table A.1.

Table A.1 - Preliminary results of collection efficiency

Particles introduced (*g*)	Injection type	Liquid flow rate (*kg/s*)	Efficiency (*%*)
300	Spray	0.019	40
	Spray	0.038	28
	Film	0.038	9
200	Spray	0.038	30
	Film	0.038	8.7

It can be observed that the results show that with the spray injection the efficiency of the venturi is higher than film injection.

Model validation

The collection efficiency experimental data were compared with predictions resulting from the theoretical model by Cruz *et al.* (1997).

Figure A.5 shows the influence of the liquid flow rates upon the collection efficiency. It is evident that the liquid loading has a strong influence in the collection efficiency, because more droplets are available for dust collection.

Higher collection efficiency can be achieved for higher liquid flow rates, due to higher droplet concentration.

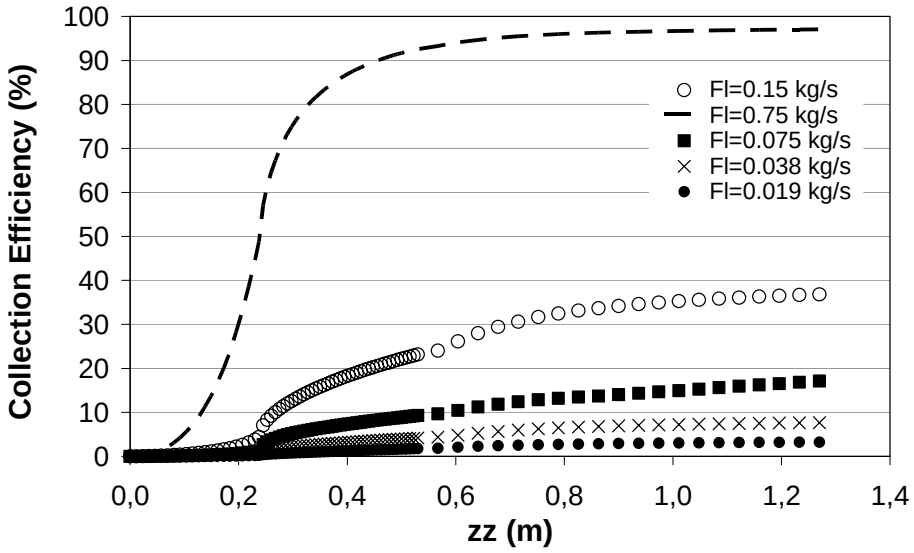

Figure A.5 - Collection efficiency: numerical prediction.

Comparing with the experimental data the results obtained are similar. For film injection type, with liquid flow rate 0.038 *kg/s* the efficiency obtained by the model is 8 % and experimentally this value is 8.7% and 9%.

As mentioned these are preliminary results and more tests should be made to validate the collection system.

A.4 Conclusions

An experimental facility of a large scale venturi scrubber was built to measure collection efficiency. The systems of introduction and collection of particles were developed and tested with reasonable results

More experiments and further improvements in the collection procedure are necessary to fully validate the efficiency of the system and make the collection efficiently experiments reliable.

References

Allen, R. W. K. (1996). *Prediction of Venturi Scrubber Grade Efficiency Curves Using the Contacing Power Law*. Power Technology, Vol. 86, p. 137-144.

Allen, R.W.K., Van Santen, A. (1996). *Designing for Pressure Drop in Venturi Scrubbers: The Importance of Dry Pressure Drop*. Chem. Eng. J., Vol. 61, p. 2003-2011.

Alonso, D.S., Gonçalves, J.A.S., Azzopardi, B.J., Coury J.R. (2001). *Drop Size Measurements in Venturi Scrubbers*. Chem. Eng. Science, Vol. 56, p. 4901-4911.

Ananthanarayanan, N.V. and Viswanathan, S. (1998). *Estimating Maximum Removal Efficiency in Venturi Scrubbers*. Environmental and Energy Engineering, AIChE Journal, Vol. 44, N. 11, p. 2549-2560.

Ananthanarayanan, N.V. and Viswanathan, S. (1999). *Effect of nozzle arrangement on venturi scrubber performance*. Ind. Eng. Chem. Res., Vol. 38, p. 4889-4900.

Atkinson D.S.F. and Strauss W. (1978). *Droplet size and surface tension in Venturi scrubbers*. J. Air Pollution Control Assoc., Vol. 28, p. 1114–1118.

Azzopardi, B.J. and Govan, A.H. (1984). *The Modeling of Venturi Scrubbers*. Filtration and Separation, Vol.21, N. 3, p. 196-200.

Azzopardi, B.J., Teixeira, S.F.C.F., Govan, A.H. and Bott, T.R. (1991). *An improved model for pressure drop in venturi scrubbers*. Trans. Inst. Chem. Eng., Vol. 69, p. 55-64.

Azzopardi, B.J. (1993). *Liquid Distribution in venturi Scrubbers: The Importance of Liquid Films on the Channel Walls*. Chem. Eng. Science, Vol. 48, N. 15, p. 2807-2813.

Azzopardi, B.J. and Teixeira, J.C.F. (1994a). *Detailed measurements of vertical annular two phase flow Part I: drop velocities and sizes*. J. Fluids Eng., Vol. 116, p. 792-795.

Azzopardi, B.J. and Teixeira, J.C.F. (1994b). *Detailed measurements of vertical annular two phase flow Part II: gas core turbulence*. J. Fluids Eng., Vol. 116, p. 796-800.

Azzopardi B.J. (1997). *Drops in Annular two-phase flow*, Int. J. Multiphase Flow, 23 Suppl., p. 1-53.

Bayvel, L.P. and Jones, (1981). A.R. *Electromagnetic scattering and its applications* .Appl. Sci. Publ., London, p. 303.

Bayvel, L.P. (1982). *The Effect of the Polydispersity of Drops on the Efficiency of a Venturi Scrubber*. Trans. I. Chem. E., Vol. 60, N. 1, p. 31-34.

Boll, R.H. (1973). *Particle Collection and Pressure Drop in Venturi Scrubbers.* Ind. Eng. Chemical Fundam. Vol. 12, N. 1, p. 40-50.

Boll, R.H., Flais, L.R., Maurer, P.W. and Thompson, W.L. (1974). *Mean Drop Size in a Full Scale Venturi Scrubber via Transmissor.* J. of Air Pollution Control Assoc. Vol. 24, N.10, p. 934-938.

Calvert, S. (1970). *Venturi and other Optimizing Scrubbers Efficiency and Pressure Drop*. AIChE J., Vol. 16, N. 3, p. 392-396.

Calvert, S., Lundgren, D., Meht, D.S. (1972). *Venturi Scrubber Performance.* J. Air Pollution Control Assoc., Vol. 22, N. 7, p. 529-532.

Castro, A.O. (2002). Caracterização de sprays de dois fluidos, MSc Thesis, University of Minho, Guimarães. (in Portuguese).

Chen, X. Q. and Pereira, J. C. F. (2000). *Computational Modeling of a Dilute Turbulent Liquid-Solid flow using Eulerian-Lagrangian approach*. International Journal of Numerical Methods for Heat & Fluid Flow, Vol. 10, N. 4, p. 409-431.

Chigier, N. (1983), *Drop size and velocity instrumentation*. Prog. Energy Combust. Sci.,

Clif, R., Grace, J.R. and Weber, M.E. (1978). *Bubble Drops and Particles.* Academic Press.

Costa, M.A.M, Henrique, P.R., Gonçalves, J.A.S. and Coury, J.R. (2004). *Droplet Size in a Rectangular Venturi Scrubber.* Brazilian Journal of Chemical Engineering. Vol. 21, N. 2, p. 335-343.

Costa, M.A.M, Ribeiro, A.P.R.A., Togneti, E.R., Aguiar, M.L., Gonçalves, J.A.S. and Coury, J.R. (2005). *Performance of a Venturi Scrubber in the Removal of Fine Powder from a Confined Gas Stream.* Materials Research. Vol. 8, N. 2, p. 177-179.

Cruz, T.M.S. (1997). *Modelação de Sistemas de Limpeza de Gases*. Master thesis, University of Minho. (in Portuguese).

Cruz, T.M.S., Teixeira, S.F.C.F. and Teixeira, J.C.F. (1997). *The role of droplets in scrubbing combustion flue gases*. Proc of the Fourth Int Conf on Technologies and Combustion for a Clean Environment, p. 67-71.

Dahl, E. (2005). *Handbook of Multiphase Flow Metering*. Revision 2. The Norwegian Society for Oil and Gas Measurement and The Norwegian Society of Chartered Technical and Scientific Professionals. Olso. ISBN 82-91341-89-3.

Espaze, A. (2005). *Floating of particles*. Internal report, University of Minho, Guimarães.

Fathikalajahi, J., Taheri, M. and Talaie, R. (1996). *Theoretical Study of Nonuniform Droplets Concentration Distribution on Venturi Scrubber Performance*. Particulate Science and Technology, Vol. 14, p. 153-164.

FLUENT 6.2 *User's Guide* (2005). Fluent Inc.

Gamisans, X., Sarra, M., Lafuente, F.J. and Azzopardi, B.J. (2002). *The Hydrodynamics of Ejector- Venturi Scrubbers and their Modelling by an Annular Flow / Boundary Layer Model*. Chem. Eng. Science, Vol. 57, p. 2707-2718.

Gaminsans, X., Sarra, M. and Lafuente, F.J. (2004a). *Fluid flow and pumping efficiency in an ejector-venturi scrubber*. Chem. Eng. Process., Vol. 43, p. 127-136.

Gamisans, X., Sarra, M., Lafuente, F. J. and Azzopardi, B. J. (2004b). *The Split of Liquid Phase in Drops and Film in an Ejector-Venturi Scrubber.* Chem. Eng. Comm., Vol. 191, p. 398-413.

Gibbons, D.B. (1985). *Drop Formation in annular two-phase flow.* Ph.D. Thesis, University of Birmingham.

Gonçalves, J.A.S., Fernandez, D.A. and Azzopardi, B. J. (1999a). *Experimental study of hydrodynamics in venturi scrubbers with two different liquid injection arrangements,* in P. Di Marco and R.K. Shah (ed.), Two-Phase Flow Modelling and Experimentation, Pisa, p. 701-707.

Gonçalves, J.A.S., Costa, M.A.M., Fernandez, D.A. and Coury, J.R. (1999b). *Perda de carga em um lavador venturi de secção transversal retangular.* Congresso Brasileiro de Sistemas Particulados, Campos do Jordão, Brazil.

Gonçalves, J.A.S. (2000). *Aspectos da modelagem matemática de lavadores venturi.* PhD Thesis. University of Federal de São Carlos. (in Portuguese).

Gonçalves, J.A.S., Alonso, D.S., Costa, M.A.M., Azzopardi, B.J. and Coury J.R. (2001). *Evaluation of the Models Available for the Prediction of Pressure Drop in Venturi Scrubbers* J. Hazardous Materials, B 81, p. 123-140.

Gonçalves, J.A.S., Costa, M.A.M., Aguiar, M.L. and Coury, J.R. (2004). *Atomization of Liquids in a Pease-Anthony Venturi Scrubber Part II. Droplet dispersion.* J. Hazardous Materials, B 116, p. 147-157.

Guilkey J.E., Harman, T.B. and Banerjee, B. (2007). *An Eulerian-Lagrangian Approach for Simulating Explosions of Energetic Devices.* Computers & Structures, Vol. 85, p. 660-674.

Hinze, J.O. (1975). *Turbulence*. McGraw-Hill Publishing Co., New York.

Holdich, R.G. (2002). *Fundamentals of Particle Technology*. Chapter 14. Midland Information Technonology and Publishing, Leicestershire, U.K. ISBN 0-9543881-0-0.

Hollands, K.G.T. and Goel, K.C. (1975). *A General Method for Predicting Pressure Loss in Venturi Scrubbers*. Ind. Eng. Chem. Fundam., Vol 14, N.1, p. 16-22.

Huang, L., Kumar, K. and Mujumdar, A.S. (2003). *A Parametric Study of the Gas Flow Patterns and Drying Performance of Co-current Spray Dryer: Results of a Computational Fluid Dynamics Study*. Drying Technology, Vol. 21, N. 6, p. 957-978.

Hutchinson, B.R. and Raithby, G.D. (1986). *A Multigrid Method based on the Additive Correction Strategy.* Numerical Heat Transfer, Vol.9, p. 511-537.

Kuan B., Yang, W. and Schwarz M.P. (2007). *Dilute Gas-Solid Two-phase Flows in a Curved 90º Duct Bend: CFD Simulation with Experimental Validation*. Chemical Engineering and Science, Vol. 62, p. 2068-2088.

Launder, B.E. and Spalding, D.B. (1972). *Lectures in Mathematical Models of Turbulence.* Academic Press.

Leith, D., Martin, K.P. and Cooper, D.W. (1985). *Liquid utilization in a venturi scrubber.* Filtration and Separation. Vol. 21, p. 191-195.

Lobarinhas, P.J.M. (2003). *Estudo Experimental em Venturi de Grandes Dimensões*. Master Thesis, University of Minho (in Portuguese).

Maliska, C.R., Silva, A.F.C., Rezende, R.V.P. and Georg, I.C. (2008). *Interface Forces Calculations for Multiphase Flow Simulation*. 1º Encontro Brasileiro sobre Ebulição, Condensação e Escoamento Multifásico Líquido-Gás, Florianópolis, 28-29 Abril.

Malvern Instruments Ltd (1991). *High Performance Systems for Particle Characterization*. 2600 Series- User Manual. England.

Mohebbi A., Taheri M., Fathikaljahi J. and Talaie M. R. (2003). *Simulation of an orifice scrubber performance based on eulerian/lagrangian method*, J. Hazard. Mater., A100, p. 13-25.

Morsi, S.A. and Alexander, A.J. (1972). *An Investigation of Particle Trajectories in Two-Phase Flow Systems.* J. Fluid Mech., Vol. 55, Part. 2, p. 193-208.

Mugele, R.A. and Evans, H.D. (1951) *Droplet size distributions in sprays,* Industrial and Engineering Chemistry, Vol. 43, p. 1317-1324.

Nasseh S., Mohebbi A., Jeirani Z. and Sarrafi A. (2007). *Predicting pressure drop in venturi scrubbers with artificial neural networks*. Journal of Hazardous Materials, Vol. 143, p. 144-149.

Norton, T and Sun, D. (2006). *Computational fluid dynamics (CFD) - an effective and efficient design and analysis tool for the food industry: A review.* Trends in Food Science & Technology, Vol. 17, p. 600 -620.

Norwegian Society for Oil and Gas Measurement and Norwegian Society of Chertered Technical and Scientific Professionals. (2005). *Handbook of Multiphase Flow Metering.* Revision 2. ISBN 82-91341-89-3.

Nukiyama, S. and Tanasawa, Y. (1938). *An experiment on the atomisation of liquid by means of air stream*. Trans. Society Mech. Eng. (Japan), Vol. 4, p. 86–93.

Pak, S.I. and Chang, K.S. (2006). *Performance estimation of a venturi scrubber using computational model for capturing dust particles with liquid spray*. J. Hazard. Mater., B138, p. 560-573.

Parker G.J. and Cheong K.C. (1973). *Air-water tests on a Venturi for entraining liquid Hlms.* Int. J. Fluid Mech. Sci., 15, p. 633–641.

Patankar, S.V. (1980). *Numerical Heat Transfer and Fluid Flow.*Hemisphere Publishing Corp.

Placek, T.D. and Peters, L.K. (1982). *Analysis of particulate removal in venturi scrubbers – Role and heat transfer.* AIChE J., Vol. 28, N.1, p. 31-39.

Rahimi, A., Taheri, M. and Fathikalajahi, J. (2004). *Prediction of Pressure Drop in a Venturi Scrubber: Effect of Liquid Film and Re-entrainment.* Chem. Eng. Comm., 191, p. 315-334.

Rahimi, A., Taheri, M. and Fathikalajahi, J. (2005). *Mathematical Modelling of Non-Isothermal Venturi Scrubbers.* The Canadian Journal of Chemical Engineering, 83, p. 401-408.

Ranz W.E. and Marshall W.R. (1952). *Evaporation from drops*. Chem. Eng. Prog., 48: 141-146, 173-180. Village Rio das Pedras, Club Med, Rio de Janeiro, 14 to 18 August 2005.

Ribeiro, A.P., Togneti, E.R., Gonçalves J.A.S. and Coury J.R. (2005). *A Study on the Collection Efficiency of Venturi Scrubber with Multi-Orifice Injection*, 2nd Mercosur Congress on Chemical Engineering.

Roberts D.B. and Hill J.C. (1981). *Atomization in Venturi scrubbers*. Chem. Eng. Commun., Vol. 12, p. 33–68.

Rudnick, S.N., Koehler, J.L.M., Martin K.P., Leith D. and Cooper, D.W. (1986). *Particle Collection Efficiency in a Venturi Scrubber: Comparison of Experiments and Theory*. Environ. Sci. Technol., Vol. 20, N. 3, p. 237-243.

Shih T.H., Liou W.W., Shabbir A., Yang Z., and Zhu J. (1995). *A New k-ε Eddy-Viscosity Model for High Reynolds Number Turbulent Flows - Model Development and Validation*. Computers Fluids, Vol. 24, N. 3, p. 227-238.

Silva, A.M., Leão, C.P., Teixeira, S.F.C.F and Teixeira J.C.F. (2008). *Droplet distribution flowing in a venturi scrubber*. Proceedings of 4th International Conference on Comparing Design in Nature with Science and Engineering, 24 to 26 of June, Algarve, Portugal.

Sun, H. and Azzopardi, B.J. (2003). *Modelling Gas-Liquid Flow in Venturi Scrubbers at High Pressure.* IchemE, Vol. 81, Part B, July, p. 250-256

Swithenbank, J., Beer, J.M., Taylor, D.S., Abbot, D. and McCreath G.C. (1976). A laser diagnostic for the measurement of droplet and particle size distribution, Department of Chemical Engineering and Fuel Technology, Sheffield University, Report Nº AD AO21/30.

Taheri, M. and Sheih, C.M. (1975). *Mathematical Modeling of Atomizing Scrubbers* AIChe J., Vol. 21, N. 1, p. 153-157

Teixeira, J.C.F. (1988). *Turbulence in annular two phase flow*. PhD Thesis. University of Birmingham.

Teixeira, J.C.F., Azzopardi, B.J. and Bott, T.R. (1988) *The Effect of Inserts on Drop Sizes in Vertical Annular Flow*. 2nd U.K. Nat. Heat Transfer Conf., Glasgow, p. 1281–1296.

Teixeira, J.C.F., Teixeira, S.F.C.F. and Azzopardi, B.J. (1994). *Modeling venturi scrubbers for combustion emissions clean up*, Proc. CROCUS'94, Salsomaggiore Terme, paper III-4.

Teixeira, S.F.C.F. (1989). *A model for the hydrodynamics of venturis applicable to scrubbers*. PhD. Thesis. University of Birmingham.

Tsai, C.J., Lin, C.H., Wang, Y-M., Hunag, C.H., Li, S.N., Wu, Z.X. and Wang F-C. (2005). *An Efficient Venturi Scrubber system to Remove Submicron Particles in Exhaust Gas*, Journal of the Air & Waste Management Association, Vol. 55, p. 319-325.

Van Werven, M., Maanen, H.R.E, Ooms, G. and Azzopardi, B.J. (2003). *Modeling Wet-Gas Annular / Dispersed Flow Through a Venturi*. AIChE J., Vol. 49, N.6, p. 1383-1391.

Versteeg, H. and Malalasekera, W. (1995). *An introduction to computational fluid dynamic. The finite volume method.* Longman Scientific & Technical, Harlow, UK.

Viswanathan, S., Gnyp, A.W. and St. Pierre, C.C. (1985). *Annular flow for pressure drop for Pease-Anthony venturi scrubbers.* AIChE Journal, Vol. 12, N. 31, p. 1947-1958.

Viswanathan, S. (1998). *Examination of liquid film characteristics in the prediction of pressure drop in Venturi scrubber*, Chem. Eng. Sci., Vol. 53, N. 17, p. 3161-3175.

Viswanathan, S., Lim, D.S. and Ray, M.B. (2005). *Measurement of drop size and distribution in an annular two-phase, two-component flow occurring in a venturi scrubber*. Ind. Eng. Chem. Res., Vol. 44, p. 7458-7468.

Wasewar, K. L.and Sarathi, J. V. (2008). *CFD Modelling and Simulation of Jet Mixed Tanks.* Engineering Applications of Computational Fluid Mechanics. Vol. 2, N. 2, p. 155-171.

White F. (2003). *Fluid mechanics.* 5th edition, McGraw-Hill.

Yakhot, V. and Orszag, S.A. (1986). *Renormalization Group Analysis of Turbulence: I Basic Theory*. Journal of Scientific Computing, Vol. 1, N.1, p. 1-51.

Yoshida T., Morishima N., Suzuki M. and Fukutome N. (1965). *Pressure loss for the acceleration of atomized droplets*. Kagaku Kogaku, Vol. 29, p. 308.

Yung S., Calvert S. and Duncan M. (1984). *Performance of gas-atomized spray scrubbers at high pressure.* J. Air Pollution Control Assoc., Vol. 34, N.7, p. 736-742.